Detailed Analysis of Biosynthetic Components for the Virulence-Associated Siderophore Petrobactin from *Bacillus anthracis*

by

Tyler Dominic Nusca

A dissertation submitted in partial fulfillment
of the requirements for the degree of
Doctor of Philosophy
(Microbiology and Immunology)
in The University of Michigan
2012

Doctoral Committee:

Professor David H. Sherman, Chair
Professor Stephen W. Ragsdale
Associate Professor Philip C. Hanna
Associate Professor Mary X. D. O'Riordan

ACKNOWLEDGMENTS

I would like to thank my advisor Professor David Sherman for his encouragement and support since the first day I joined his lab, and for showing me the high degree of consideration and multiple opportunities that all his students are fortunate enough to experience. The Sherman group is a competent, compassionate and fun place to do research where I am happy to have the friendship, mentorship, and assistance of many members. A thank you is also extended to my graduate committee including Dr. Phil Hanna, Dr. Mary O'Riordan, and Dr. Stephen Ragsdale for their general enthusiasm and many eye-opening conversations.

During my graduate career, I have been fortunate to be included on multiple publications including those described in this dissertation. These advances would not have been possible without the contribution and collaboration of my coauthors (in alphabetical order): Carl J. Arawang, Erica C. Anderson, Nicholas H. Bergman, Paul E. Carlson, Gregory L. Challis, Shandee D. Dixon, William H. Eschenfeldt, Philip C. Hanna, Stephanie D. Himpsl, Andrzej Joachimiak, Brian K. Janes, Youngchang Kim, Jung Yeop Lee, Natalia Maltseva, Harry L. Mobley, Daniel Oves-Costales, Melanie M. Pearson, Christopher M. Rath, Jamie B. Scaglione, Michael M. Schofield, and Lucy L. Stols.

A few additional members of U of M deserve recognition and appreciation: Ms. Shamilya Williams for administrative support and whose sense of humor and patience is

well appreciated when dealing with absent-minded scientists; Mr. Tom McQuade of the Center for Chemical Genomics is remarkably approachable and fun as well as a wealth of knowledge in the area of high-throughput screens; the facilities management and custodial staff of U of M work very hard to keep something as complex as a biochemistry research building running smoothly and comfortably; Professor Carol Fierke provided useful insight on enzymology discussed in this work; and, the Gestwicki and Lim lab at the Life Sciences Institute have been very generous in use of their equipment.

Finally and very important to me, I would like to express my gratitude for the love and support of my family members: I shut myself out from the world sometimes, but I hope you realize that whether genetically related or not—or in some cases even a human or not—I don't know how I could have made it through hard times at all or enjoyed good times more without you. Thanks!!!

PREFACE

This written dissertation encapsulates the majority of labor and thought invested in my graduate studies, which surround the topic of siderophore biosynthesis and how this relates to *Bacillus* iron acquisition and microbial life cycles. This body of work is divided into four chapters. Chapter 1 introduces iron in biology and aspects of microbial iron acquisition. An emphasis is placed on current research surrounding biological iron-scavenging molecules called siderophores.

Chapter 2 describes work my colleagues and I performed on the unique 3-dehydroshikimate dehydratase enzyme AsbF and its contribution to formation of the siderophore petrobactin. This research has been published as an article in the Proceedings of the National Academy of Sciences (Pfleger, B. F., Y. Kim, T. D. Nusca, N. Maltseva, J. Y. Lee, C. M. Rath, J. B. Scaglione, B. K. Janes, E. C. Anderson, N. H. Bergman, P. C. Hanna, A. Joachimiak, and D. H. Sherman. 2008. "Structural and functional analysis of AsbF: Origin of the stealth 3,4-dihydroxybenzoic acid subunit for petrobactin biosynthesis." *Proceedings of the National Academy of Sciences* 105:17133-17138.).

Remaining questions surrounding petrobactin biosynthesis are addressed by work put forth in Chapter 3, in which I attempted reconstitution of petrobactin biosynthesis *in vitro* using purified proteins and substrates. These findings are coordinated with further characterization of petrobactin siderophore synthetases guided by the crystal structure of

the AsbB enzyme. The research put forth in Chapter 3 has been published in the Journal of Biological Chemistry (Nusca, T. D., Y. Kim, N. Maltseva, J. Y. Lee, W. H. Eschenfeldt, L. Stols, M. M. Schofield, J. B. Scaglione, S. D. Dixon, D. Oves-Costales, G. L. Challis, P. C. Hanna, B. F. Pfleger, A. Joachimiak, and D. H. Sherman. 2012. "Functional and structural analysis of the siderophore synthetase AsbB through reconstitution of the petrobactin biosynthetic pathway from Bacillus anthracis". *J Biol Chem*. Pub. Online.)

As a closing section, Chapter 4 aims to summarize the research presented in Chapters 2 and 3 as well as its possible implications in the fields of microbiology and biochemistry. Connections are made between results discussed within this work and previously published aspects of cellular metabolism, macromolecular protein assembly, and small molecule synthesis. Generally, Chapter 4 encompasses hypothetical and future avenues of experimentation that were made more apparent by the body of this dissertation; however, in some instances, preliminary data is presented.

TABLE OF CONTENTS

Acknowledgments……...……...ii

Preface…….……...iv

List of Figures…….…….....ix

List of Tables…….……..…..xi

List of Abbreviations……...xii

Abstract…….……...xiv

Chapter 1…….…….....1

Introduction…….…….....1

1.1 Overview…….…….....1

1.2 Iron in Nature and Organisms…...…….…….…….....2

1.3 Molecular Biology of Iron Starvation During Inhalational Anthrax..…..….....5

1.4 Siderophore Biosynthesis and Classification..…….....7

NRPS-derived Natural Products……...……...9

NRPS-independent Siderophore Synthetases…...……11

1.5 Siderophore Recognition, Uptake, and Iron Release..…….....14

1.6 Stealth Siderophores..…….....17

1.7 Petrobactin Biosynthesis: Recent Discoveries and Unanswered Questions....18

1.8 References……...….....21

Chapter 2…….…….....26

Structural and Functional Analysis of AsbF: Origin of the Stealth 3,4-Dihydroxybenzoic Acid Subunit for Petrobactin Biosynthesis….....26

2.1 Introduction……..26

2.2 Results and Discussion…….29

2.3 Materials and Methods……..…..41

2.4 Supplemental……....47

2.5 Notes……....57

2.6 References…….....58

Chapter 3…….....60

Functional and Structural Analysis of the Siderophore Synthetase AsbB through Reconstitution of the Petrobactin Biosynthetic Pathway from *Bacillus anthracis*……...…….…….....60

3.1 Introduction……..60

3.2 Results……..65

3.3 Discussion……84

3.4 Experimental Procedures.……89

3.5 Supplemental……....98

3.6 Notes……..106

3.7 References…….....107

Chapter 4…….…….....111

Discussion of Research…….....111

4.1 Summary……...……...……..111

4.2 Microbial Primary Metabolism and the Secondary Metabolism of Siderophore Biosynthesis……...…..…….……..……...112

4.3 Macromolecular Organization of the Petrobactin Biosynthetic Complex….116

4.4 Chemical and Therapeutic Application……...……...……...122

Siderophore-related antimicrobial strategies……...123

De novo chemoenzymatic production of novel compounds...…..…..…...125

Applying isolated natural products…...……...……129

4.5 References……...…….……...……...131

Appendix…….135

Further Comparison of Putative *asb* Gene Clusters……...135

LIST OF FIGURES

Figure

1-1 An overview of iron in the environment, host, and bacterium……..3

1-2 Sample structures of siderophores derived from nonribosomal peptide synthetase (NRPS) and NRPS-independent siderophore (NIS) synthetase pathways..……..8

1-3 An overview of NIS synthetases……...……..12

1-4 Schematic of petrobactin-facilitated iron uptake…….15

1-5 Known components of the petrobactin biosynthetic pathway encoded by the *asbABCDEF* operon……19

2-1 AsbF catalyzes dehydration of 3-dehydroshikimate (3-DHS) to 3,4-dihydroxy-benzoic acid (3,4-DHBA) in *B. anthracis*..……..…...28

2-2 Structural analysis of AsbF……...……...33

2-3 Proposed mechanism for AsbF-catalyzed conversion of 3-DHS to 3,4-DHBA…….38

2-S1 Attenuation of virulence of the Δ*asbF* mutant of *B. anthracis* in mice……50

2-S2 Conservation of AsbF among diverse prokaryotes……...……51

2-S3 Detecting AsbF activity. ……...……52

2-S4 Further modeling of AsbF…….....53

2-S5 AsbF with homologous proteins in sequence……54

2-S6 AsbF-catalyzed D_2O exchange of 3-DHS…….55

3-1 Structure and biosynthesis of petrobactin, the virulence-associated siderophore of *Bacillus anthracis*……61

3-2 *In vitro* reconstitution of petrobactin biosynthesis…….67

3-3 Structure of the type C NIS synthetase AsbB……..70

3-4 Comparison of AsbB to other NIS synthetases..……...…..72

3-5 Modeling the substrate binding pocket of AsbB...……...…..74

3-6 AsbA and AsbB display varying selectivity for nucleophilic substrates……79

3-7 3,4-dihydroxybenzoylation by the aryl transferase components encoded by *asbCDE*……82

3-S1 Fluorescamine derivatization of prepared standards.…….….101

3-S2 Sequence comparison of AsbB, AlcC, AcsD and AsbA.……..……..….102

3-S3 Modeling of ADP binding in the AsbB active site..……..……...…..….103

3-S4 Activity plots for quantification of enzymatic efficiency....……..…...…..….104

3-S5 Reaction of AsbE with spermidine and 3,4-DHBA……105

4-1 Preliminary data suggesting interaction of AsbC, AsbD, and AsbE……..…118

4-2 Hypothetical quaternary structure of natively expressed *asb* gene products……..…120

4-3 Repurposing petrobactin biosynthesis for creation of novel compounds……..126

4-4 Incorporation of unnatural aromatic moieties utilizing thiophenol derivatives……128

A-1 Synteny in *asb* genes from select species……..…136

A-2 Divergence of selected *asb* products……137

A-3 Phylogeny of select species harboring an *asb*-like gene cluster…..……....138

LIST OF TABLES

Table

2-1 Kinetic parameters for AsbF mutants……..36

2-2 AsbF data collection, phasing and refinement...……..46

2-S1 Quantification of 3,4-dihydroxybenzoic acid (3,4-DHBA)..……..……..56

3-1 Summary of the AsbB crystallographic data…….……...……..93

3-S1 Gene, vector, strain, and expression conditions. ……....……100

LIST OF ABBREVIATIONS

3-DHS	3-dehydroshikimate
3,4-DHBA	3,4-dihydroxybenzoic acid
BHI	brain-heart infusion
D_2O	deuterated water
ddH_2O	double-deionized water
HPLC	high-performance liquid chromatography
IDM	iron-depleted medium
IPTG	β-D-1-thiogalactopyrinoside
LB	Luria-Bertani medium
LC-MS	liquid chromatography mass spectrometry
MeCN	acetonitrile
MeOH	methanol
MESG	2-amino-6-mercapto-7-methylpurine ribonucleoside
MS/MS	tandem mass spectrometry
NIS	NRPS-independent siderophore
NRPS	non-ribosomal peptide synthetase
SeMet	selenomethionine
SIM	selective ion monitoring
TCA	trichloroacetic acid

TCEP	tris(2-carboxyethyl) phosphine
TLC	thin-layer chromatography
TB	terrific broth

ABSTRACT

Iron is an essential cofactor in biology, yet most organisms' acquisition of iron is hampered by inaccessibility of this metal in ferric complexes. Thus, life on Earth has developed diverse strategies to obtain necessary levels of free iron, one of the most prominent among microbes being the biosynthesis of specific, high-affinity chelators called siderophores. *Bacillus anthracis*, the causative agent of anthrax, requires the siderophore petrobactin for full virulence. Prior studies have demonstrated the *asbABCDEF* operon encodes biosynthetic machinery for this secondary metabolite: The virulence-associated "NRPS-independent siderophore (NIS) synthetase" protein family includes the enzymes AsbA and AsbB, which condense the common metabolites citrate and spermidine; meanwhile, the AsbCDE complex promiscuously transfers 3,4-dihydroxybenzoic acid (3,4-DHBA) to primary amines. 3,4-DHBA moieties on petrobactin allow the siderophore to evade neutralization by innate immune mechanisms, yet the origin of 3,4-DHBA as well as the function of the protein encoded by the final gene in the *asb* operon, *asbF*, has remained unclear. The data presented herein reveals that the primary metabolite 3-dehydroshikimate is converted to 3,4-DHBA via AsbF catalysis. Subsequent mass spectrometric studies demonstrate that five gene products encoded by the *asb* operon are necessary and sufficient for conversion of endogenous metabolic precursors to petrobactin using an *in vitro* system. In this pathway, the siderophore synthetase AsbB catalyzes formation of amide bonds crucial for petrobactin

assembly through use of biosynthetic intermediates, as opposed to primary metabolites, as carboxylate donors. Structural characteristics of AsbB were applied to provide new insight into how this enzyme, and its partner synthetase AsbA, can bind and adenylate multiple citrate-containing substrates, followed by incorporation of both natural and unnatural polyamine nucleophiles. Subsequent enzymatic assays with the nonribosomal peptide synthetase-like AsbC, AsbD, and AsbE polypeptides indicate two products of AsbB are further converted to petrobactin, verifying previously proposed convergent routes to formation of this siderophore. Combined, these studies establish new avenues for the chemoenzymatic synthesis of novel compounds and investigate key biosynthetic enzymes of petrobactin assembly with the purpose of promoting better understanding of bacterial host iron acquisition and identifying new antimicrobial strategies to protect against *B. anthracis* and other pathogenic bacteria.

Chapter 1

Introduction

1.1 Overview

Nearly all organisms on Earth have evolved to use iron as a cofactor in a variety of essential metabolic processes (*1*). Despite the ubiquity of this metal in biology, the acquisition of free iron from the environment and within the host is hampered by its inaccessibility in ferric complexes. Thus, to obtain necessary levels of free iron, cells have developed diverse strategies, one of the most prominent among microbes being the biosynthesis of iron-specific, high-affinity chelators called siderophores (*2*) (Fig. 1-2).

In *Bacillus anthracis*, the causative agent of anthrax, two siderophores, petrobactin and bacillibactin (Fig. 1-2), play a significant role during iron acquisition (*3-5*), but only petrobactin is absolutely essential for full virulence within a mammalian host (*6*). This mixed catechol-carboxylate siderophore was first isolated from the Gram-negative marine microbe *Marinobacter hydrocarbonoclasticus* (7), but recent genetic and chemical analysis suggests that petrobactin biosynthesis may also be a prerequisite for virulence in numerous *Bacillus* species (*8*). These studies highlight the importance of elucidating the mechanisms of siderophore production in pathogenic microbes as a target for halting infection by organisms like *B. anthracis*, a rapidly virulent organism and potential bioterrorism agent. Based on these factors, my colleagues and I have conducted studies designed to investigate key biosynthetic enzymes for petrobactin assembly with

the purpose of further understanding bacterial host iron acquisition and establishing new anti-microbial strategies to protect against anthrax.

1.2 Iron in Nature and Organisms

After the first billion years of the Earth's formation, soluble iron was abundant in the shallow, turbulent oceans of Earth. Ancestral organisms readily took advantage of this ion's electrochemical properties in the evolution of their enzymology. The multiple charge states of iron allowed for catalysis of biological redox reactions including nitrogen fixation (*9*), metabolite degradation (*10, 11*), and molecular hydrogenation during fermentation (*12*). By the Cambrian explosion 500 million years ago, flourishing photosynthetic microbes had created one of the grandest geological changes in our planet's history: Earth's atmosphere was at the height of becoming poisoned with oxygen (*13, 14*). This had a drastic effect on many aspects of the earth's surface including oxidation of available ferrous iron and its resultant unavailability in largely insoluble ferric complexes (*2, 14*). Billions of years of evolution incorporating the utility of iron could not suddenly be changed, thus organisms began to evolve methods for obtaining and retaining the now scarce element.

Microorganisms have developed multiple ways to obtain iron from the extracellular environment (Fig. 1-1). Transporters designed for the recognition of free metal are ubiquitous, but methods for solubilizing large amounts of iron often are not very efficient except at extreme conditions (*15, 16*). Cohabitation with other organisms has also allowed for expansive uptake of metal bound to heme (*17*). Indeed many

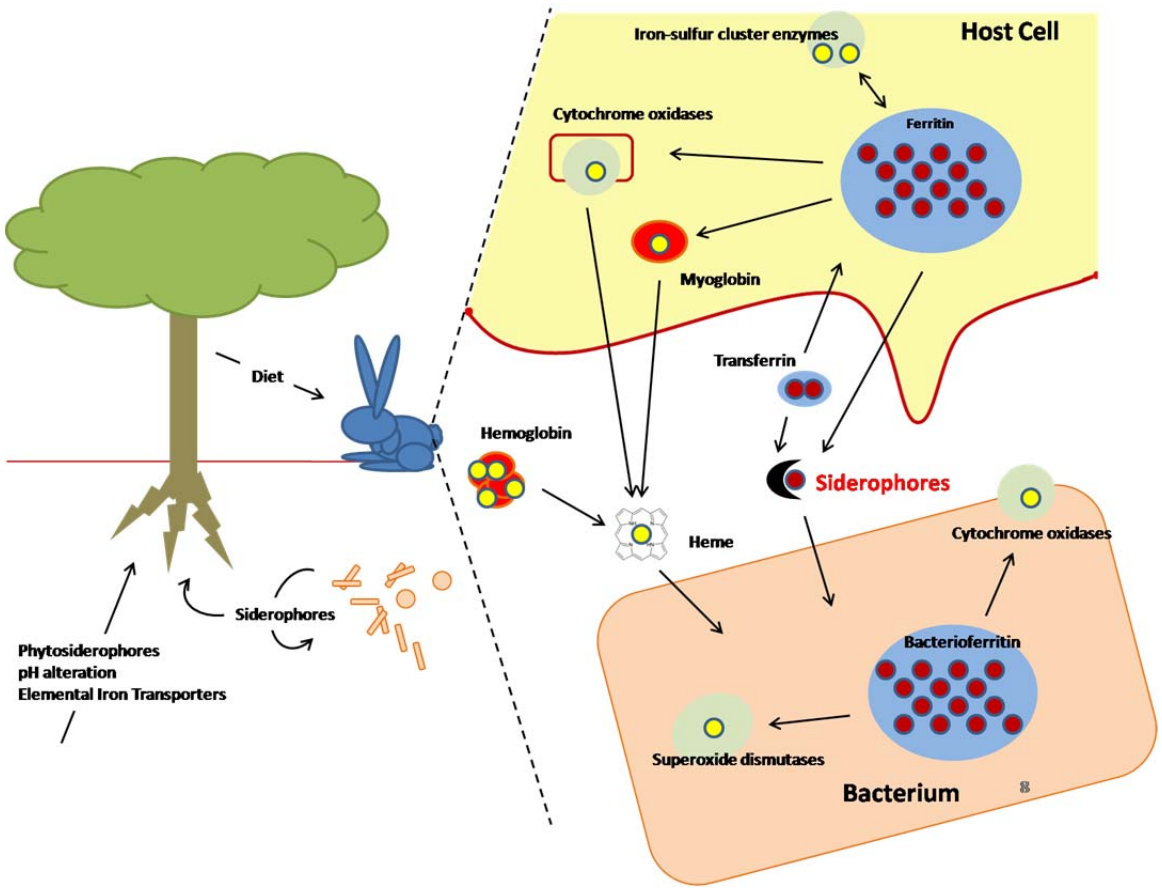

Figure 1-1. An overview of iron in the environment, host, and bacterium. Free iron is not readily available in the oxidative environment; meanwhile, it is tightly sequestered by host molecules during an infection. Bacteria have evolved multiple methods to overcome this including heme scavenging and secretion and reuptake of siderophores.

pathogens maintain heme recognition and uptake systems as virulence factors, and this system has been extensively studied in *Staphylococcus aureus* (*18*) and *Escherichia coli (19)*. *Bacillus anthracis* also expresses a heme uptake system that may contribute to virulence (*20-22*); however, not to the same extent that siderophore production does (*21, 23, 24*). Indeed siderophores are one of the more widely distributed iron acquisition methods utilized by both prokaryotes and fungi in growth conditions ranging from marine to terrestrial habitats to infections of both animal and plant hosts. A more detailed description of siderophores appears in a following section.

Iron obtained by higher eukaryotes through diet, or in the instance of plants, through alteration of local soil pH and siderophore-like chelators (*16, 25*), is kept sequestered in specialized biological molecules (Fig. 1-1). This extends to the human host which contains approximately 4 to 5 grams of iron when well-nourished, yet nearly all of this metal is bound by a myriad of proteins (*26-28*). Aforementioned enzymes utilize iron as a cofactor and the oxygen storage molecules hemoglobin and myoglobin (*28, 29*). Additionally, intracellular ferritin is the predominant intracellular reserve for iron (*28, 30*). A homolog of this, bacterioferritin, is found in prokaryotes and serves a similar function but differs slightly from eukaryotic ferritin by multiple copies of a single polypeptide sequence as opposed to a heavy and light chain in the formation of a large multimer (*2*). Meanwhile, the iron-scavenging protein transferrin is freely diffuse in the plasma (*31, 32*) and conveys ferrous iron atoms throughout the body (Fig. 1-1). Studies indicate transferrin is a main source of iron for many pathogens during infection. Indeed, the formation constants of molecules ($K_f = {}^{[complex]}/_{([molecule][ligand])}$) like transferrin and ferritin for their ferric iron complexes are around 10^{23}/M, many orders of magnitude

lower than the formation constant of most siderophores which can range between 10^{29}-10^{52}/M (*2*).

Multicellular organisms tightly regulate the amount of stored and free iron in the cell. In vertebrates, ferritin and transferrin levels as well as copy number of iron cation transporters exposed on the cell membrane are controlled by the liver-derived hormone hepcidin (*27, 33*). The purpose of tight iron regulation in multicellular organisms is two-pronged. Primarily, free iron is highly toxic, catalyzing the formation of free radicals from reactive oxygen species (ROS) in respiring cells (*27, 34*). Ironically, this same property of iron is capitalized on by heme-containing catalase and superoxide dismutase to harmlessly convert ROSs to water (*34*). The stringent limitation of available iron has a secondary benefit as well more pertinent to this work, and that is restricting development of any invading pathogen. Even in instances where microbes have evolved mechanisms to scavenge iron in the host, optimal intracellular levels of iron found in culture are rarely reached (*2, 15, 28*). Furthermore, siderophore biosynthesis, production of heme-scavenging protein complexes, or degradation of ferric host protein has a high metabolic price. Hence, low iron retards pathogen cellular replication, giving a host an "edge" required to combat infection.

1.3 Molecular Biology of Iron Starvation during Inhalational Anthrax

In the inhalational route of infection, the spore is the infectious form of *Bacillus anthracis*(*35*)**.** Once latent spores make their way to the lung epithelium, host antigen-presenting cells—primarily macrophages—internalize the infectious particle and shuttle it to other parts of the lymphatic system. It is at this later stage of host entry where the

spore finally germinates into vegetative cells in a position to rapidly replicate to extremely high titers in the blood and, through the effects of secreted toxins, cause severe edema that directly contributes to lethality (*21, 36*). Iron facilitates activities including DNA replication, amino acid synthesis, and lipid conversion that can be associated with the rampant cell division observed by *B. anthracis* in the blood. During early stages of infection, iron is also necessary for mounting bacterial countermeasures against host immune defenses. The release of reactive oxygen species by neutrophils and other immune cells has a strong antibacterial effect, and infection by *B. anthracis* is highly reliant on proteins requiring iron as a cofactor, including cystathionine β-synthase, responsible for accumulation of reductive H_2S (*37*), and a suite of redundant superoxide dismutases (SODs) to mitigate oxidative stress (*38, 39*). Interestingly, copies of SOD constitute one of the three main iron reservoirs in *B. anthracis* along with the bacterioferritin Dps2 and ferredoxin (*40*) (Fig 1-1).

The bacterial response to iron starvation is largely mediated by the ferric uptake response (Fur) regulator (*2, 21, 41*). The actual Fur protein is a dimeric AraC-like repressor that undergoes a conformational change in the absence of iron, resulting in release of bound DNA. A canonical AT-rich DNA sequence constituting the "Fur box" precedes many iron acquisition genes in *Bacillus* spp., including *dhb*, responsible for bacillibactin biosynthesis, the elemental iron importer Ywb, and multiple ABC transporters responsible for siderophore and heme uptake (*21, 42*). In *E. coli*, an additional Fur-regulated gene constitutes a second level in low-iron response through expression of the siRNA RyhB, and the product FsrA appears to serve the analogous role in *Bacillus* species (*43, 44*). These polynucleotides post-transcriptionally affect multiple

mRNAs with the end result of increasing precursor pools for siderophore biosynthesis, repressing translation of iron-dependent proteins, and repression of further expression of *fur* (*43-45*). Global expression studies of *Bacillus* species demonstrate an overlap in expression profiles between response to oxidative stress and iron starvation (*46-48*). In addition to the aforementioned requirement for iron-containing enzymes to prevent redox damage, an oxidative environment directly contributes to a loss of cytoplasmic and protein-bound ferrous (Fe^{2+}) iron (*49*).

Genetic and chemical analysis of *B. anthracis* revealed the *asb* biosynthetic operon, responsible for petrobactin biosynthesis, to be critical for infection of macrophages and in a mouse model (*3, 23, 48*). Interestingly, while petrobactin production is induced in iron-deficient conditions, there is no canonical Fur-box preceding any *asb* genes. While there is some upstream sequence that may confer Fur-like regulator binding, the fact that petrobactin production is also affected by paraquat-induced oxidative stress, variation in temperature, and oxygen availability suggests additional levels of control in *asb* expression exists (*46, 48, 50*).

1.4 Siderophore Biosynthesis and Classification

Generally, the biosynthetic origin of siderophores can be divided into two classes: non-ribosomal peptide sythetases (NRPS) and the relatively newly characterized class of NRPS-independent siderophore (NIS) synthetases (*51-54*) (Fig. 1-2). *B. anthracis* has one of each of these systems. Bacillibactin is synthesized via an NRPS pathway that

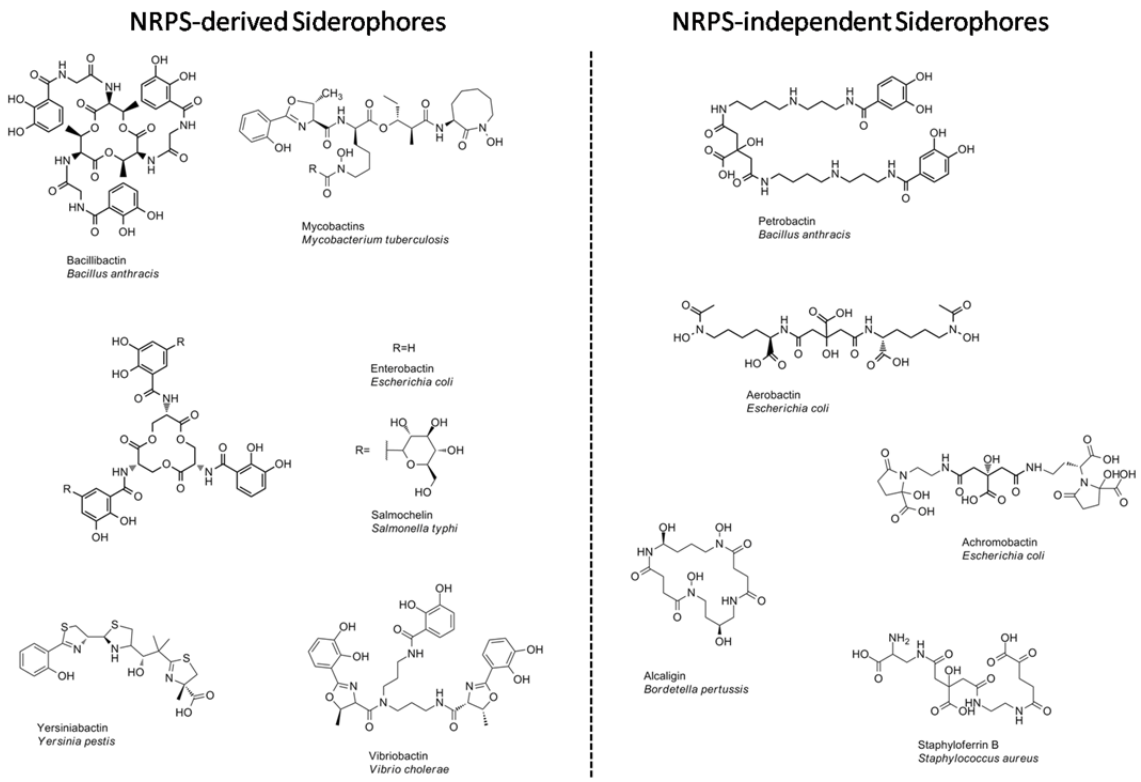

Figure 1-2. Sample structures of siderophores derived from non-ribosomal peptide synthetase (NRPS) and NRPS-independent siderophore (NIS) synthetase pathways.

is not required for virulence in mice but may still play anotherrole. Petrobactin, however, is required for virulence of all *Bacillus* species and derived from NIS mechanisms (*55*).

NRPS-derived Natural Products

In addition to siderophores, many other bacterial and fungal natural products are derived from NRPS pathways. These include compounds with such useful applications as antibiotics, like erythromycin (*56*), and cryptophycin anticancer agents (*57, 58*). Metabolites derived from this process are either linear or cyclic, appearing as chains consisting of multiple subunits united by a series peptide bonds. The incorporation of each NRP subunit is facilitated by a single module that is comprised of three essential catalytic domains: a carrier domain that is modified with a phosphopantethine arm that forms thioester bonds with NRP subunits; an adenylation domain that recruits substrates and loads the subunit to the carrier domain; and a condensation domain that catalyzes the condensation of a nucleophilic portion of the loaded subunit with the thioester of the preceding module's carrier domain and subunit. In most instances, multiple NRPS modules are encoded by a single ORF (*56, 57*). The resultant individual polypeptides in turn form tight, noncovalent interactions via docking domains with additional NRPS modules encoded by separate genes within the same biosynthetic cluster. The end result is a heteromer that acts as a molecular "assembly line", recruiting substrates that are adenylated and condensed to one another through repeating peptide bonds in a specific order (*56, 57*). Many NRPS biosynthetic pathways will contain domains in addition to the adenylation, condensation, and carrier described above, including tailoring enzymes like reductases, halogenases, epimerases, and methyltransferases. A final thioesterase

domain releases the generated NRP and in some cases also cyclizes the completed molecule (*56, 57*). While a single NRPS system represents a protein macromolecule several hundred kilodaltons in size, electron micrography of *Bacillus subtilis*, a close relative to *Bacillus anthracis*, discovered multiple copies of the bacillaene hybrid NRPS-polyketide synthase (PKS) system organized into an organelle-like megastructure (*59*). Such a finding suggests other natural product biosynthetic machinery, including that of siderophores, may be organized in a similar fashion.

Many NRPS-derived siderophores are implicated in bacterial virulence (*2, 51, 53*). *Yersinia pestis* research regularly uses a strain attenuated for yersiniabactin production (*60*) while *Mycobacterium* species synthesize an array of mycobactins to shuttle iron from the environment, past the cell wall, and into the bacterial cytoplasm (*61*) (Fig. 1-2). *Pseudomonas aeruginosa* produces two NRPS-derived siderophores, pyochelin and pyoverdin, that are also implicated in quorum sensing (*62*). Despite all these examples, perhaps the most researched NRPS-derived siderophore is enterobactin (Fig. 1-2). Originally characterized in *E. coli*, it has been attributed to the iron acquisition of multiple commensal and pathogenic Gram-negative species including *Salmonella enterica* serovar Typhi, and has the highest ferric iron affinity of any natural compound (*2, 51, 52, 63*). This radially symmetrical molecule is comprised of three chelating 2,3-dihydroxybenzoic acids (2,3-DHBA) individually bound to serine. These three serines are in turn incorporated into a central trilactone ring (*51*). Interestingly, bacillibactin from *B. anthracis* shares many structural features with enterobactin, though methylserines comprise the trilactone ring which is linked to 2,3-DHBA through an additional glycine subunit (*52, 55, 64*). Shared structural motifs are no coincidence: not

only did the biosynthetic pathways for all NRPS-derived siderophores likely arise from common precursors, but the similarity combined with slight (but apparent) deviation of bacillibactin from enterobactin's structure allow for *Bacillus* species to recognize and use both highly effective siderophores, while Gram-negative enterobacteriaciae have generally only evolved to use enterobactin (*64, 65*).

NRPS-independent Siderophore Synthetases

A second method of siderophore biosynthesis utilizes a family of enzymes logically referred to as NRPS-independent siderophore (NIS) synthetases (*51, 66*) (Fig. 1-2, 1-3). Much like an NRPS module, NIS synthetases catalyze condensation reactions resulting in the formation of peptide, and occasionally ester, bonds; however, the mechanisms by which this occurs is somewhat different (Fig. 1-3 B). While NRPS gene products typically contain multiple catalytic domains, an NIS synthetase polypeptide occupies a rough "cupped hand" structure that contains one active site that coordinates multiple substrates. As a first step of NIS synthetase reaction, ATP is recruited to a deeply-set binding pocket, followed by coordination of a carboxylate-containing substrate. These two compounds are placed in a strained coordination that makes the adenylation of this carboxylic acid favorable (Fig. 1-3 C). Once incorporated, the AMP is positioned as an ideal leaving group for SN2 attack by a final nucleophilic substrate. All final products of this reaction, including the newly formed siderophore intermediate, AMP, and pyrophosphate (PP_i) are released following the condensation and have been used to track the progress of NIS synthetase reactions (*51, 54, 66-68*). While the

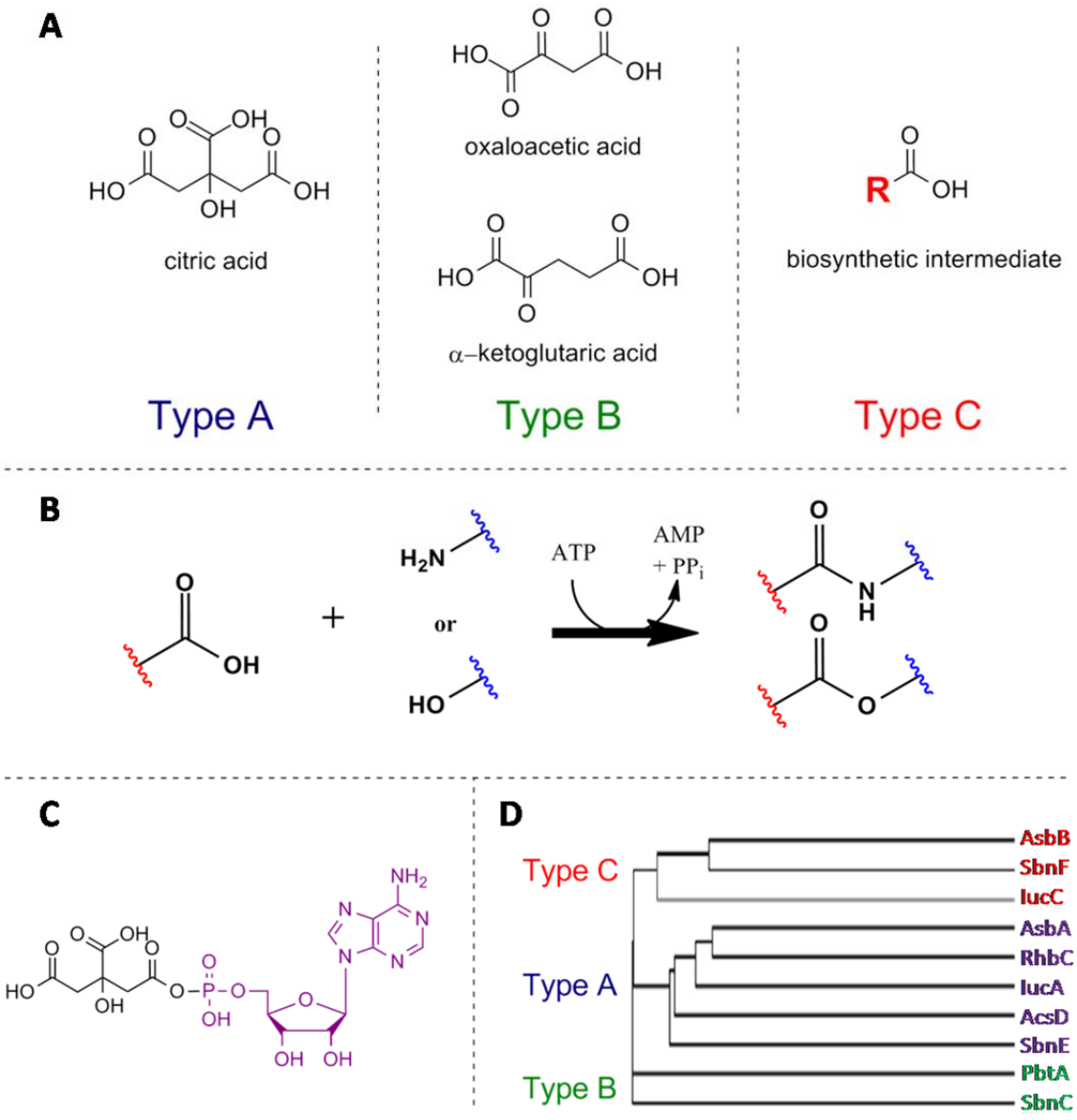

Figure 1-3. An overview of NIS synthetases. A. NIS synthetases are classified based on their preference of carboxylate-containing substrate. B. The general activity of an NIS synthetase involve adenylation of a substrate's terminal caboxylate, followed by attack and resultant condensation with a primary amine or an alcohol, forming an amide or ester bond, respectively. C. The adenylated intermediate of a type A NIS synthetase like AsbA. D. Clade separation comparing primary structure of related NIS synthetases. Enzymes group in accordance to substrate preference over native organisms' phylogeny (analyzed in *ClustalW*).

implicit order of substrate binding is known (ATP, carboxylic acid, nucleophile), exact points at which carboxylate adenylation, nucleophile binding, and eventual condensation occurs is not (*51, 54, 66-68*).

NIS synthetases are further defined by what type of carboxylate substrate they coordinate (Fig. 1-3 A): Type A synthetases bind citric acid; type B originally denoted synthetases that utilize α–ketoglutaric acid, but more recently discovered enzymes falling in this family preferentially bind closely related primary metabolites like oxaloacetatic or glutaric acid instead. Finally, Type C synthetases do not preferentially bind simple primary metabolites, but instead more complex intermediates in NIS biosynthesis (*51, 66*). Interestingly, sequence analysis of NIS synthetases is capable of revealing carboxylic substrate affinity; thus, if a handful of NIS genes are subjected to clade separation they will be segregated by type A, B, or C (Fig. 1-3 D). Thus far, every NIS synthetase characterized to date contains a single catalytic domain, unlike the multi-domained and often multimodular NRPS genes. This said, there are examples of iterative NIS synthetases that first function as a type A or B enzyme, synthesizing their own substrate for subsequent type C synthetase activity (*66, 69, 70*). Furthermore, cursory experiments suggest specific, noncovalent interactions between multiple NIS biosynthetic enzymes in the possible formation of a defined macromolecular machine similar to the "conveyor belt" scheme of NRPSs (described in Chapter 4).

Typically, because NIS pathway substrates are polar metabolites, the products of these reactions are also highly polar (*51, 66, 70*). While charged and polar functionalities are useful in chelating iron and increasing the solubility of siderophores in aqueous environments, this chemical characteristic also makes standard methods for secondary

metabolite isolation largely ineffective. Thus organic extractions are often abandoned for use of more polar solvents, resins, and chromatography methods (*71*). Petrobactin is unique in this instance as it is the only NIS-derived siderophore found thus far to have aromatic functionalities, increasing its hydrophobicity and UV absorbtivity for standard chromatographic methods, and making it an amenable model for investigating NIS biosynthetic pathways.

1.5 Siderophore Recognition, Uptake, and Iron Release

Once complexed with extracellular iron, a ferri-siderophore complex must be recognized by a specific surface-associated receptor for bacterial uptake (*2, 72-74*). This receptor in turn interacts with an ATPase-binding cassette (ABC) transporter system to facilitate siderophore-associated iron uptake through the plasma membrane into the cytoplasm (*74, 75*). In the instance of Gram- negative microbes, a TonB-associated outer membrane receptor is also required for import of ferri-siderophore into the periplasm (*74, 76*). The permease of an ABC transporter is comprised of either a single peptide with repeating domains or dimer of polypeptides that form a channel across the plasma membrane. The extracellular portion of the permease interacts with specific ligand receptors while the cytoplasmic side binds soluble ATPases that function in a dimer to drive internalization of the ligand (*75*). Recent research has shown that while multiple receptors of diverse species are capable of binding petrobactin, only one ABC-transport associated receptor gene, *fpuA*, facilitates petrobactin uptake in *B. anthracis* (*24, 72, 73*). FpuA, in turn interacts with two possible permease structures, each of which require their own ATPase set (Fig. 1-4). This branching redundancy of a single receptor to multiple

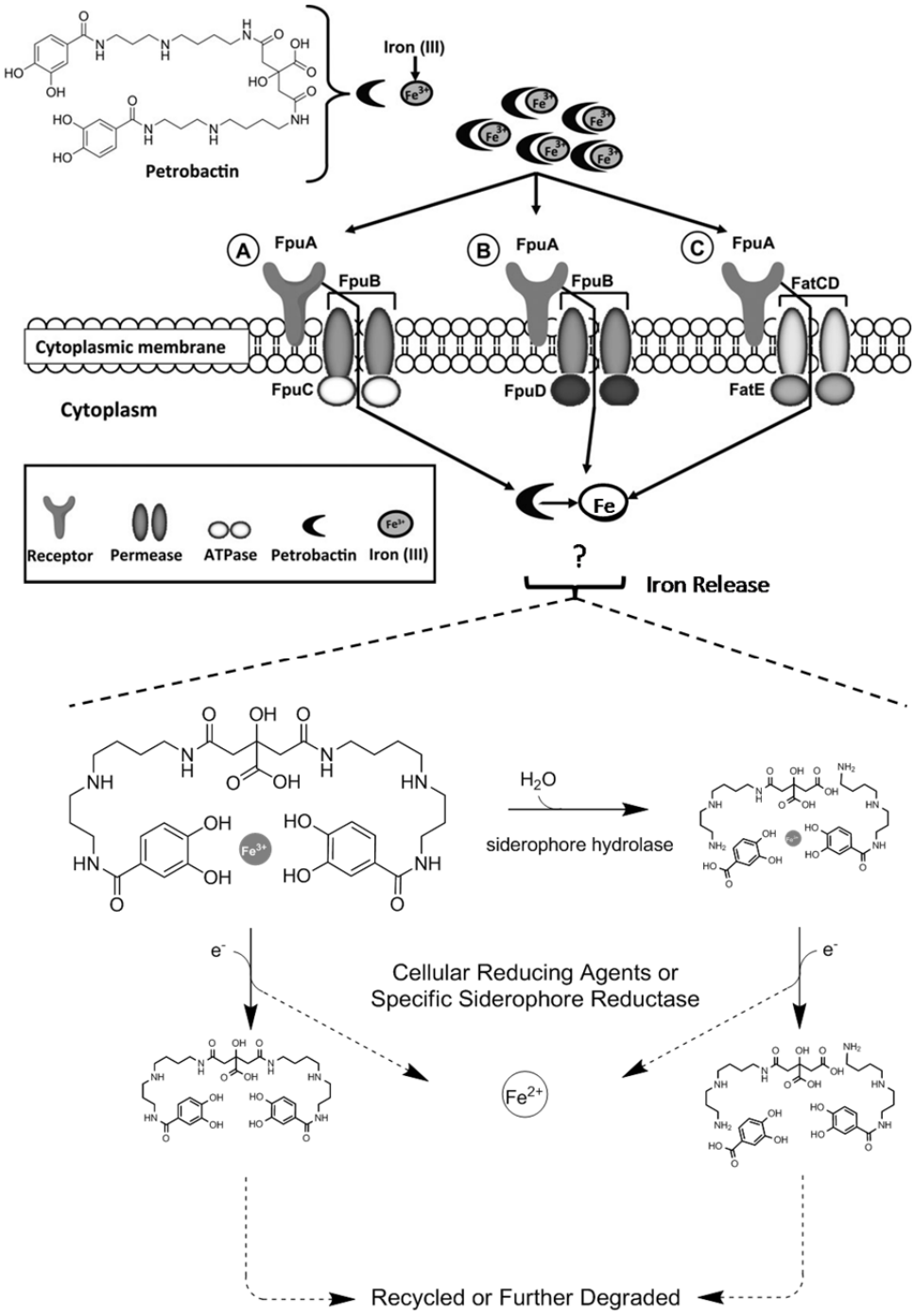

Figure 1-4. Schematic of petrobactin-facilitated iron uptake. The extracellular receptor FpuA recognizes petrobactin. Three possible ABC import complexes are comprised of ATPase and permease components that display some functional redundancy. The method for iron release of presumably internalized petrobactin remains unknown, but may involve enzymatic siderophore degradation and iron reduction. *Portions of this figure courtesy of* ***Shandee D. Dixon*** *of the Hanna group and adapted from reference 77.*

ATPases is unique in ABC-transport mechanisms and highlights many new targets in inhibiting virulence-associated iron acquisition (*77*).

Prior to usage by the bacterial cell, iron must be released from the siderophore. The strategy employed for iron removal to occur largely depends on the affinity the chelator has for ferric iron (*53*). Reduced ferrous iron is not bound strongly to siderophores, thus the overall reductive environment of the cytoplasm is sufficient for dissociation of iron from relatively weaker siderophores (K_f ~10^{20}) (*53, 78*). This mechanism has been speculated for desferrioxamine in which iron dissociation can be facilitated by general cellular reducing agents like FADH (*78*). In some instances, specific ferri-siderophore reductase genes have been identified, including FhuF and YqjH, which interact with hydroxamates and catecholates respectively in *E. coli* (*79, 80*). A unique example of reductases is found in *Mycobacterium* species in which iron reduction occurs extracellularly, and only the dissociated ion, as opposed to the siderophore-iron complex, is internalized (*81*). Tris-catecholate siderophores like bacillibactin and enterobactin (and its salmochelin derivatives), have the highest affinity for ferric iron of any known natural compounds, thus creating a redox potential unfavorable for conversion of bound iron to the ferrous ion, even enzyamtically. In these instances, the siderophore must first be degraded by a specific hydrolase—FesA in *E. coli* and YuiI in *Bacillus* spp.—before iron liberation can occur (*53*). Interestingly, specific siderophore degradation enzymes have also been observed in some cases that are not required for iron utilization, and thus seemingly serve another unknown metabolic function (*82*). The structure of petrobactin includes both carboxylate and catechol chelation points which combine to confer a unique binding affinity for iron, thus the

methods employed by *Bacillus* spp. for petrobactin iron release remains enigmatic as does the fate of the siderophore after interaction with the ABC transporter (Fig. 1-4).

1.6 Stealth Siderophores

As an added level of complexity in competition for iron during an infection, the host innate immune protein siderocalin neutralizes many catechol-containing siderophores secreted by invading pathogens. Siderocalin does not sequester petrobactin, however, and this "stealth siderophore" quality is significant when considering the dependence of *B. anthracis* on this compound during an anthrax infection. Modeling and binding studies implicate steric hindrance created by the positioning of the hydroxyls on 3,4-dihydroxybenzoic acid (3,4-DHBA) subunits of petrobactin in preventing its interaction with siderocalin (*83*). Alternatively, most other catecholate siderophores contain 2,3-dihydroxybenzoic subunits, including bacillibactin, and are effectively neutralized by this protein during the host response to infection (*83-85*).

Further examples exist of stealth siderophores. The tris-catecholate siderophore enterobactin possesses one of the highest formation coefficients for iron-complexation, yet presence of 2,3-DHBA moieties allows it to still be neutralized by siderocalin (*85*). Salmochelins are enterobactin molecules covalently modified by the glucosyltransferase IroB (*63*) (Fig. 1-2). The presence of glucose on the catechol moieties creates a steric hindrance similarly to 3,4-DHBA, but through a different biosynthetic route (*84*). Another triscatecholate, vibriobactin from *Vibrio cholerae*, coordinates iron with only five of its six catechol oxygens in a unique 3-dimensional conformation that prevents binding to siderocalin (*86*). A larger collection of siderophores simply avoid

sequestration by siderocalin through the absence of catechol groups in their structure, including the salicylate-containing yersiniabactin and mycobactin, which are only loosely bound by the immune protein, and hydroxamate or carboxylate siderophores like aerobactin and staphyloferrin B, that largely avoid siderocalin altogether (*84*) (Fig. 1-2).

1.7 Petrobactin Biosynthesis: Recent Discoveries and Unanswered Questions

Previous mutagenesis and biochemical studies have shown that products of the polycistronic operon consisting of the six genes *asbABCDEF* contribute to assembly of petrobactin in bacteria. Furthermore, petrobactin arises from three simple metabolic precursors: the common primary metabolites citric acid and spermidine, and the unique subunit 3,4-DHBA (Fig. 1-5 A) (*4, 55, 67, 87-90*). As described above, AsbA and AsbB are members of a growing family of gene products referred to as non-ribosomal peptide synthetase - independent siderophore (NIS) synthetases (*87, 91, 92*). AsbA can be classified more specifically as a type A NIS synthetase due to its utilization of citrate as a substrate for adenylation. This is followed by condensation with spermidine leading to *N*8-citryl-spermidine (Fig. 1-5 B) as a first step in petrobactin biosynthesis (*87*). AsbB is similar in activity to AsbA, but classified as a type C NIS synthetase due to its preference for advanced intermediates in siderophore biosynthesis as substrates including *N*8-citryl-spermidine (*4, 89*). Both AsbA and AsbB incorporate the asymmetric polyamine spermidine from only one (*N*8) of its two primary amine termini (Fig. 1-5 B) (*87, 89, 91*). Currently, the mechanism by which this regioselectivity is achieved is not well understood.

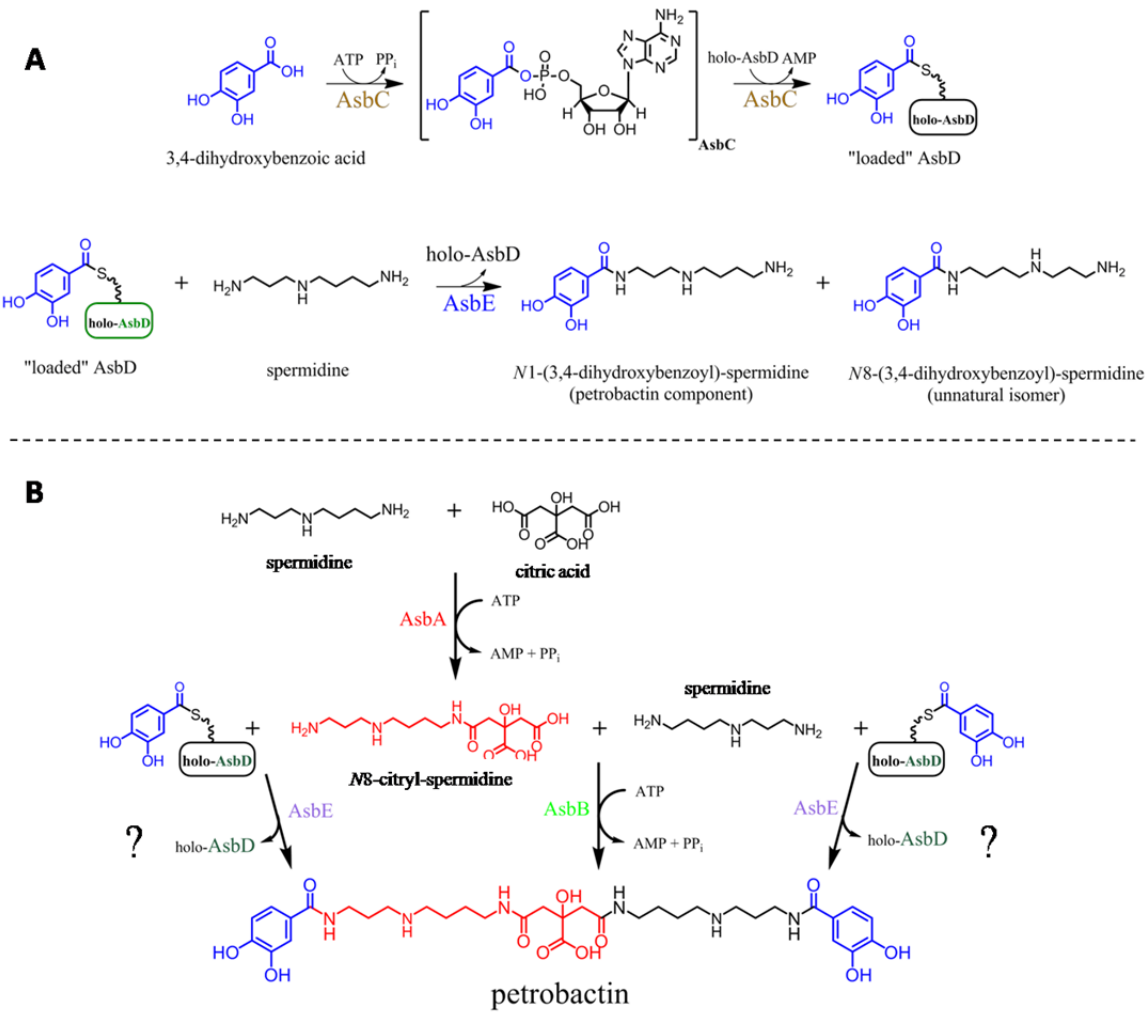

Figure 1-5. Known components of the petrobactin biosynthetic pathway encoded by the *asbABCDEF* operon. A. NRPS-like polypeptides AsbC,-D, and –E transfer 3,4-DHBA to spermidine, but how this activity is integrated with native petrobactin biosynthesis is not fully understood. B. The NIS synthetases AsbA and AsbB incorporate spermidine arms to a central citrate moiety. 3,4-DHBA must be incorporated at some point for formation of the complete siderophore.

In addition to citrate and spermidine, which are readily available primary metabolites in bacteria, petrobactin biosynthesis requires the unusual precursor 3,4-DHBA. It was hypothesized that the *asb* operon would likely code for synthesis of this crucial catecholate; indeed, it was indicated by earlier reports (*93*), precursor incorporation studies (*94*), and through previous analysis that supernatants of a *B. anthracis* Sterne culture contain 3,4-DHBA. Specifically, the Sherman group demonstrated that supernatants of an *asbABCDEF* mutant fail to accumulate this key petrobactin subunit, indicating that one or more *asb*-encoded polypeptides are involved in its synthesis. 3,4-DHBA is critical for petrobactin to function as a virulence factor as it facilitates the siderophore's stealth ability and forms four of the six chelating functionalities on the molecule. Subsequent experimentation is required to explain the biochemical origin of this important molecule.

Once available, linkage of the 3,4-DHBA moieties to spermidine is facilitated *in vitro* by interactions of three other *asb* products: AsbC catalyzes adenylation of 3,4-DHBA followed by transfer via thioester bond formation to the phosphopantetheinylated aryl carrier protein AsbD (*67*). Subsequently, AsbE functions to catalyze amide bond formation between 3,4-DHBA ("loaded" on AsbD) and a suite of linear molecules bearing a primary amine (*67*) (Fig. 1-5 A). Products of this reaction cannot be efficiently incorporated enzymaticlly into a petrobactin molecule; however, there are several proposed petrobactin precursors that have an available amino group, thus a systematic investigation is required to establish which metabolic intermediates function as natural substrates for AsbE during petrobactin biosynthesis.

Siderophore production in pathogenic bacteria has gained considerable attention due to its crucial function in essential iron uptake by many microbes and the relevance of siderophore-associated proteins as molecular markers of various infectious agents (*95*). Eliminating petrobactin in pathogenic microbes is particularly important among catecholate siderophores, as it escapes sequestration by the mammalian immune protein siderocalin (*83, 84*) and is required for virulence. The genes responsible for mediating production of this metabolite have remained partially undefined as has the biochemical mechanism of its assembly. Elucidation of these unknown aspects in petrobactin biosynthesis and describing how this may be applied toward the generation of novel compounds and design of new antibiotics are the motivating forces behind my thesis work.

1.8 References

1. P. Lindley, Lindley, *Rep Prog Phys* **59**, 867 (1999).
2. S. C. Andrews, A. K. Robinson, F. Rodriguez-Quinones, *FEMS Microbiol Rev* **27**, 215 (2003).
3. A. T. Koppisch *et al.*, *Biometals* **18**, 577 (Dec, 2005).
4. J. Y. Lee *et al.*, *J Bacteriol* **189**, 1698 (Mar, 2007).
5. M. K. Wilson, R. J. Abergel, K. N. Raymond, J. E. Arceneaux, B. R. Byers, *Biochem Biophys Res Commun* **348**, 320 (Sep 15, 2006).
6. S. Cendrowski, W. MacArthur, P. Hanna, *Mol Microbiol* **51**, 407 (Jan, 2004).
7. K. Barbeau, G. Zhang, D. H. Live, A. Butler, *J Am Chem Soc* **124**, 378 (Jan 23, 2002).
8. A. T. Koppisch *et al.*, *Biometals*, (May 6, 2008).
9. X. M. Xu, S. G. Moller, *Antioxid Redox Signal* **15**, 271 (Jul 1, 2011).
10. P. Hlavica, M. Lehnerer, *Curr Drug Metab* **11**, 85 (Jan, 2010).

11. D. E. Torres PazmiÃ±o, M. Winkler, A. Glieder, M. W. Fraaije, *Journal of Biotechnology* **146**, 9.
12. DavidÂ W. Mulder *et al.*, *Structure* **19**, 1038.
13. M. Dole, *J Gen Physiol* **49**, Suppl:5 (Sep, 1965).
14. J. Farquhar, A. L. Zerkle, A. Bekker, *Photosynth Res* **107**, 11 (Jan).
15. M. L. Guerinot, *Annu Rev Microbiol* **48**, 743 (1994).
16. M. L. Guerinot, Y. Yi, *Plant Physiol* **104**, 815 (Mar, 1994).
17. C. L. Nobles, A. W. Maresso, *Metallomics* **3**, 788 (Aug, 2011).
18. N. D. Hammer, E. P. Skaar, *Annual Review of Microbiology* **65**, 129.
19. S. Cescau *et al.*, *Biometals* **20**, 603 (2007).
20. E. S. Honsa, M. Fabian, A. M. Cardenas, J. S. Olson, A. W. Maresso, *J Biol Chem* **286**, 33652 (Sep 23).
21. E. S. Honsa, A. W. Maresso, *Biometals* **24**, 533 (Jun).
22. Y. Tarlovsky *et al.*, *J Bacteriol* **192**, 3503 (Jul, 2010).
23. S. Cendrowski, W. MacArthur, P. Hanna, *Mol Microbiol* **51**, 407 (2004).
24. P. E. Carlson Jr *et al.*, *Mol Microbiol* **75**, 900 (2009).
25. J. Jeong, M. L. Guerinot, *Trends in Plant Science* **14**, 280 (2009).
26. C. Ratledge, L. G. Dover, *Annual Review of Microbiology* **54**, 881 (2000).
27. N. C. Andrews, *New England Journal of Medicine* **341**, 1986 (1999).
28. J. Wang, K. Pantopoulos, *Biochem J* **434**, 365 (Mar 15, 2011).
29. A. Roy, A. Kucukural, Y. Zhang, *Nat Protoc* **5**, 725.
30. K. M. Ehrensberger, A. J. Bird, *Trends in Biochemical Sciences* **36**, 524.
31. C. Ratledge, L. G. Dover, *Annu Rev Microbiol* **54**, 881 (2000).
32. C. Wandersman, P. Delepelaire, *Annu Rev Microbiol* **58**, 611 (2004).
33. T. Ganz, E. Nemeth, *Biochimica et Biophysica Acta (BBA) - Molecular Cell Research*.
34. K. Jomova, M. Valko, *Toxicology* **283**, 65.
35. T. A. Bartrand, M. H. Weir, C. N. Haas, *Risk Analysis* **28**, 1115 (2008).
36. A. E. Frankel *et al.*, *Front Biosci* **14**, 4516 (2009).
37. K. Shatalin, E. Shatalina, A. Mironov, E. Nudler, *Science* **334**, 986 (November 18, 2011).

38. R. J. Cybulski *et al.*, *Infection and Immunity* **77**, 274 (January 2009, 2009).
39. K. D. Passalacqua, N. H. Bergman, A. Herring-Palmer, P. Hanna, *Journal of Bacteriology* **188**, 3837 (June 1, 2006, 2006).
40. W. Y. Tu *et al.*, *Journal of Bacteriology* **194**, 932 (March 1, 2012).
41. B. M. Carpenter, J. M. Whitmire, D. S. Merrell, *Infection and Immunity* **77**, 2590 (July 2009, 2009).
42. J. Ollinger, K.-B. Song, H. Antelmann, M. Hecker, J. D. Helmann, *Journal of Bacteriology* **188**, 3664 (May 15, 2006, 2006).
43. A. Gaballa *et al.*, *Proceedings of the National Academy of Sciences* **105**, 11927 (August 19, 2008, 2008).
44. G. T. Smaldone *et al.*, *Journal of Bacteriology*, (March 2, 2012).
45. E. MassÃ©, H. Salvail, G. Desnoyers, M. l. Arguin, *Current Opinion in Microbiology* **10**, 140 (2007).
46. K. D. Passalacqua, N. H. Bergman, J. Y. Lee, D. H. Sherman, P. C. Hanna, *Journal of Bacteriology* **189**, 3996 (June 1, 2007, 2007).
47. S. Pohl *et al.*, *PROTEOMICS* **11**, 3036.
48. J. Y. Lee, K. D. Passalacqua, P. C. Hanna, D. H. Sherman, *PLoS One* **6**, e20777 (2011).
49. P. Cornelis, Q. Wei, S. C. Andrews, T. Vinckx, *Metallomics* **3**, 540.
50. M. K. Wilson, R. J. Abergel, J. E. Arceneaux, K. N. Raymond, B. R. Byers, *Biometals* **23**, 129 (Feb, 2009).
51. S. M. Barry, G. L. Challis, *Curr Opin Chem Biol* **13**, 205 (Apr, 2009).
52. R. C. Hider, X. Kong, *Natural Product Reports* **27**, 637 (2010).
53. M. Miethke, M. A. Marahiel, *Microbiol. Mol. Biol. Rev.* **71**, 413 (September 1, 2007, 2007).
54. D. Oves-Costales, N. Kadi, G. L. Challis, *Chemical Commun (Camb)*, 6530 (2009).
55. K. Hotta, C. Y. Kim, D. T. Fox, A. T. Koppisch, *Microbiology* **156**, 1918 (Jul, 2010).
56. J. L. Meier, M. D. Burkart, *Chemical Society Reviews* **38**, 2012 (2009).
57. A. C. Jones *et al.*, *Natural Product Reports* **27**, 1048 (2010).

58. N. A. Magarvey *et al.*, *ACS Chemical Biology* **1**, 766 (2012/03/17, 2006).
59. R. A. Butcher *et al.*, *Proceedings of the National Academy of Sciences* **104**, 1506 (January 30, 2007, 2007).
60. C. Pelludat, M. Hogardt, J. r. Heesemann, *Infection and Immunity* **70**, 1832 (April 1, 2002, 2002).
61. R. G. Marcela, *Trends in Microbiology* **14**, 320 (2006).
62. P. Nadal Jimenez *et al.*, *Microbiology and Molecular Biology Reviews* **76**, 46 (March 1, 2012).
63. S. Müller, M. Valdebenito, K. Hantke, *Biometals* **22**, 691 (2009).
64. R. J. Abergel, A. M. Zawadzka, T. M. Hoette, K. N. Raymond, *Journal of the American Chemical Society* **131**, 12682 (2012/03/17, 2009).
65. F. Peuckert *et al.*, *Chemistry & Biology* **18**, 907.
66. N. Kadi, G. L. Challis, *Methods Enzymol* **458**, 431 (2009).
67. B. F. Pfleger *et al.*, *Biochemistry* **46**, 4147 (Apr 3, 2007).
68. S. Schmelz *et al.*, *Nat Chem Biol* **5**, 174 (Mar, 2009).
69. H. Y. Kang, T. J. Brickman, F. C. Beaumont, S. K. Armstrong, *Journal of Bacteriology* **178**, 4877 (August 1, 1996, 1996).
70. N. Kadi, D. Oves-Costales, F. Barona-Gomez, G. L. Challis, *Nat Chem Biol* **3**, 652 (Oct, 2007).
71. J. Cheung, F. C. Beasley, S. Liu, G. A. Lajoie, D. E. Heinrichs, *Mol Microbiol* **74**, 594 (2009).
72. A. M. Zawadzka, R. J. Abergel, R. Nichiporuk, U. N. Andersen, K. N. Raymond, *Biochemistry* **48**, 3645 (Apr 28, 2009).
73. A. M. Zawadzka *et al.*, *Proc Natl Acad Sci U S A* **106**, 21854 (Dec 22, 2009).
74. B. Chu *et al.*, *Biometals* **23**, 601.
75. A. L. Davidson, E. Dassa, C. Orelle, J. Chen, *Microbiology and Molecular Biology Reviews* **72**, 317 (June 2008, 2008).
76. A. l. GarÃ©naux, M. l. Caza, C. M. Dozois, *Veterinary Microbiology* **153**, 89.
77. S. D. Dixon, B. K. Janes, P. E. Carlson, Jr., P. C. Hanna, *Mol Microbiol*, (2012).
78. J. Harrington, A. Crumbliss, *Biometals* **22**, 679 (2009).
79. M. Miethke, J. Hou, M. A. Marahiel, *Biochemistry* **50**, 10951 (2012/03/18).

80. B. F. Matzanke, S. AnemÃ¼ller, V. SchÃ¼nemann, A. X. Trautwein, K. Hantke, *Biochemistry* **43**, 1386 (2012/03/18, 2004).
81. C. Ratledge, *Tuberculosis* **84**, 110 (2004).
82. V. TomisÌŒicÌ , S. Blanc, M. Elhabiri, D. Expert, A.-M. Albrecht-Gary, *Inorganic chemistry* **47**, 9419 (2012/03/18, 2008).
83. R. J. Abergel *et al.*, *Proc Natl Acad Sci U S A* **103**, 18499 (December 5, 2006, 2006).
84. M. A. Fischbach, H. Lin, D. R. Liu, C. T. Walsh, *Nat Chem Biol* **2**, 132 (Mar, 2006).
85. R. J. Abergel, E. G. Moore, R. K. Strong, K. N. Raymond, *J Am Chem Soc* **128**, 10998 (Aug 30, 2006).
86. N. Li *et al.*, *Journal of Biological Chemistry* **287**, 8912 (March 16, 2012).
87. D. Oves-Costales *et al.*, *J Am Chem Soc* **129**, 8416 (Jul 11, 2007).
88. D. T. Fox, K. Hotta, C. Y. Kim, A. T. Koppisch, *Biochemistry* **47**, 12251 (Nov 25, 2008).
89. D. Oves-Costales *et al.*, *Chem Commun (Camb)*, 4034 (Sep 14, 2008).
90. B. F. Pfleger *et al.*, *Proc Natl Acad Sci U S A*, (Oct 27, 2008).
91. D. Oves-Costales, L. Song, G. L. Challis, *Chem Commun (Camb)*, 1389 (Mar 21, 2009).
92. G. L. Challis, *Chembiochem* **6**, 601 (Apr, 2005).
93. B. L. Garner, J. E. Arceneaux, B. R. Byers, *Curr Microbiol* **49**, 89 (Aug, 2004).
94. A. T. Koppisch *et al.*, *J Org Chem* **73**, 5759 (Aug 1, 2008).
95. S. C. Andrews, A. K. Robinson, F. Rodriguez-Quinones, *FEMS Microbiol Rev* **27**, 215 (Jun, 2003).

Chapter 2

Structural and Functional Analysis of AsbF: Origin of the Stealth 3,4-Dihydroxybenzoic Acid Subunit for Petrobactin Biosynthesis

2.1 Introduction

Siderophore production in pathogenic bacteria has gained considerable attention due to its crucial function in essential iron uptake by many microbes and the relevance of siderophore-associated proteins as molecular markers of various infectious agents (*1*). Recent genetic and chemical analysis suggests that biosynthesis of the siderophore petrobactin (Fig. 2-1 A) may also be a prerequisite for virulence in related *Bacillus* species (*2*). These studies highlight the importance of elucidating the mechanisms of siderophore production in pathogenic microbes as a target for abrogating infection by organisms like *B. anthracis*, a rapidly virulent microbe with proven potential as a bioterrorism agent. Based on these factors, we have initiated studies to investigate key biosynthetic enzymes for petrobactin assembly in efforts to establish new anti-microbial targets to protect against anthrax. Eliminating petrobactin in pathogenic microbes is particularly important among catecholate siderophores, as the 3,4-DHBA moiety enables the molecule to escape sequestration by the mammalian immune protein siderocalin (*3, 4*). However, the genes responsible for mediating production of this metabolic precursor have remained undefined as has the biochemical mechanism of its assembly.

Biosynthesis of petrobactin in *B. anthracis* requires citrate, spermidine and 3,4-DHBA as biosynthetic units (*5, 6*). While citrate and spermidine are readily available primary metabolites in bacteria, the presence of a 3,4-DHBA in the precursor pool is unusual. Since 3,4-DHBA is critical for petrobactin to function as a virulence factor, we hypothesized that the *asb* operon would likely code for its synthesis. Indeed, it was indicated by earlier reports (*7*), precursor incorporation studies (*8*) and through our own analysis that supernatants of a *B. anthracis* Sterne culture contain 3,4-DHBA. Specifically, we demonstrated that supernatants of an *asbABCDEF* mutant fail to accumulate this key petrobactin subunit, indicating that one or more *asb*-encoded polypeptides are involved in its synthesis. Further examination of supernatants isolated from cultures of individual *asb* deletion mutants (*5*) revealed that each strain is capable of producing 3,4-DHBA except Δ*asbF*. In order to substantiate its functional role, we sought to determine the biochemical function of recombinant AsbF exogenously expressed and purified from *E. coli*. X-ray crystallographic analysis of AsbF provides structural details of this unique polypeptide and has enabled new insights into AsbF enzymatic activity and a proposed mechanism in formation of the 3,4-DHBA moiety essential to petrobactin biosynthesis. Moreover, this study identifies AsbF as a potential new target in efforts to identify inhibitors for development of effective therapeutics against *B. anthracis*, and other pathogens where petrobactin operates as a stealth virulence factor.

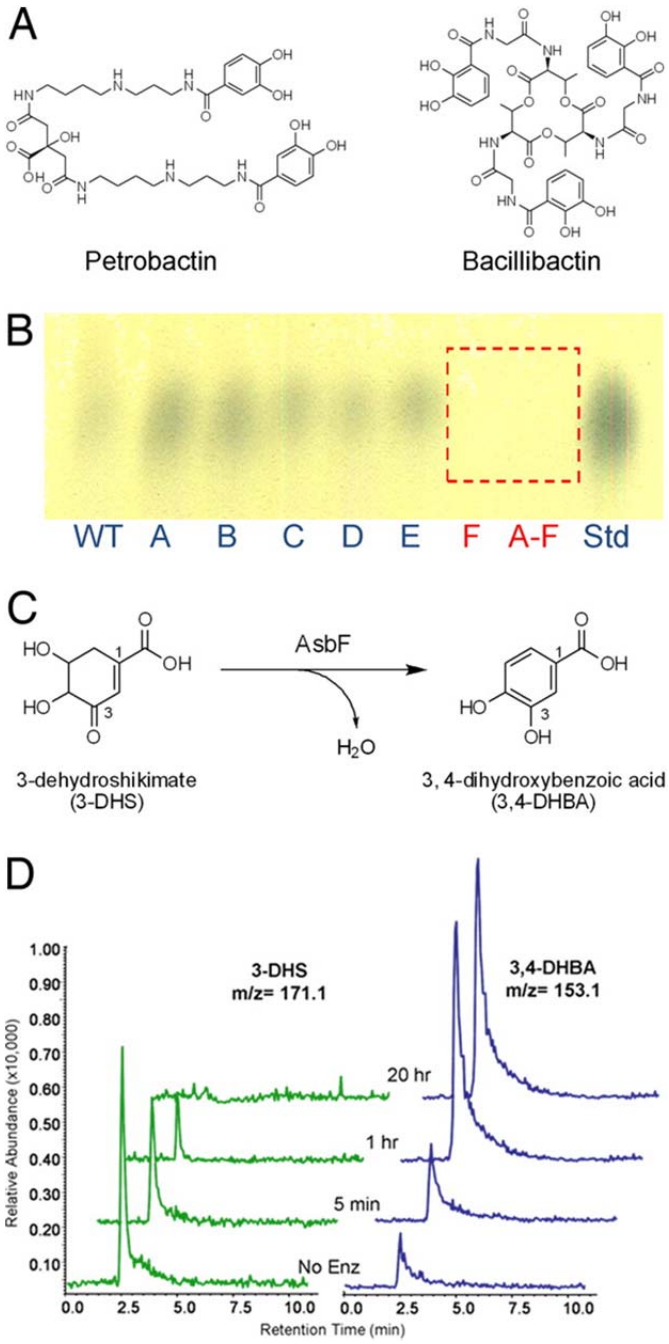

Figure 2-1. AsbF catalyzes dehydration of 3-dehydroshikimate (3-DHS) to 3,4-dihydroxybenzoic acid (3,4-DHBA) in *B. anthracis*. (A) Structures of petrobactin and bacillibactin, two siderophores of *Bacillus anthracis*. (B) TLC analysis of culture supernatants from Δ*asb* mutant strains stained with $FeCl_3$. All strains generated a spot that co-migrated with an authentic 3,4-DHBA standard except Δ*asbABCDEF* and Δ*asbF*. (C) Chemical transformation showing the dehydration of 3-DHS, a common bacterial metabolite, to generate the unique siderophore precursor 3,4-DHBA. (D) LC-MS traces of the AsbF reaction quenched at sequential time points to illustrate conversion of 3-DHS to 3,4-DHBA. *No Enz*: no enzyme control incubated for 20 hours.

2.2 Results and Discussion

The requirement for AsbF is revealed through analysis of B. anthracis mutant strains.

The role of AsbF was initially assessed by determining the level of 3,4-DHBA production from various *B. anthracis* strains, including Δ*asbA*, Δ*asbB*, Δ*asbC*, Δ*asbD*, Δ*asbE*, Δ*asbF*, and Δ*asbABCDEF* (*5*), as well as a wild type Sterne 34F2 that were grown in iron-depleted medium (IDM) (*5*). The presence of 3,4-DHBA was assayed by cellulose plate TLC on organic solvent extracts obtained from filtrates of the IDM cultures of each strain. TLC analysis revealed a single spot corresponding to the iron-chelating compound 3,4-DHBA evident in the extracts of *B. anthracis* Sterne $34F_2$ and the mutants *ΔasbA*, *ΔasbB*, *ΔasbC*, *ΔasbD*, and *ΔasbE* at R_f 0.91-0.93 (Fig. 2-1 B). In contrast, spots corresponding to the subunit were absent in the Δ*asbF* and Δ*asbABCDEF* strains. The ferri-DHBA complex is a strong chromophore, forming blue-colored complexes when sprayed with 1% $FeCl_3$ after TLC development. Extract samples were further analyzed by HPLC using a C18 reverse phase semi-preparative column. The retention time and UV spectrum of the corresponding 3,4-DHBA peaks in each sample were coincident with an authentic standard (data not shown). Peak areas were determined, quantified and compared based on a standard curve constructed by injecting a series of six concentrations (ranging from 0 to 500 μg/ml) of authentic 3,4-DHBA (Supplemental Table 2-S1). Analysis of these *B. anthracis* mutants provided compelling evidence for the function of the BA1986 gene product (AsbF) as the 3,4-DHBA synthase necessary for petrobactin production. Moreover, in a mouse model of inhalation anthrax (*9*), the Δ*asbF* mutant strain was found to be completely avirulent at day 10, whereas the

parental Sterne strain (34F2) resulted in 50% fatality over the same period (Supplemental Fig. 2-S1).

Bioinformatic analysis revealed that the *asb* cluster is conserved in a variety of bacterial genomes, including both Gram-positive and Gram-negative organisms (Supplemental 2-S2 A). Interestingly, these microbes do not share a common niche; they are found in diverse environments with marine species dominating. The significance of this trend is unclear as it is difficult to assess how widespread petrobactin synthesis is within marine bacterial genomes. However, the relative phylogenetic diversity of bacteria bearing an *asb*-type operon (Supplemental Fig. 2-S2 B) together with evidence that these gene clusters appear to have been acquired long ago (they have diverged considerably in sequence, and each has assumed the global sequence characteristics of its host genomes), suggests that petrobactin may confer a competitive advantage in iron acquisition within the ocean environment as well. We expect that as the number of sequenced bacterial genomes increases, the evolutionary history of the *asb* cluster will become clearer, and clues to the significance of petrobactin in various habitats will emerge.

AsbF is responsible for conversion of 3-dehydroshikimate to 3,4-DHBA.

To guide our initial studies of AsbF catalytic activity, bioinformatic analyses were conducted to identify potential functional homologs and to suggest reaction substrates. However, these efforts revealed only sequence similarity to conserved proteins of unknown function or irrelevant catalytic properties (data not shown). Alternatively, a search of the biochemical pathway databases revealed several anabolic processes leading to assembly of 3,4-DHBA, in addition to the many well studied catabolic pathways. In

some bacteria (exemplified by *Pseudomonas putida* PobA), 3,4-DHBA is generated by hydroxylation of 4-hydroxybenzoic acid (4-HBA) in order to utilize the substrate as a carbon source (*10*). However, reaction of purified AsbF with 4-HBA and NAD(P)H failed to yield 3,4-DHBA (data not shown).

We considered an alternative metabolic process found in *Neurospora crassa* (*qa-4*), *Aspergillus nidulans* (*qutC*), and *Klebsiella pneumoniae* (*aroZ*) where 3,4-DHBA is generated by dehydration of 3-dehydroshikimate (3-DHS), a shikimate pathway intermediate, in order to utilize aromatic compounds as a carbon source (Fig. 2-1 C) (*11-13*). A reaction mixture including AsbF with 3-DHS (purified from cultures of recombinant *E. coli* (*14*)), resulted in a product bearing a new absorbance maximum at 290 nm that corresponded to a DHBA chromophore (Supplemental Fig. 2-S3 A). Upon analysis by LC-MS in negative SIM mode, the same reaction mixture resulted in disappearance of 3-DHS (m/z = 171), and generation of a product consistent with the structure of 3,4-DHBA (m/z = 153) (Fig. 2-1 D). Both starting material and product eluted from a C18 reverse phase column with retention times identical to authentic standards (data not shown).

Enzymatic Characterization.

With a clear catalytic role for AsbF identified as a 3-dehydroshikimate dehydratase, we next sought to determine the efficiency of the AsbF-catalyzed 3-DHS dehydration (3,4-DHBA production) reaction. The reaction rate at room temperature increased monotonically with increasing pH (from 6.0 to 9.2) with a plateau between 7.2 and 8.0 (Supplemental Fig. 2-S3 B). Earlier studies of a fungal 3-DHS dehydratase suggested a requirement for divalent cations (*12, 13*). Significantly, the AsbF catalyzed dehydration

reaction was inhibited at EDTA concentrations above 0.1 mM. Supplementation of this experimental reaction mixture with 5 mM $MgCl_2$ restored activity. Following this observation, a suite of metals was titrated into reactions containing AsbF inactivated by EDTA. While a series of divalent cations including cobalt, calcium, and magnesium reactivated the enzyme, manganese was found to maximize catalytic efficiency while equal concentrations of zinc completely abrogated it. In conjunction with these biochemical findings, a fluorescent scan of crystallized recombinant AsbF showed manganese to be the predominant enzyme-bound metal (data not shown, see below). Similar dependencies, in which manganese is the preferred metal and zinc is inhibitory, are found among a structural class of sugar isomerases (*15*).

Kinetic parameters for AsbF at pH 7.5 were determined spectrophotometrically. Recorded initial velocities were fit to a Michaelis-Menten curve demonstrating the enzyme to have a K_m ~ 290 μM and k_{cat} ~80 min^{-1}. The Km value is on a similar order of magnitude to those reported by groups describing fungal dehydroshikimate dehydratases from *N. crassa* (590 μM) (*12*) and *A. nidulans* (530 μM) (*13*).

Structural Characterization of AsbF Bound to its Product 3,4-DHBA.

Due to the lack of sequence similarity to known 3-DHS dehydratases, we sought the crystal structure of AsbF and to explore a potential reaction mechanism based on these insights. The structure of AsbF adopts a $(\beta/\alpha)_8$-barrel (TIM barrel) configuration (Fig. 2-2 A). As expected from a prior TEV protease cleavage experiment (Materials and Methods), the N-terminus of the structure is partially buried at the bottom part of the barrel while the C-terminus is completely exposed to the solvent channel. With the His_6-tag in place, the C-termini could be involved in lattice interactions with neighboring

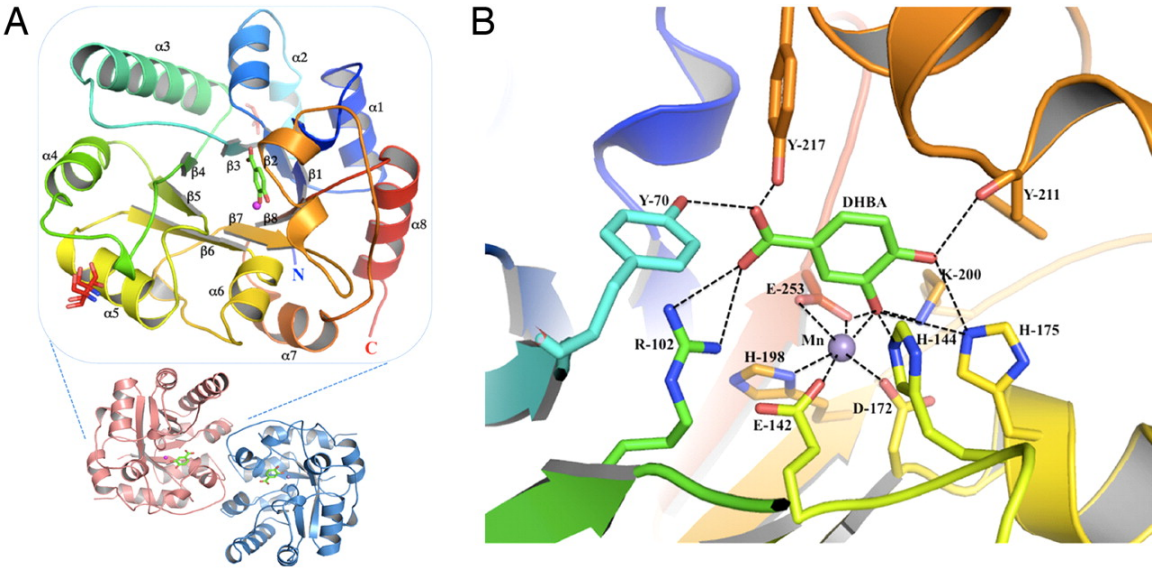

Figure 2-2. Structural analysis of AsbF. (A) Crystal structure form of AsbF. Overall view of the AsbF monomer is enlarged and rotated 90° relative to the dimeric structure below. Monomer is depicted with a color ramp of blue to red (amino to carboxyl terminus). The manganese atom is shown as a purple sphere in the middle of the TIM barrel adjacent to the ligand molecule 3,4-DHBA (green). Numbering of main TIM barrel secondary structures is shown as α1-8 and β1-8. (B) Active site of liganded AsbF showing 3,4-DHBA coordinated to manganese interacting with side chains. Manganese is coordinated with four carboxyl group oxygen atoms from two glutamate residues and an aspartate as well as an amine of His ranging in distance between 2.08 to 2.38 Å. All hydrogen bonds are indicated in dashed lines.

protein molecules, which might have led to twinning.

AsbF belongs to AP endonuclease 2 TIM barrel proteins (*16*) with the closest homologues including xylose isomerase and the myo-inositol catabolism protein IolI (*17*). The internal section of AsbF is well packed by relatively large side chains with a narrow bottom part of the barrel relative to the top. The barrel opens up at the top to form a pocket with a number of hydrophilic residues including His, Glu, Thr, Lys, Tyr, and Gln to contain a specific ligand. Unexpectedly, the 3,4-DHBA reaction product was found in the active/binding site of AsbF, surrounded by several aromatic amino acid residues including F255, F211, F104, H144 and Y217. The 3,4-DHBA molecule makes direct contacts with hydroxyl groups of Y70 and Y217, a guanidinium of R102, an amine of K200, an imine of H175, a carboxyl of E253, and the main chain carbonyl of F211 using mainly hydrogen bonding interactions. Moreover, 3,4-DHBA is capped tightly under the helical loop (residues 206 – 224) located between the seventh β-strand (β7) and the seventh α-helix (α7), and is directly coordinated with a Mn^{2+} ion that is also found in the structure (Fig. 2-2 A). Both 3,4-DHBA and a metal ion were evident from the electron density map calculation using experimental phases with the weighted coefficient (Fw). Metal identity was determined from the specific emission peak during the fluorescence spectrum scan. Inspection of the AsbF structure reveals that Mn^{2+} is coordinated with the carboxylic acid side chains of E142, D172, E253 (both oxygen atoms), the deprotonated imine of H198, and the 3-hydroxy group of 3,4-DHBA, with the distance range of 2.08 – 2.38 Å that is typical of Mn^{2+} ions (Fig. 2-2 B) (*18*). Although there is only one AsbF protein molecule in the asymmetric unit, they apparently form a dimer (Fig. 2-2 A) that excludes 2460 Å of surface area according to PISA (*19*).

Analysis by static light scattering and size exclusion chromatography also supports a dimeric state of the enzyme in solution (data not shown).

Structural comparisons revealed that AsbF can be reasonably well superimposed with the 3-dehydroquinate dehydratase (DHQ) from *Salmonella typhimurium* (1qfe) (Supplemental Fig. 2-S4 A), an enzyme that functions as part of the shikimate pathway for biosynthesis of aromatic compounds (*16*). Indeed the AsbF structure is generally homologous to this type of dehydratase enzyme comprised of a TIM barrel fold with a few variations, including the lid loop located at the top of the pocket. For AsbF, this lid loop extends from residue 202 – 227 as the partly α-helical loop between strands β7 and α7. In contrast, for the enzyme DHQ it comes from the loop between β3 and α3 spanning residues 82 - 93 covering approximately the opposite side of the pocket mouth. Another important difference in DHQ is an additional small β ribbon at the C-terminus that closes the bottom of the β-barrel. Each ligand in its corresponding binding pocket occupies a different location and orientation (Supplemental Fig. 2-S4 A). One of the key distinctions between TIM barrel enzymes is the location of metal binding sites and the type of metal involved. The AsbF manganese ion is bound to six atoms, including one from 3,4-DHBA and five amino acid residues that may also contribute to catalysis by stabilizing an intermediate ligand and/or a product ligand differing from other dehydratases, particularly DHQ (such as 1qfe) that does not contain a metal cofactor (*16*).

Proposed Mechanism for AsbF Dehydratase.

With the crystal structure as a guide, we employed site-directed mutagenesis to probe further the key amino acid residues involved in catalysis of AsbF. This analysis

Mutant	K_m, μM	k_{cat}, min^{-1}	% activity
WT	288.72 ± 38.93	79.84 ± 0.96	100
K200E	—	—	Inactive
K200A	—	—	Inactive
K200R	30.25 ± 8.48	2.56 ± 0.05	3.2
H144A	—	—	Inactive
H175A	—	<1	Trace
R102A	—	—	Inactive
Y70A,Y217A	≈2,511	48.35 ± 3.82	60.6

Table 2-1. Kinetic parameters for AsbF mutants. Site directed mutagenesis was performed on BA 1986 (*asbF*) to probe for residues involved in catalysis. The K_m of WT AsbF is comparable to two eukaryotic 3-DHS dehydratases. Inactive mutants are presumably disrupted in coordination of the metal or substrate. Replacement of Y70 and Y217 is likely to expose the active site to solvent and reduce substrate specificity while loss of the proposed catalytic H144 renders the enzyme inactive.

revealed that a K200R mutant form of the protein was partially active, confirming the lack of a covalent imine intermediate shown to occur in structurally similar DHQs (19). Characterization of additional AsbF site-directed mutants demonstrated (Table 1) that most inactive forms of the enzyme lacked residues believed to be crucial for metal or substrate coordination ascertained through inspection of the 3,4-DHBA orientation within the AsbF crystal structure (Fig. 2-2 B).

Based on the crystal structure and mutant analysis, the surrounding amino acid residues comprising the putative AsbF active site suggest an E_1CB (elimination unimolecular via conjugate base) mechanism that requires a base to abstract the axial proton from the adjacent aliphatic carbon atom (C4) of 3-DHS (Fig. 2-3). In the AsbF structure, H144 is orthogonal to the catechol ring of the 3,4-DHBA product, an ideal position for removal the C4 axial proton (the hydroxyl is equatorial) of the substrate. H144 and E142 are both well conserved among members of the xylose isomerase family (Supplemental Fig. 2-S5). The nearby E142 could elevate basicity of H144 by forming a hydrogen bond to NE2 of H144, improving its proton abstraction ability. Histidine functions as a base for initial proton removal during many enzymatic reactions, including some type I 3-dehydroquinate dehydratases (*20, 21*). Furthermore, while the activity of a H175A mutant is attenuated, the adjacent AsbF H144A mutant is completely inactive. Proton removal from the C4 position of 3-DHS leads to formation of a non-covalently bound enolate intermediate with the resulting negative charge stabilized by the divalent Mn^{2+} cation.

To assess enolate formation as a first step in conversion of 3-DHS to 3,4-DHBA, we conducted a deuterium labeling experiment using the AsbF reaction in D_2O buffer. Rapid

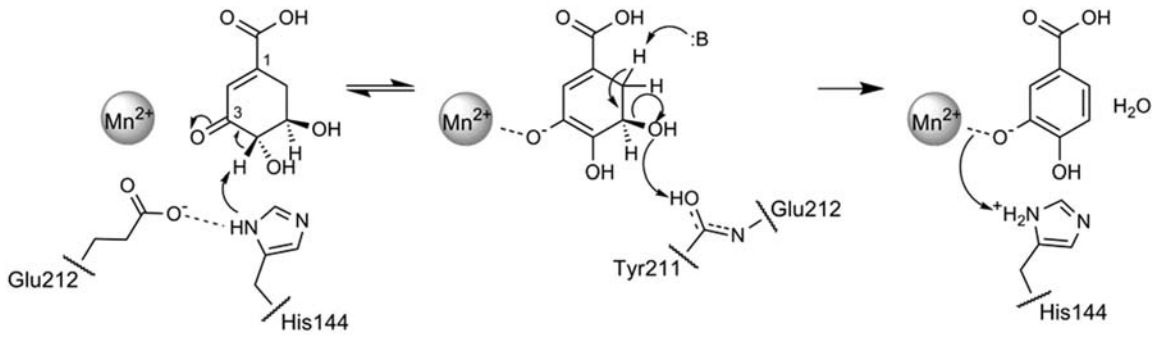

Figure 2-3. Proposed mechanism for AsbF-catalyzed conversion of 3-DHS to 3,4-DHBA. Mn^{2+} stabilizes an enolate intermediate after proton removal at C4 by H144. This is followed by dehydration/aromatization of the molecule to generate the key petrobactin subunit 3,4-DHBA.

and reversible exchange of deuterium from the conversion of C3 keto to enol (Fig. 2-3) was expected to result in accumulation of the substrate bearing a one mass unit increase detectable by FT ICR MS. This rapid exchange was readily detectable (Supplemental Fig. 2-S6) supporting the proposed mechanistic hypothesis regarding initial formation of the 3-DHS enolate upon substrate binding to AsbF.

In a second, more rapid step of the reaction, dehydration presumably occurs through a general acid-catalyzed elimination of the C5 hydroxyl and product formation following aromatization (Fig. 2-3). The most likely candidate for the acid-catalyzed removal of the C5 hydroxyl is the main chain carbonyl of Y211 located at the C-terminus of the short α-helix as a part of the helical loop between β7 and α7 capping the binding pocket. A main chain carbonyl is generally not a good acid, but the main chain carbonyl of Y211 is the closest to C5 and its acidity is likely to be elevated by positioning at the C-terminus of the α-helix (with partial negative charge from the helix dipole) that includes conserved amino acid residues among the family (Fig. 2-2 B).

To understand further the role of specific active site residues in catalysis, we modeled 3-DHS in place of the 3,4-DHBA in AsbF (Supplemental Fig. 2-S4 B). This motivated analysis of Y217 and Y70 that were initially believed to be necessary for excluding solvent from the active site. Both were found to be inconsequential for normal enzymatic function when mutated individually, and only reduced activity by 40% when the corresponding double Tyr mutation was constructed (Table 1). Unexpectedly, an R102A mutation completely inactivates AsbF indicating its role in maintaining a proper active site conformation, while substitution of K200 for arginine significantly reduces substrate binding and overall catalytic efficiency.

Elucidation of the AsbF Structure and Function is Important to Understanding Siderophore Biosynthesis of B. anthracis.

Recently, other pathogenic *Bacillus* sp. were found to produce petrobactin (*2*), while the ability for uptake and utilization of exogenous petrobactin is even more widespread among prokaryotes (*22*). Moreover, some evidence suggests that the siderophore or its analogs play additional biological roles beyond iron sequestration (*23-25*). Though we have now characterized the enzymatic activity of AsbF as well as its role in iron acquisition, the complete nature of the enzyme within bacteria has yet to be fully understood. Indeed research on other members of the *asb* gene cluster suggests a pool of 3,4-DHBA, and thus functioning AsbF, is necessary for the initial steps of petrobactin biosynthesis (*5, 6*).

The acquisition of the *asb* gene cluster by *Bacillus* exemplifies evolution of a pathogen to adapt to adverse conditions established by its host (in this case, iron availability). AsbF itself, with its metal coordination structure reminiscent of other proteins, most likely evolved from enzymatic precursors with a purpose very different from siderophore biosynthesis. The presence of the unusual 3,4 isomer of DHBA in petrobactin is vital to its ability to acquire iron for the bacterium while avoiding detection by innate host defenses. Without petrobactin, *B. anthracis* would be limited to the ability of bacillibactin to compete for free iron, a process that is highly compromised due to siderocalin sequestration (*3*). Since the generation of 3,4-DHBA is a key step for petrobactin biosynthesis (*6*), AsbF represents an attractive target for small molecule antibiotic therapy. In addition to the prevention of petrobactin assembly, disrupting AsbF function would thwart uptake of any iron bound by 3,4-DHBA subunits that may be

exported out of the cell (*6*). This approach is supported by the fact that *B. anthracis* cells carrying an *asbF* gene deletion grow significantly more poorly in iron depleted media (*5*) and display a highly attenuated lethality to mice (Supplemental Fig. 2-S1). The search for AsbF inhibitors with possible therapeutic application is already underway. Questions regarding how AsbF is regulated and the precise timing and order of 3,4-DHBA incorporation into petrobactin will be addressed in future studies. This research will serve to further articulate how even insidious microbes are fundamentally reliant on finding a method to surpass innate immune defenses in the acquisition of nutrients, and likely uncover innovative strategies for combating life-threatening infections.

2.3 Material and Methods

Analysis of Sterne Strain Mutants. *B. anthracis asb* mutant strains, Δ*asbA*, Δ*asbB*, Δ*asbC*, Δ*asbD*, Δ*asbE*, Δ*asbF*, and Δ*asbABCDEF* (*5*) as well as a wild type Sterne 34F2 were generated as described previously and grown in iron-depleted medium (IDM (*5*)). Filtrates (100 ml) of the growth medium were prepared as described previously (*5*). Sample preparation for TLC analysis and quantification of 3,4-DHBA was performed by extracting acidified (pH 2.0) IDM culture supernatants (10 ml) with an equal volume of ethyl acetate three times. The organic layers were pooled and the solvents were concentrated to dryness *in vacuo*. The dried pellets were dissolved in 50 µl of methanol and used for analysis. Thin-layer chromatography (TLC) was performed with the extracts on a cellulose plate (Merck). TLC plates were developed with a solvent system of butanol-acetic acid-water (12:3:5, v/v/v), and 3,4-DHBA was detected by spraying with 1% (w/v) ferric chloride.

For quantification of 3,4-DHBA (Table 2-S1), samples were analyzed by HPLC. Analytical results and detailed methods are available following Table 2-S1 in section 2.4 of this chapter.

Intratracheal Inoculation of DBA/2 Mice. Mouse infection was performed as described previously (*9*). All mouse experiments were performed using protocols approved by the University of Michigan Committee on the Use and Care of Animals.

Cloning and DNA Manipulation. The *asbF* gene of *B. anthracis* Sterne strain was cloned into the expression vector pMCSG7 (29) using ligation independent cloning (LIC) (*26*). Detailed cloning and mutagenesis methods are available as supplemental methods in section 2.4 of this chapter.

Bioinformatic Analysis. Bioinformatic analyses of the *B. anthracis asb* cluster and homologs were performed using tools implemented within the Integrated Microbial Genomes website (http://img.jgi.doe.gov), and the EMBL-EBI website (http://www.ebi.ac.uk/).

Protein Purification for Enzymatic Analysis. All pMCSG7-*asbF* constructs were subsequently used to transform BL21 expression cells (Novagen). The enzyme was purified using standard His-tag Ni-affinity chromatography. Detailed protein purification methods are available as supplemental methods in section 2.4 of this chapter.

Enzymatic Assays. Initial substrate determination assays were performed with 75 mM HEPES pH 7.5, 100 mM substrate (3-DHS), and 1 µM enzyme. 50 µl reactions were tracked spectrophotometrically by observing ΔA_{290} using a SpectraMax M5 plate reader (Molecular Devices). Standard serial dilutions of synthesized 3,4-DHBA (Fluka) in similar reaction conditions were used to quantify product yield. LC-MS analysis of

substrate to product conversion was performed by addition of nine reaction volumes of methanol followed by evaporation of the resulting supernatant and loading onto a 3.5 µm C18 reverse-phase column (Waters) in-line with a Shimadzu LCMS-2010A for detection. Elution was performed with a stepwise 5-70% gradient of MeCN in 20 mM aqueous NH_4HCO_3. Changes to reaction conditions were performed as noted in the text. Characterization of kinetic parameters was performed with 75 mM HEPES pH 7.5, 250 nM enzyme, and varying concentrations (0 - 2 mM) 3-DHS in 80 µl reactions. Both substrate and enzyme were equilibrated in reaction buffer at ambient temperature for 15 minutes before the reaction was initiated by mixing. 3,4-DHBA production was tracked by observing ΔA_{290} using a Flexstation III plate reader (Molecular Devices). Reactions were run in quadruplicate and nonlinear regression using Kaleidagraph software (Synergy) was performed on a plot of V_0 vs [3-DHS] for determination of K_m and V_{max}.

Gene Cloning, Expression and Protein Purification for Structure Determination. After failing to obtain diffraction quality crystals from the initial pMCSG7-*asbF* construct, *asbF* was cloned in pMCSG26 vectors with two variations, including an un-cleavable C-terminal His_6-tag and a C-terminal His_6-tag with a TEV protease cleavage site.Recombinant *E. coli* cells for AsbF overexpression were grown using selenomethionine (Se-Met)-containing enriched M9 medium (pink medium) under conditions known to inhibit methionine biosynthesis (*27, 28*). Protein was purified by two-step Ni-affinity chromatography following the standard protocol described previously (*29*). Detailed cloning, overexpression, and purification methods are available as supplemental methods in section 2.4 of this chapter.

Protein Crystallization. Crystallization screening was executed for all AsbF protein variants, including the one bearing an N-terminal His_6-tag (expressed from pMCSG7) and the ones from pMCSG26 vectors with and without the C-terminal His_6-tag cleavage. They were screened for crystallization conditions using a Mosquito robot (TTP Labtech) using sitting drops in 96-well plates (Greiner), with drops of 0.4 µl of protein at 60 mg/ml mixed with 0.4 µl of crystallization screen solutions and equilibrated over 135 µl of crystallization screen solutions in the well at 18^{o}C. A number of commercially available screens including Index (Hampton Research) and ANL-1 and ANL-2 (Qiagen) were used for crystallization screening. AsbF with N-terminal His_6-tag failed to yield a diffraction quality crystal. The best crystals of AsbF without the TEV cleavage site appeared after 1 - 2 days from Index #25 containing 3.5M sodium formate pH 7.0. The same condition and a few others including ANL-2 #88 and #89 gave diffraction quality crystals for the AsbF without the C-terminal His_6-tag. Prior to data collection crystals were flash-frozen in liquid nitrogen in the presence of a number of different cryo-protectants. The chunky plate-shape of a 0.15 mm side crystal of the AsbF with the C-terminal tag diffracted to 2.0 Å. However, the data were twinned and the phasing stalled. One of the rod shape crystals of AsbF lacking a His_6-tag from condition ANL-2 #89 (0.1M Tris pH 8.5; 3.2M sodium chloride) with the saturated sucrose cryo-protectant diffracted to 2.12 Å and was used for data collection.

Data Collection, Structure Determination, Refinement and Deposition. The single wavelength anomalous dispersion (SAD) data near the Se absorption edge (0.9793Å) up to 2.12 Å were collected from a single Se-Met labeled rod shape protein (30 * 30 * 300 µm) crystal at 100º K at the 19ID beam line of the Structural Biology Center at the

Advanced Photon Source, Argonne National Laboratory. The crystal was exposed for 5 sec. per 1.0° rotation of ω with the crystal to detector distance of 320 mm. The data were recorded on ADSC Q315 detector by the scanning of 200º. The space group was $P6_522$ with cell dimension of $a = b = 134.48$ Å $c = 72.81$ Å. All data were processed and scaled with HKL3000 (*30*) (Table 2).

The structure was determined by SAD phasing utilizing the anomalous signal from Se atoms with HKL3000 (*30*), SHELX (31), SOLVE/RESOLVE (*32*), MLPHARE (*33*), DM (*34*), CCP4 (*35*) and arp/Warp (*36*) using the peak data to 2.12 Å. The model from HKL3000, after the high resolution model building routine by arp/Warp contained most of the residues with side chains except four N-terminal residues, seven C-terminal residues and all artificial residues from cloning. The extra electron density for the 3,4-DHBA was evident from the electron density map calculated from the experimental phases. The subsequent refinement was performed iteratively by REFMAC 5.2 (*37*) in CCP4 and manual adjustment using Coot (*38*) until it converged to the R factor of 0.148, and the free R of 0.178 with the rms bond distances of 0.017 and the rms bond angles of 1.47º. The final model included residues 1 - 274 of one chain of AsbF, one molecule of 3,4-DHBA, a Mn ion, a disordered Tris, a glycerol molecule, and 320 ordered water molecules. The C-terminus residues including those introduced during cloning could not be resolved. The stereochemistry of the structure was checked with PROCHECK (*39*) and the Ramachandran plot. Atomic coordinates and experimental structure factors of AsbF have been deposited in PDB under the code 3DX5.

Data Collection (anomalous peak)	
Wavelength, Å	0.9793
Resolution (last shell), Å	49.4 to 2.11 (2.19 to 2.11)
Reflections measured/unique	22,726/2,210
Multiplicity	13.9 (12.3)
Completeness (last shell), %	99.9 (99.4)
R sym (last shell), %*	14.4 (53.4)
I/σ (last shell)	9.1 (7.1)
Phasing	
Resolution, Å	49.4 to 2.12
Phasing power	1.06
Figure of merit	0.112
After density modification	0.801
Refinement	
Resolution, Å	49.4 to 2.12
R work/R free†	14.8/17.8
rms deviation bond lengths, Å	0.017
rms deviation bond angles, Å	1.47
PDB code	3DX5

Table 2-2. AsbF data collection, phasing and refinement. * $R_{sym} = \Sigma\Sigma j|Ij - \langle I\rangle|/\Sigma Ij$, where Ij is the intensity measurement for reflection j, and <I> is the mean intensity for multiply recorded reflections. † $R_{work}/R_{free} = \Sigma||F_{obs}| - |F_{calc}||/|F_{obs}|$, where the working and free R factors are calculated by using the working and free reflections sets. The free reflections (5% of the total) were held aside throughout refinement.

2.4 Supplemental

Preparation of AsbF for Enzymatic Assays: The *asbF* gene of *B. anthracis* Sterne strain was cloned into the expression vector pMCSG7 (Midwest Center for Structural Genomics) using ligation independent cloning (LIC) (*26*). The pMCSG7 vector, bearing a TEV protease cleavage site, creates a construct with a cleavable His_6-tag fused into the N-terminus of the target protein with three artificial residues (SerAsnAla). Site-directed mutagenesis was performed on this construct in modification of a StrataGene QuickChange protocol: Primers containing the desired mutation were kept at a constant concentration while varying amounts of template DNA were titrated. 10 U Phusion DNA polymerase (Finnzymes) was used per 50 µl reaction. Reactions shown by gel electrophoresis to contain amplified vector were incubated with 10 U DpnI (New England Biolabs) for 2 hours to remove template and used to transform chemically competent XL1-Blue cells for amplification. All DNA manipulation was confirmed by DNA sequencing.

All pMCSG7-*asbF* constructs were transformed into Z-competent (Zymo Research) BL21 expression cells (Novagen). An overnight LB starter culture was used to inoculate 1 L (or in the case of point mutants, 250 ml) of Terrific Broth (TB) medium and shaken at 190 rpm at 37°C until an OD_{600} of ~1 was reached. Cultures were cooled to 18°C over the course of an hour and induced with 250 µm IPTG for incubation overnight. Resulting cell pellets were resuspended in 5 ml of lysis buffer (20 mM HEPES pH 8.0, 300 mM NaCl, 20 mM imidazole, 1 mM DTT, 10% glycerol) per gram of pellet and lysed by sonication. Soluble lysate was incubated with pre-equilibrated Ni-NTA resin (Qiagen) for 3 hours at 4°C, poured through a glass column, washed with 6x the lysate volume of lysis buffer, and eluted with an imidazole solution (20 mM HEPES pH 8.0,

300 mM NaCl, 300 mM imidazole, 1 mM DTT, 10% glycerol) into 1 ml fractions. The expected mass of 35 kDa was observed for the isolated His-tagged fusion-protein (below). Eluted fractions shown to contain enzyme and a minimal amount of contaminants were pooled, concentrated, and buffer exchanged in an Amicon Ultra 30 kDa MW cutoff filter (Millipore) with 20 mM HEPES pH 8.0, 20 mM NaCl, 1 mM DTT, 10% glycerol. Protein concentration was determined using A_{280} and Bradford assay, then preparations were flash-frozen in liquid nitrogen and stored at -80°C.

Preparation of AsbF for Crystallization: After failing to obtain diffraction quality crystals with the initial pMCSG7-*asbF* construct, *asbF* was cloned in pMCSG26 vector with two variations, including an un-cleavable C-terminal His_6-tag and a C-terminal His_6-tag with a TEV protease cleavage site. The *asbF* gene was overexpressed in *E. coli* BL21 (DE3) - Gold (Stratagene) harboring an extra plasmid encoding three rare tRNAs (AGG and AGA for Arg, ATA for Ile).

Cell cultures were grown at 37°C to an OD_{600} of ~0.95 then cooled down before adding Se-Met and 0.5 mM isopropyl β-D-1-thiogalactopyranoside (IPTG) to induce, and maintained at 18°C overnight. The harvested cells were lysed by sonication in the presence of 1 mg/ml of lysozyme and a protease inhibitor cocktail tablet (Complete, Roche) in 35 ml of lysis buffer containing 50 mM HEPES pH 8.0, 500 mM NaCl, 10 mM imidazole, 10 mM β-mercaptoethanol, and 5% v/v glycerol. The lysate was clarified by centrifugation at 30,000 x g (RC5C-Plus centrifuge, Sorval) for 75 min, followed by filtration through a 0.45 μm filter (Gelman) before loading onto a 5 ml Ni-Histrap column (GE Healthcare) for purification.

Protein was purified by two-step Ni-affinity chromatography following the standard protocol described previously (*29*). Immobilized metal affinity chromatography (IMAC-I) was conducted using a 5-ml HiTrap Chelating HP column charged with Ni^{2+} ions and buffer-exchange chromatography on a HiPrep 26/10 desalting column (GE Healthcare) on *ÄKTAxpress™* (GE Healthcare). Both AsbF expressed from the pMCSG26 vector with a TEV cleavage site and the protein with an N-terminal His_6-tag that could not be cleaved were dialyzed in crystallization buffer (20 mM HEPES pH 8.0, 250 mM NaCl, 2mM DTT) and concentrated to 82 mg/ml using an Amicon Ultra centrifugal filter device (Millipore). For AsbF expressed from pMCSG26 vector with a TEV cleavage site, the His_6-tag was removed using recombinant TEV protease (a gift from Dr. D. Waugh, NCI) in a 1:30 ratio by incubating at 4°C for 72 hours. The TEV protease cleavage left six artificial residues (ENLYFQ) remaining at the C-terminus. The AsbF protein was then further purified by a 5 ml manually packed Ni-superflow affinity column (GE Healthcare). The protein eluted as a flow-through from the column in lysis buffer with 20mM imidazole, was dialyzed in crystallization buffer containing 20 mM HEPES pH 8.0, 250 mM NaCl, 2mM DTT, and concentrated to 85 mg/ml using an Amicon Ultra centrifugal filter device (Millipore).

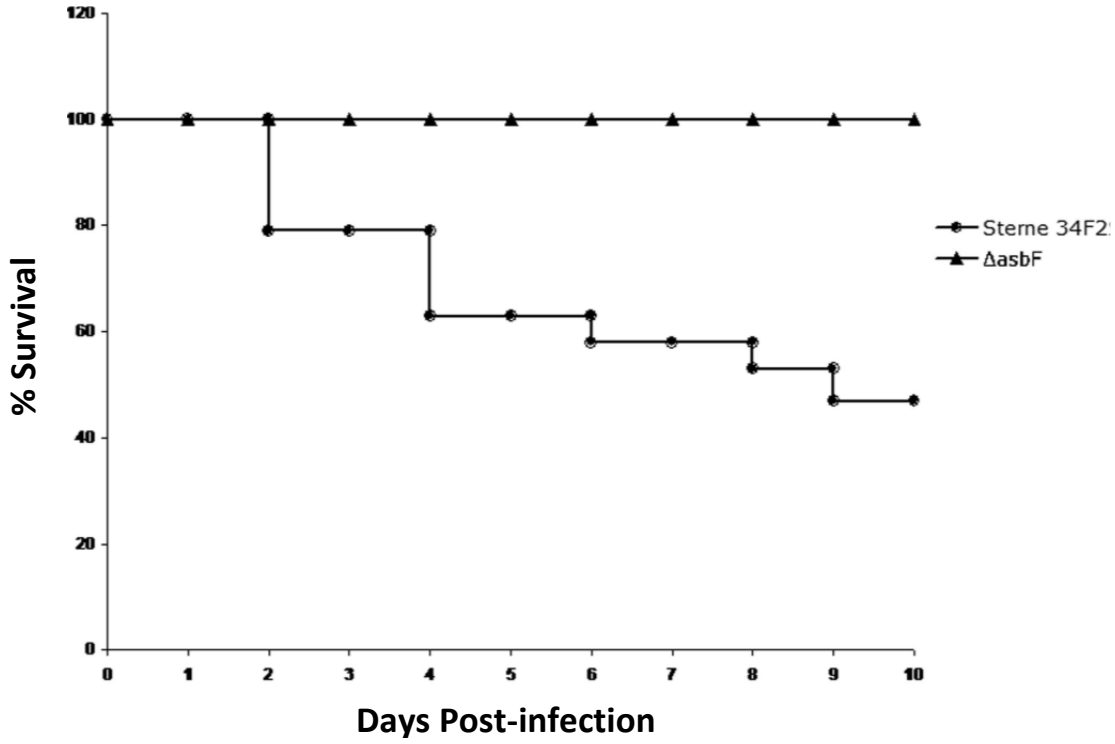

Figure 2-S1. Attenuation of virulence of the Δ*asbF* mutant of *B. anthracis* in mice. DBA/2 mice were inoculated with ~ 1 X 10^4 spores of either the parental (Sterne 34F2) or mutant (Δ*asbF*) strain of *B. anthracis* via intratracheal injection. The group sizes were 19 mice (Sterne 34F2) and 20 mice (Δ*asbF*) respectively.

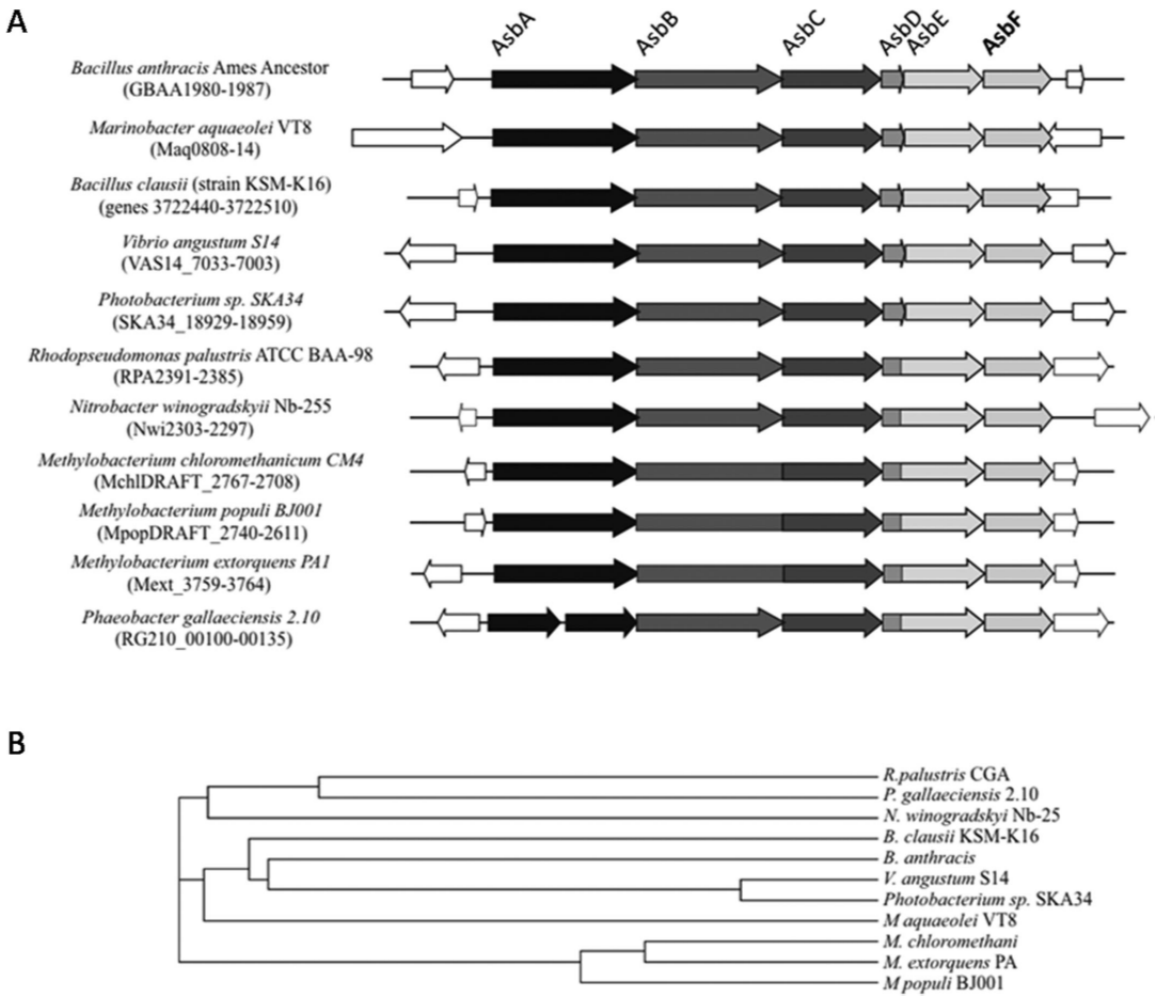

Figure 2-S2. Conservation of AsbF among diverse prokaryotes. (A) Synteny between the *B. anthracis asb* cluster and homologous clusters from other species. The translated *B. anthracis asb* locus (GBAA1981-6, corresponding to *asbA-F*) is shaded and shown at top, and the corresponding translated loci from each homologous cluster are shown beneath and shaded to reflect homology with AsbA-F. There is no similarity between genes that are not shaded. (B) A cladogram showing the evolutionary relationship (most likely branching order) between AsbF and homologs found in other bacterial genomes. The tree shown was constructed using the ClustalW server at EBI.

Further sequence comparison of putative *asb* gene products can be found in the Appendix of this dissertation.

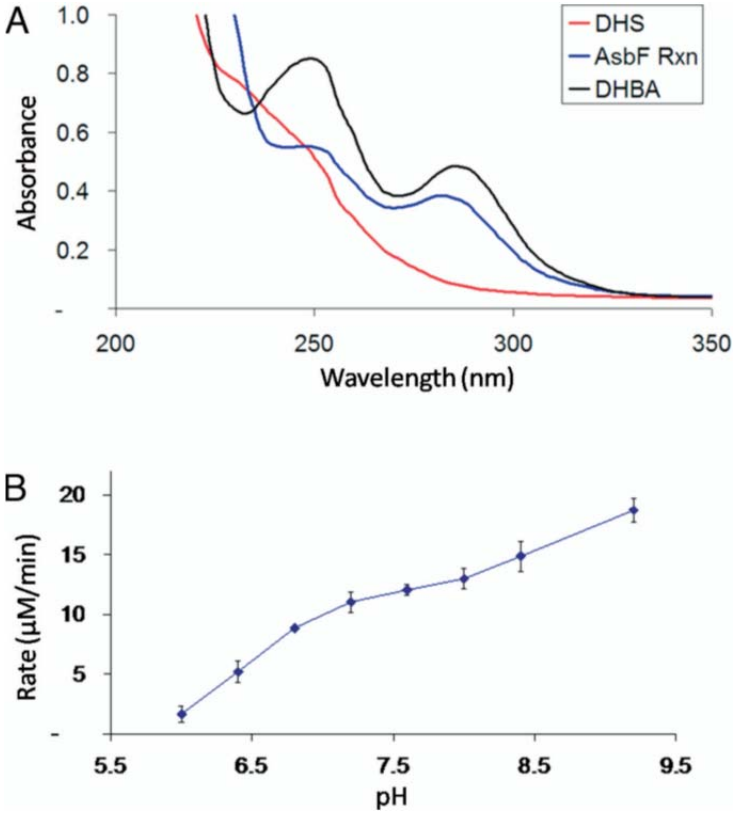

Figure 2-S3. Detecting AsbF activity. (A) Absorbance spectrum of (—) DHS, (—) DHBA, and (—) AsbF reaction. 3,4-DHBA is highly absorptive at 290 nm while in relation, the 3-DHS substrate and His_6-AsbF enzyme is not. AsbF reaction progression is observed by monitoring at this wavelength. Conditions for the AsbF reaction follow those described in Materials and Methods; (B) Dependence of the dehydration reaction on pH at 100 mM 3-DHS, 75 mM HEPES, 5 mM $MgCl_2$ and 250 μM AsbF.

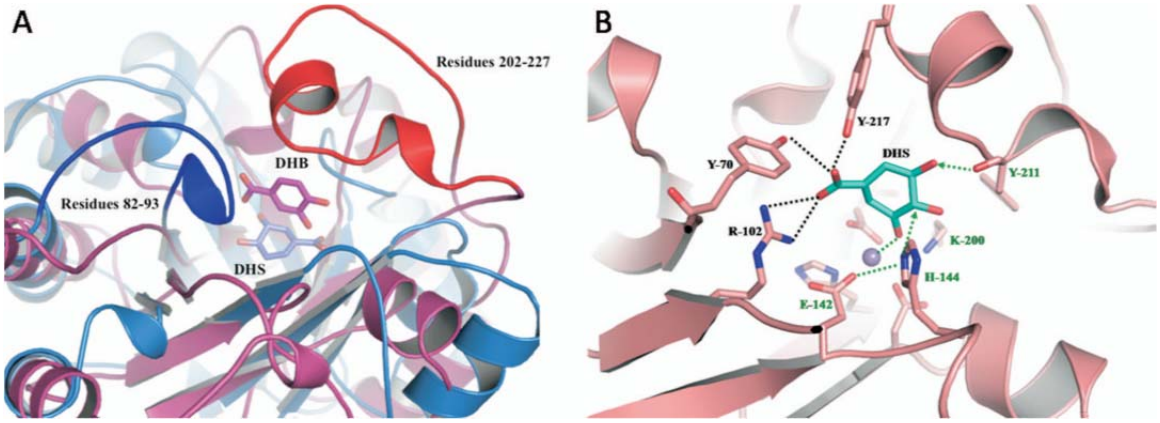

Figure 2-S4. Further modeling of AsbF. (A) Superposition of the AsbF ribbon (pink) drawing with the DHQ (1qfe) structure (sky blue). 3,4-DHBA in pink stick and 3-DHS in blue are also presented. The lid loops are highlighted in red (for AsbF) and blue (for 1qfe). The 3,4-DHBA molecule in AsbF is located near the top of the pocket right under the lid loop with the aromatic ring facing the barrel wall while the dehydroshikimate molecule in DHQ is placed flat at the lower part of the pocket where the H198 side chain resides in the AsbF structure. The carboxylate of 3,4-DHBA is held by the R102 and two tyrosine residues Y217 and Y70, while R82 of DHQ occupies the analogous position of AsbF R102 interacting with C4 OH of DHS in the pocket. The carboxylate of DHS is also found to interact with R213 in DHQ. (B) 3-DHS molecule is modeled (cyan) in the AsbF binding pocket in approximate place of 3,4-DHBA. Green dashed arrows indicate potential catalytic activities and potential catalytic residues are shown in green.

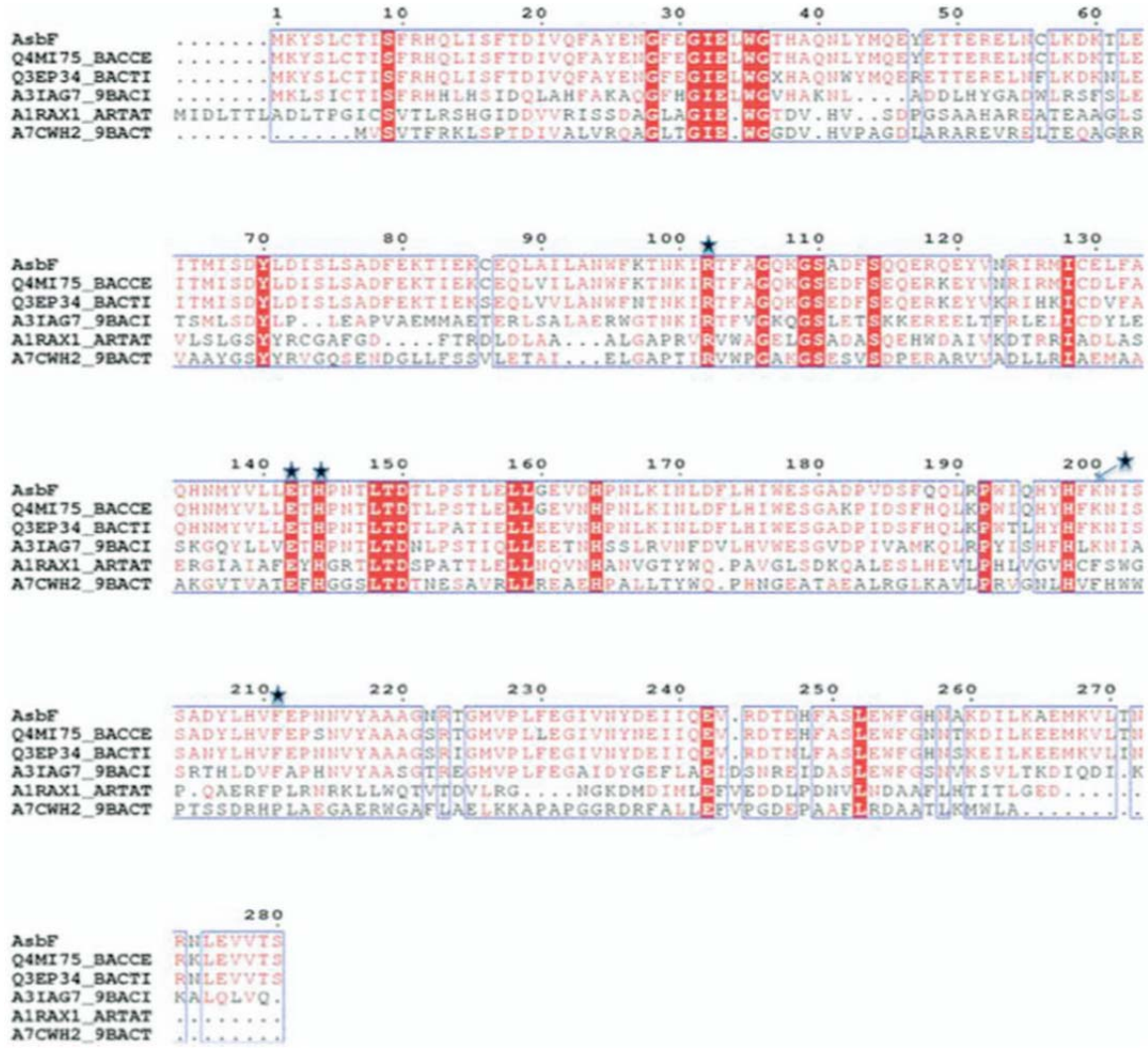

Figure 2-S5. AsbF with homologous proteins in sequence. Conserved residues are indicated in red, red blocks indicating highest homology. Potential catalytic residues are indicated as asterisks at the top of the residues. Q4MI75_BACCE: Putative uncharacterized protein *from B. cereus*; Q3EP34_BACTI: Uncharacterized cytosolic protein *from B. thuringiensis serovar israelensis* ATCC 35646*:* A3IAG7_9BACI: Putative uncharacterized protein *from Bacillus sp. B14905;* A1RAX1_ARTAT: Putative AP endonuclease, family 2 protein *Arthrobacter aurescens;* A7CWH2_9BACT: Xylose isomerase domain protein TIM barrel, *Opitutaceae bacterium TAV2.*

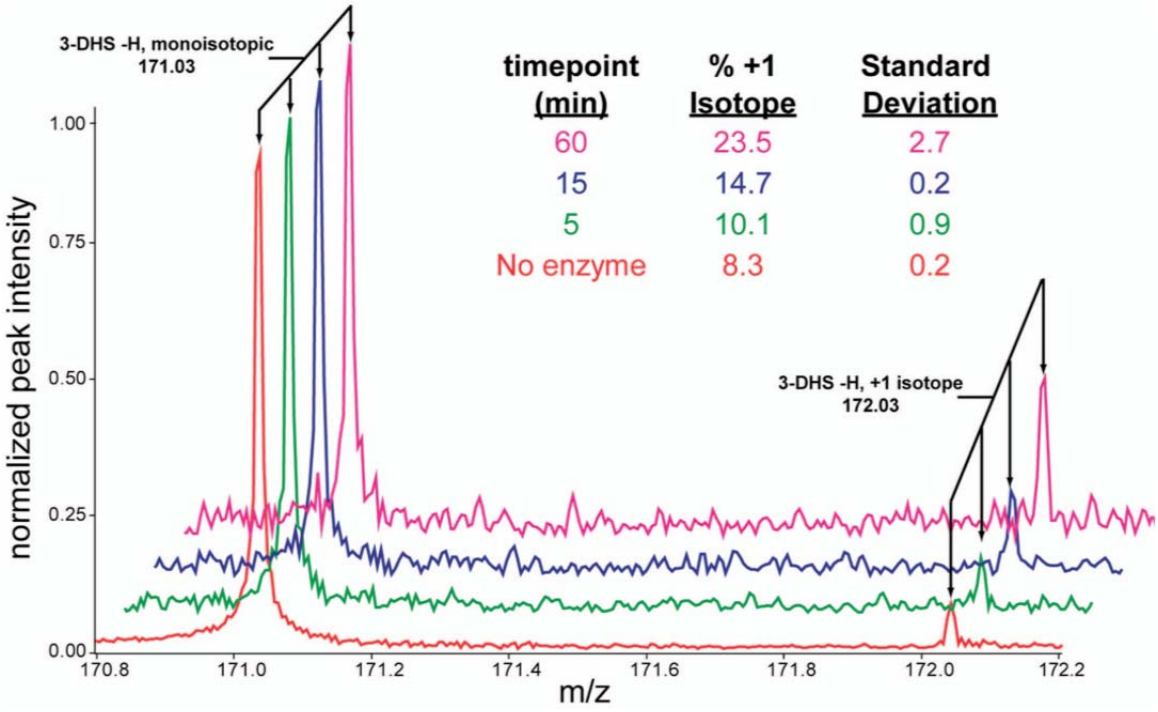

Figure 2-S6. AsbF-catalyzed D_2O exchange of 3-DHS.

100 µl deuterium exchange reactions were run with 10 mM HEPES, 1 mM 3-DHS (from a stock dissolved previously in D_2O), and 1 µM AsbF (pre-soaked in D_2O at 4° C for 15 min). The reaction was started with the addition of enzyme and quenched at designated time points by acidification with 0.5 µl formic acid and immediate extraction with ethyl acetate. Reactions were then dried under N_2 and stored at -20° C. Immediately prior to Fourier Transform Ion Cyclotron Resonance Mass Spectrometric (FT-ICR MS) analysis, samples were resuspended in 50:50 / IPA:H_2O. The extracted 3-DHS samples were analyzed by an FT-ICR MS (APEX-Q with Apollo II ion source and actively shielded 7T magnet, Bruker Daltonics, Billerica, MA). Data was gathered from m/z 50-1,000 utilizing direct infusion electrospray ionization in negative ion mode. Electrospray was conducted at 2,000 volts with 16 scans per spectra utilizing 1s external

ion accumulation in the hexapole prior to analysis in the FT-ICR using a loop value of 3. Data analysis was performed in Data Analysis (Bruker Daltonics, Billerica, MA).

The monoisotopic peak for 3-DHS at 171.03 Da, corresponding to the hydroxyl-deprotonated form in negative mode is readily observed. Since all time points were normalized to the monoisotopic peak, an increase in intensity over time is observed at the +1 isotope peak, corresponding to increasing incorporation of a non-exchangeable deuterium. This data is supported with the numerical values observed, and tight standard deviations with triplicate samples. Since 3-DHS is irreversibly converted to 3,4-DHBA due to aromatization, the overall intensity of the 3-DHS peaks does decrease with time (data not shown), even as the monoisotopic and +1 peak ratios shift.

Strains	3,4-DHBA (g/mL IDM supernatant)
Sterne 34F2	152.25 ± 18.43
Δ*asbA*	457.70 ± 38.61
Δ*asbB*	359.22 ± 42.60
Δ*asbC*	306.03 ± 28.18
Δ*asbD*	239.64 ± 31.02
Δ*asbE*	304.38 ± 29.79
Δ*asbF*	0.09 ± 0.01
Δ*asbABCDEF*	0.07 ± 0.02

Table 2-S1. Quantification of 3,4-dihydroxybenzoic acid (3,4-DHBA). Samples from supernatants of *Bacillus anthracis asb* mutant cultures were analyzed by HPLC.

Quantification of 3,4-DHBA. HPLC using a C18 reverse phase semi-preparative column (SymmetryPrep C18, 7 μM, 7.8 X 300 mm, Waters). HPLC was performed on a Beckman Coulter System with a diode-array detector using a linear stepwise gradient from 10% to 100% aqueous acetonitrile in 0.1% (v/v) trifluoroacetic acid (TFA) at a flow

rate of 1.5 ml/min over 40 minutes for 3,4-DHBA analysis. The retention time and UV spectrum of the corresponding 3,4-DHBA HPLC peaks in each sample were compared with an authentic 3,4-DHBA standard (Sigma). Peak areas were determined and compared with a standard curve constructed by injecting a series of six concentrations (ranging from 0 to 500 μg/ml) of authentic 3,4-DHBA for quantification.

2.5 Notes

Portions of this chapter were originally published in the following:

> Pfleger, B. F.[†], Y. Kim[†], T. D. Nusca[†], N. Maltseva, J. Y. Lee, C. M. Rath, J. B. Scaglione, B. K. Janes, E. C. Anderson, N. H. Bergman, P. C. Hanna, A. Joachimiak, and D. H. Sherman. 2008. "Structural and functional analysis of AsbF: Origin of the stealth 3,4-dihydroxybenzoic acid subunit for petrobactin biosynthesis." *Proceedings of the National Academy of Sciences* 105:17133-17138.
>
> [†]Equal contribution to the work.

Prof. John Frost provided 3-DHS for assays; William Eschenfeldt and Lucy Stols created the vectors used in this project; AsbF structure was made possible by helpful members of the Structural Biology Center at Argonne National Laboratory at the 19ID beamline. This work was supported by a development grant from the Great Lakes Regional Center of Excellence for Bio-defense and Emerging Infectious Diseases (Grant U54AI57153), by the Hans W. Vahlteich Professorship (to Prof. David Sherman), and by National Institutes of Health Grant HHSN266200400059C/N01-AI-40059 (to Prof. Phil Hanna).

2.6 References

1. S. C. Andrews, A. K. Robinson, F. Rodriguez-Quinones, *FEMS Microbiol Rev* **27**, 215 (Jun, 2003).
2. A. T. Koppisch *et al.*, *Biometals*, (May 6, 2008).
3. R. J. Abergel *et al.*, *Proc Natl Acad Sci U S A* **103**, 18499 (December 5, 2006, 2006).
4. M. A. Fischbach, H. Lin, D. R. Liu, C. T. Walsh, *Nat Chem Biol* **2**, 132 (Mar, 2006).
5. J. Y. Lee *et al.*, *J Bacteriol* **189**, 1698 (Mar, 2007).
6. B. F. Pfleger *et al.*, *Biochemistry* **46**, 4147 (Apr 3, 2007).
7. B. L. Garner, J. E. Arceneaux, B. R. Byers, *Curr Microbiol* **49**, 89 (Aug, 2004).
8. A. T. Koppisch *et al.*, *J Org Chem* **73**, 5759 (Aug 1, 2008).
9. N. Fisher *et al.*, *J Bacteriol* **188**, 1301 (Feb, 2006).
10. K. Hosokawa, R. Y. Stanier, *J Biol Chem* **241**, 2453 (May 25, 1966).
11. J. W. Frost, K. M. Draths, *Annu Rev Microbiol* **49**, 557 (1995).
12. P. Stroman, W. R. Reinert, N. H. Giles, *J Biol Chem* **253**, 4593 (Jul 10, 1978).
13. K. A. Wheeler, H. K. Lamb, A. R. Hawkins, *Biochem J* **315 (Pt 1)**, 195 (Apr 1, 1996).
14. J. Yi, K. Li, K. M. Draths, J. W. Frost, *Biotechnol Prog* **18**, 1141 (Nov-Dec, 2002).
15. M. Fuxreiter, O. Farkas, G. Naray-Szabo, *Protein Eng* **8**, 925 (Sep, 1995).
16. D. G. Gourley *et al.*, *Nat Struct Biol* **6**, 521 (Jun, 1999).
17. R. G. Zhang *et al.*, *Proteins* **48**, 423 (Aug 1, 2002).
18. H. Zheng, M. Chruszcz, P. Lasota, L. Lebioda, W. Minor, *J Inorg Biochem*, (May 28, 2008).
19. E. Krissinel, K. Henrick, *J Mol Biol* **372**, 774 (Sep 21, 2007).
20. R. K. Deka, C. Kleanthous, J. R. Coggins, *J Biol Chem* **267**, 22237 (Nov 5, 1992).
21. A. P. Leech *et al.*, *J Biol Chem* **273**, 9602 (Apr 17, 1998).
22. R. J. Abergel, A. M. Zawadzka, K. N. Raymond, *J Am Chem Soc* **130**, 2124 (Feb 20, 2008).

23. R. A. Gardner, R. Kinkade, C. Wang, O. Phanstiel, *J. Org. Chem.* **69**, 3530 (2004).
24. W. R. Harris, S. A. Amin, F. C. Kupper, D. H. Green, C. J. Carrano, *J Am Chem Soc* **129**, 12263 (Oct 10, 2007).
25. S. J. Hickford *et al.*, *J Nat Prod* **67**, 1897 (Nov, 2004).
26. C. Aslanidis, P. J. de Jong, *Nucleic Acids Res* **18**, 6069 (Oct 25, 1990).
27. G. D. Van Duyne, R. F. Standaert, P. A. Karplus, S. L. Schreiber, J. Clardy, *J Mol Biol* **229**, 105 (Jan 5, 1993).
28. M. A. Walsh, I. Dementieva, G. Evans, R. Sanishvili, A. Joachimiak, *Acta Crystallogr D Biol Crystallogr* **55**, 1168 (Jun, 1999).
29. Y. Kim *et al.*, *J Struct Funct Genomics* **5**, 111 (2004).
30. W. Minor, M. Cymborowski, Z. Otwinowski, M. Chruszcz, *Acta Crystallogr D Biol Crystallogr* **62**, 859 (Aug, 2006).
31. G. M. Sheldrick, . *Acta. Cryst.* **A64**, 112 (2008).
32. T. C. Terwilliger, *Acta Crystallogr D Biol Crystallogr* **59**, 38 (Jan, 2003).
33. Z. Otwinowski, paper presented at the Daresbury Study Weekend Proceedings, 1991.
34. K. K. C. Cowtan, 31, p34-38., *Joint CCP4 and ESF-EACBM Newsletter on Protein Crystallography* **31**, 34 (Dec, 1994).
35. paper presented at the Acta Cryst, 1994.
36. R. J. Morris, A. Perrakis, V. S. Lamzin, *Methods Enzymol* **374**, 229 (2003).
37. G. N. Murshudov, A. A. Vagin, E. J. Dodson, *Acta Crystallogr D Biol Crystallogr* **53**, 240 (1997).
38. P. Emsley, K. Cowtan, *Acta Crystallogr D Biol Crystallogr* **60**, 2126 (Dec, 2004).
39. R. A. Laskowski, M. W. MacArthur, D. S. Moss, J. M. Thornton, *J. Appl. Crystallogr.* **26**, 283 (1993).

Chapter 3

Functional and Structural Analysis of the Siderophore Synthetase AsbB through Reconstitution of the Petrobactin Biosynthetic Pathway from *Bacillus anthracis*

3.1 Introduction

During a microbial infection, iron is largely sequestered in complex with host proteins, keeping available pools of this biologically essential metal at levels prohibitive to replication of invading pathogens (*1, 2*). To circumvent this, microbial cells have developed diverse strategies to obtain iron, one of the most prominent among bacteria being the biosynthesis of iron-specific, high-affinity chelators called siderophores (*2*).

Bacillus anthracis, the causative agent of anthrax and a known bioterrorism agent, is capable of synthesizing two siderophores, bacillibactin and petrobactin (*3, 4*). Bacillibactin, a catechol-containing trilactone, is generated by a non-ribosomal peptide synthetase (NRPS) pathway encoded by the *dhb* operon (*5*); however, this metabolite is dispensable during pathogenesis and likely not secreted during an anthrax infection (*6-9*). Conversely, a second siderophore, petrobactin (Fig. 3-1 A) is essential for virulence within current infection models (*6, 10*), and has since become a focus of multiple

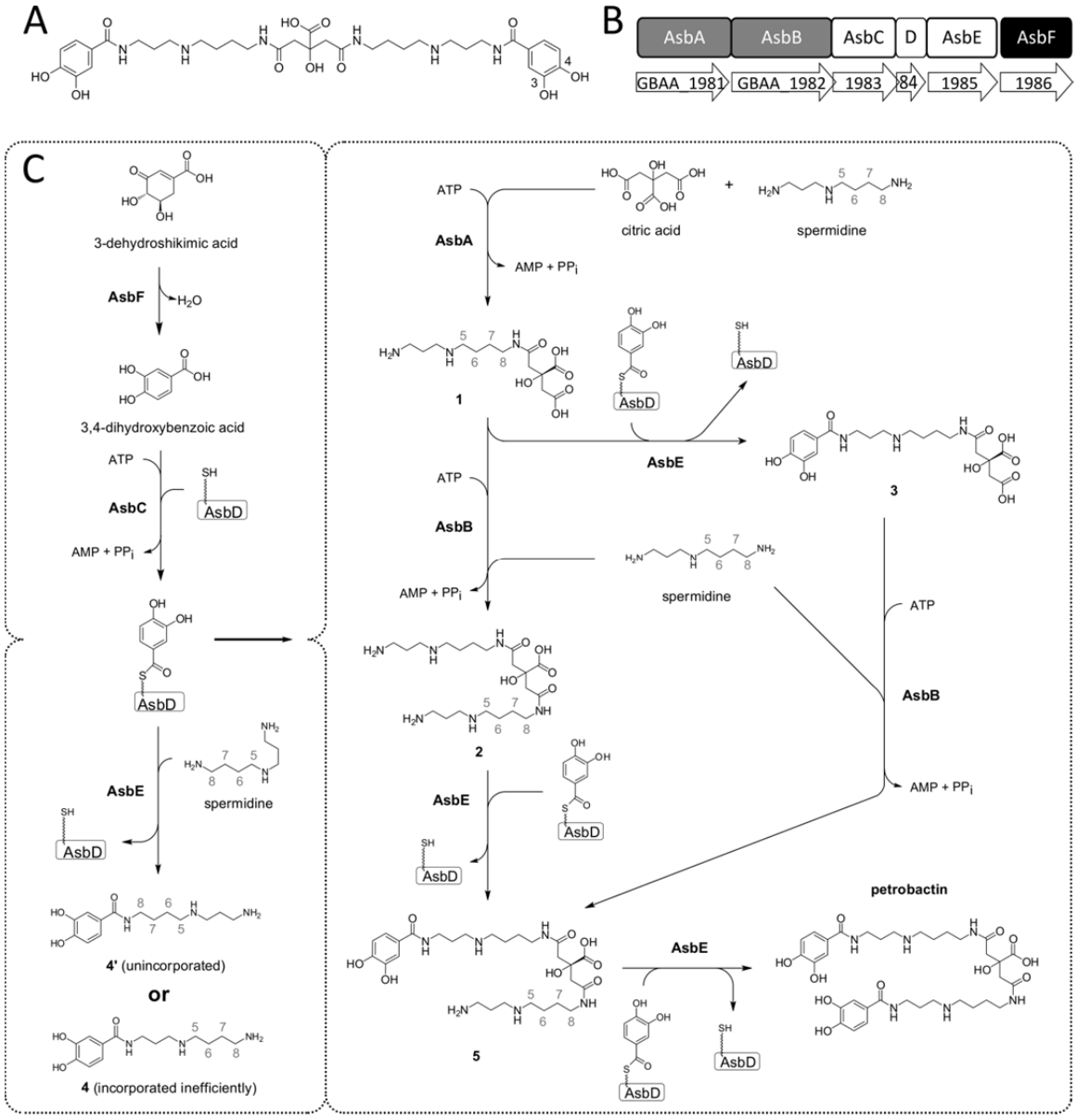

Figure 3-1. Structure and biosynthesis of petrobactin, the virulence-associated siderophore of *Bacillus anthracis*. (A) Petrobactin is a symmetrical, mixed catechol-hydroxy-carboxylate siderophore comprised of a central citric acid moiety, two spermidine arms, and two 3,4-dihydroxybenzoic acid (3,4-DHBA) moieties. The unique 3,4- position of the hydroxyl groups in the catechol confer the stealth characteristics of petrobactin during host infection. (B) The *asbABCDEF* gene cluster, shown with *B. anthracis* str. Ames labels, encodes the enzymatic machinery required for biosynthesis of petrobactin. Products include NIS synthetases (gray), an NRPS-like aryl transferase system (white), and a 3-dehydroshikimate (3-DHS) dehydratase/3,4-DHBA synthase (black). (C) The proposed pathway for petrobactin biosynthesis. Left panel: AsbF converts 3-DHS to 3,4-DHBA which is in turn adenylated by AsbC and loaded onto the phosphopantetheine thiol of the aryl-carrier protein AsbD. *In vitro*, AsbE transfers the 3,4-dihydroxybenzoyl group from AsbD to the primary amino groups of spermidine.

Right panel: Through regioselective condensation of spermidine with citric acid, AsbA and AsbB form intermediates that subsequently react with 3,4-dihydroxybenzoyl units. The flexibility of AsbB *in vitro* suggests multiple possible routes for the biosynthesis of petrobactin.

microbiological, genetic and biochemical studies (*3, 7, 9-20*). This mixed catechol-carboxylate siderophore was first isolated from the Gram-negative marine microbe *Marinobacter hydrocarbonoclasticus* (*21*). Transcriptional analysis of *B. anthracis* mutants deficient for growth in iron-depleted conditions enabled identification of a pathway responsible for siderophore biosynthesis with enzymatic machinery encoded by the *B. anthracis* siderophore biosynthesis (*asb*) operon, and a metabolite identical to the marine-derived siderophore petrobactin (*6, 7, 22*).

Previous mutagenesis and biochemical studies have shown that products of the polycistronic operon consisting of the six genes *asbABCDEF* (Fig. 3-1 B) contribute to assembly of petrobactin in bacteria. Furthermore, petrobactin arises from three simple metabolic precursors: the common primary metabolites citric acid and spermidine, and the unique subunit 3,4-dihydroxybenzoic acid (3,4-DHBA) (Fig. 3-1 C) (*4, 10-14, 17*). AsbA is a member of a growing family of gene products referred to as non-ribosomal peptide synthetase - independent siderophore (NIS) synthetases (*12, 18, 23*). Generally, in a multistep process, NIS synthetases function by binding and adenylating a substrate carboxylate group, thus activating it for condensation with a nucleophilic polyamine or amino alcohol resulting in formation of an amide or ester bond, respectively (*24-26*).

AsbA can be classified more specifically as a type A NIS synthetase due to its utilization of citrate as a substrate for adenylation. This is followed by condensation with spermidine leading to *N*8-citryl-spermidine (compound **1,** Fig. 3-1 C) as a first step in petrobactin biosynthesis (*12*). AsbB is similar in activity to AsbA, but classified as a type C NIS synthetase due to its preference for advanced intermediates in siderophore biosynthesis as substrates including **1** (*11, 17*). Both AsbA and AsbB incorporate the

asymmetric polyamine spermidine from only one (*N*8) of its two primary amino group termini (Fig. 3-1 C) (*12, 17, 18*). Currently, the mechanism by which this regioselectivity is achieved is not well understood.

It is significant to note that the dependence of anthrax on petrobactin during host infection results from the iron chelator's ability to evade sequestration by the host innate immune protein siderocalin, which is largely capable of neutralizing most other catechol-containing siderophores. More specifically, petrobactin owes this "stealth siderophore" quality to steric hindrance created by its 3,4-DHBA subunit when interacting with siderocalin (*27*). Most other catecholate siderophores contain 2,3-dihydroxybenzoic subunits, which are effectively neutralized by this protein during the host response to infection (*27-29*). Previous work has shown that *asbF*, the final gene of the petrobactin biosynthetic operon, encodes a dehydratase responsible for conversion of 3-dehydroshikimate (3-DHS) to 3,4-DHBA (*10, 14*) (Fig. 3-1 C). Once available, linkage of the 3,4-DHBA moieties to an exposed primary amine is facilitated by interactions of three other *asb* products: AsbC catalyzes adenylation of 3,4-DHBA followed by transfer to the phosphopantetheinylated aryl carrier protein AsbD. Subsequently, AsbE functions to catalyze amide bond formation between 3,4-DHBA and molecules bearing a primary amine (*13*) (Fig. 3-1 C). As there are several proposed petrobactin precursors that have an available amino group, we were motivated to ascertain which metabolic intermediates function as substrates for AsbE during petrobactin biosynthesis.

Studies on aspects of petrobactin assembly (*10-14, 17, 18, 23-25*), ligand binding (*22, 30*), and identification of the endogenous cellular receptor (*20, 31*) have enhanced our understanding of iron acquisition by *B. anthracis* during pathogenesis. The broad

eubacterial distribution of NIS systems (*10, 23, 25*) indicates that new information about petrobactin biosynthesis and transport will provide insights into these iron acquisition strategies. In this work, we sought to resolve remaining questions about the petrobactin biosynthetic pathway. Individual enzymatic activities were combined to reconstitute siderophore assembly *in vitro*, thus demonstrating formation of a functional Asb biosynthetic enzyme system. Moreover, determining the crystal structure of AsbB provides the first complete enzymatic and structural characterization of a type C NIS synthetase, with mechanistic insights regarding substrate selection and catalytic activity. Furthermore, information derived from AsbB product formation supports a biosynthetic scheme in which multiple substrates of AsbB function as intermediates in the convergent biosynthesis of petrobactin. This information defines new targets that may facilitate development of effective antibiotics, and expands our fundamental knowledge of NIS synthetases as widely distributed, multi-component biochemical machines for iron acquisition.

3.2 Results

In vitro *reconstitution of petrobactin biosynthesis.*

Previous studies on individual petrobactin biosynthetic enzymes have assigned a metabolic function to all products of the *asb* operon (Fig. 3-1 B) (*10-14, 17, 18, 23-25*); however, whether these proteins are sufficient for petrobactin production *in vitro* has not been determined. *asbA-asbE* were individually amplified from *B. anthracis* Sterne strain $34F_2$ genomic DNA by PCR and cloned into individual expression vectors. All five genes were over-expressed and the resulting proteins were purified by metal-affinity

chromatography for use in enzymatic assays. Recombinant His_6-tagged AsbA, AsbB, AsbC, AsbD, and AsbE were incubated with ATP, $MgCl_2$, and the three metabolic precursors to petrobactin: spermidine, citric acid, and 3,4-DHBA. This reaction was quenched at varying time points and subjected to LC-MS analysis, which revealed an accumulating product with *m/z* matching that expected for petrobactin (expected *m/z* for $[M+2H]^{2+}$: 360.40; observed: 360.35) (Fig. 3-2 A). This compound was not detected in reactions lacking ATP or all five recombinant proteins (Fig. 3-2 B). The enzymatically-derived product was confirmed to be petrobactin through tandem mass spectrometry yielding a fragmentation pattern and spectra (Fig. 3-2 A) that is identical to that of a previously-characterized authentic standard (*22*). Thus, the *asb* gene products are sufficient for producing petrobactin from 3,4-DHBA, spermidine, and citrate and furthermore act *in trans* when individually purified to reconstitute siderophore biosynthesis *in vitro*.

Isolation of pathway components in petrobactin biosynthesis.

Additional pathway reconstitution experiments were motivated by previous characterization of *B. anthracis* mutant strains that demonstrated a detectable amount of petrobactin to be generated even in the absence of the *asbA* gene (*11*), the product of which has been shown to catalyze condensation of spermidine and citric acid (Fig. 3-1 C) (*12*). In an effort to investigate this phenomenon *in vitro*, the biosynthetic reconstitution reaction was performed using AsbB, AsbC, AsbD and AsbE. Following incubation with

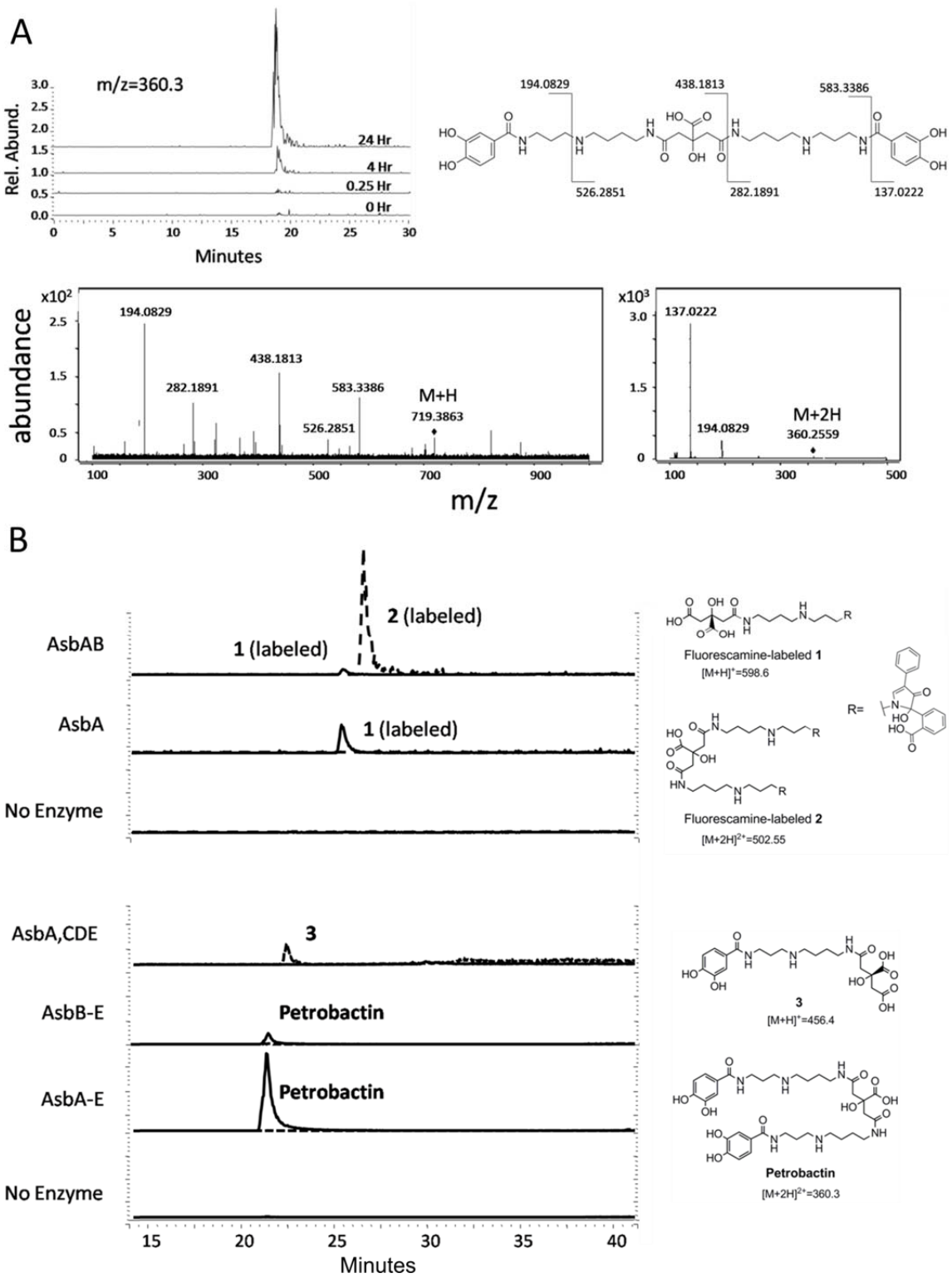

Figure 3-2. *In vitro* reconstitution of petrobactin biosynthesis. Heterologously expressed *asb* products were combined with metabolic precursors spermidine, citric acid, and 3,4-DHBA and the necessary substrate ATP and cofactor Mg^{2+}. (A) LC-MS data demonstrates accumulation of *m/z*=360.3 over time, corresponding to the $[M+2H]^{2+}$ of

petrobactin. The compound associated with this peak was analyzed by MS/MS and shown to have a fragmentation pattern identical to that of authentic petrobactin. (B**)** Products from various combinations of *asb* enzymes were investigated by LC-MS. In order to detect zwitterionic intermediates generated by the NIS synthetases AsbA and AsbB, reactions were acid quenched and products were derivatized with fluorescamine (top two traces). Other organic products were extracted with methanol for analysis (lower traces). Omission of AsbA still results in a modest accumulation of petrobactin, suggesting a compensatory role is filled by the type C NIS synthetase AsbB. Traces show relative intensity of selected *m/z* for each compound.

the required substrates (spermidine, citrate, and ATP) and co-factor (Mg^{2+}), a readily detectable, albeit small, amount of petrobactin was observed by LC-MS (Fig. 3-2 B). In this instance, the remaining NIS synthetase AsbB is able to generate *N*8-citryl-spermidine (**1**), thus functioning as a partial substitute for AsbA.

Further analysis revealed that no other single-enzyme omissions yielded petrobactin. Therefore, AsbA does not play a compensatory role for the missing enzymatic activity of other *asb* gene products. Instead, removal of AsbB from the reaction conditions again resembles a phenotype of *B. anthracis* grown in IDM (Fig. 3-2 B), where the Δ*asbB* mutant accumulates the proposed intermediate *N*1-(3,4-dihydroxybenzoyl)-*N*8-citryl-spermidine (**3**) (*11*). Indeed accumulation of **3** occurs due to its confirmed role as a substrate for AsbB *in vitro*(*17*).

*N*8-citryl-spermidine (**1**) and *N*8,*N*'8-citryl-bis(spermidine) (**2**) are products of AsbA and AsbB, respectively, and likely intermediates in petrobactin biosynthesis (*4, 12, 17*). Since they are zwitterionic molecules that are difficult to separate from other salts for analysis by mass spectrometry, a rapid derivatization method was developed to label the primary amines of **1** and **2** with fluorescamine. With addition of this label to compound **2** or compound **1**, *m/z* values corresponding to the fluorescaminylated derivatives were observed by LC-MS (di-fluorescaminylated **2**: $[M+2H]^{2+}$=502.55; fluorescaminylated **1**: $[M+H]^{+}$=598.6) (Supplemental Fig. 3-S1). Similarly, direct addition of fluorescamine to the *in vitro* pathway reconstitution mixture (AsbA or AsbA and AsbB, with substrates and co-factors) enabled ready confirmation of the presence of the derivatized forms of enzymatically-produced **1** and **2** by LC-MS (Fig. 3-2 B, top two traces).

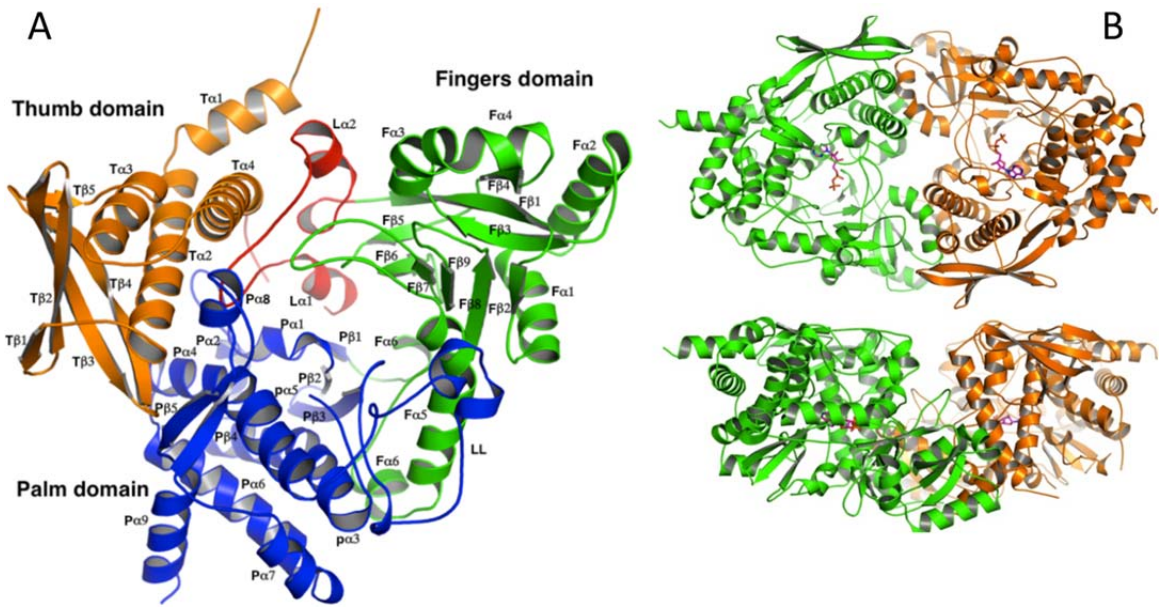

Figure 3-3. Structure of the type C NIS synthetase AsbB. (A) Overall monomer structure of AsbB showing the numbering scheme. The N-terminal thumb domain (orange, 1 -136) is composed of four α-helices (a small N-terminal helix followed by a three-helix bundle) and a four stranded anti-parallel β-sheet. A long loop (red, 137-183) consisting of three small α–helices and two short α-helices with connecting turns is a part of the substrate-binding pocket and separates the thumb domain and the fingers domain. Sandwiched between these domains, the extended loop is stabilized by a number of hydrophilic and hydrophobic interactions involving several well-conserved residues (Supplemental Fig. 3-S2). The fingers domain (green 184-384) contains five α-helices and an 8-stranded antiparallel β-sheet, which twists to form part of the cup-shape binding/active site. The C-terminal palm domain (blue, 380-601) of 10 α-helices and five β-strands (two β-sheets; three stranded antiparallel and a β-ribbon) connects the other two domains and forms a major part of the substrate-binding pocket. (B) The dimeric form of AsbB as the asymmetric unit. The top model shows the large substrate binding pocket; the bottom model is rotated around the x-axis by 90° relative to the top model and highlights the pocket formed by the two dimers.

Crystal structure of AsbB

To gain greater insight into the structural basis for petrobactin formation, the crystal structure of AsbB was solved at 2.40 Å resolution (Fig. 3-3 A). The monomer of the AsbB structure is similar to that of AlcC, *alc*aligin biosynthesis protein C (PDBIDs 2X0O, 2X0P, 2X0Q), from *Bordetella bronchiseptica* (*32, 33*) and that of AcsD (2W02, 2W03, 2W04) from *Pectobacterium crysanthemi* (*34*). AcsD was previously described as a type A NIS synthetase (*33*), which catalyzes one of the initial steps in the biosynthesis of achromobactin, a siderophore implicated in phytopathogenicity of *P. chrysanthemi* (*35, 36*).

Two chains of the AsbB polypeptide occupy the asymmetric unit of the orthorhombic $P2_12_12_1$ crystal as a dimer (Fig. 3-3 B). A monomer of the AsbB structure superposes with AcsD (2W02) (*33*) closely (rmsd 2.52Å, 448 α-carbon atoms over 597 AsbB residues), although there is only a 20% sequence identity (Fig. 3-4 A and Supplemental Fig. 3-S2). Briefly, AsbB has three domains, the thumb domain, the palm domain, and the fingers domain (following the AcsD notation), arranged in a structure resembling a cupped hand. Although the overall fold is similar, as expected from the low sequence identity, the details of each domain are different from AcsD. All three domains together make up a round-bottom, cup-shaped active site and are described in detail in Fig. 3-3A. Additionally, in the pocket, partial electron density corresponding to an ADP molecule (although not fully ordered) is found in chain B (Supplemental Fig. 3-S3) that is consistent in conformation with the ATP molecule of the AlcC structure (2X0Q) (*34*).

The positioning of the homodimer interface between AsbB (or AlcC) and AcsD varies considerably (Fig. 3-4 A and 3-4B). However, as in the case with AcsD, a dimeric

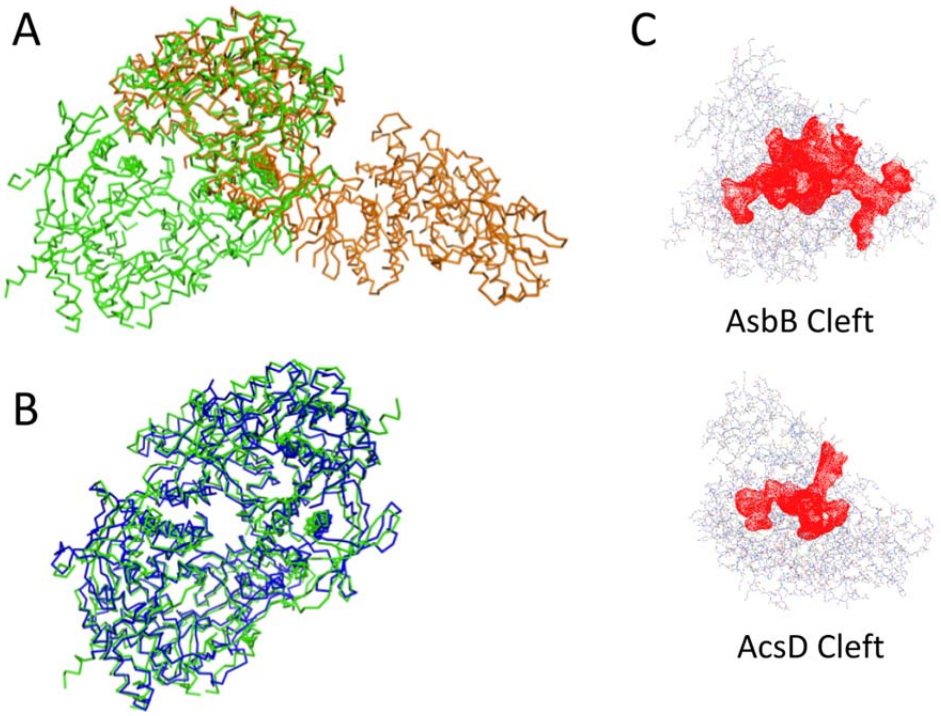

Figure 3-4. Comparison of AsbB to other NIS synthetases. Calculations regarding structural similarity (SSM) were made using PDBeFold (*37*). (A) Superposition of AsbB (green) and the type A NIS synthetase AcsD (orange) demonstrating similar monomeric structures with different dimers. Between the two proteins, the sequence identity is 20.5 %, the RMSD on α-carbon atom positions is 2.52 Å with 448 amino acids compared. (B) Superposition of AsbB (green) and the type C NIS synthetase AlcC (blue) indicating the same fold with similar dimers. For these two proteins, the sequence identity is 24.6 %, the RMSD on α-carbon atom positions is 1.79 Å with 516 amino acids compared. **C.** Ligand binding pockets (red) of AsbB and AcsD. The cleft sizes of AsbB and AcsD are 8614 and 3593 $Å^3$, respectively, as calculated by Profunc (*38, 39*) and plotted by Jmol (*40*).

AsbB found in the crystal structure is corroborated by size-exclusion chromatography and computational analysis, suggesting that the dimeric form exists *in vivo* as well. In the AsbB structure, helices of Tα1, Tα2 and Tα4 in the thumb domain from one chain and a curved helix spanning Fα3 – Fα4 in the fingers domain from the other chain bundle up to form a symmetric half of the dimer interface with a number of hydrophobic or hydrophilic residues exchanging interactions. In the AlcC structure, all the same matching helices maintain interactions to form a similar dimer (Fig. 3-4 B). However, in the AcsD structure, one of the key helices (Tα1) is missing. Instead, a loop (42-61) containing a turn of α-helix from each chain is inserted between Tα1 and Tα2 and contributes to a major part of the interface to make up a dimer, which is quite different from that of the AsbB structure (Fig. 3-4 A).

While AcsD is a type A NIS synthetase, and employs citric acid as the substrate for adenylation, AsbB (and AlcC) is a type C NIS synthetase. The fact that AsbB must adenylate a substrate that is more complex than citrate is reflected in the structural differences between these two highly related proteins. AsbB has a significantly larger binding pocket with about 8500 $Å^3$ encompassing 18.3 Å at its widest part, compared to AcsD that bears a 13.9 Å binding pocket measured between identical amino acid residues with the cleft volume of approximately 3500 $Å^3$ (Fig. 3-4 C). Furthermore, a solvent exposed channel is visibly connecting the active site/binding pocket of one AsbB monomer to the corresponding pocket in the other monomer (Fig. 3-3 B).

AsbB Substrate-Binding Site

Our efforts to co-crystallize AsbB with citryl substrate, spermidine, ATP and/or ADP, were not successful. However, it is reasonable to suggest that these ligands assume

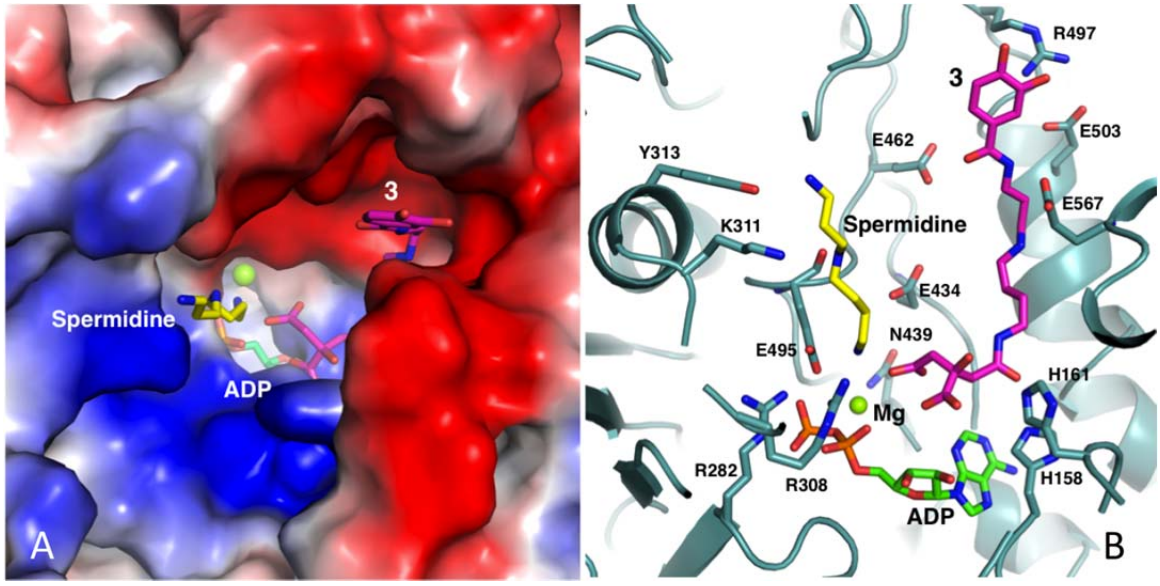

Figure 3-5. Modeling the substrate binding pocket of AsbB. (A) The binding pocket of the AsbB monomer shown in a charge potential surface drawing with ADP (green) as well as a manually modeled spermidine (yellow) and compound **3** (pink). For the ligands, oxygen, nitrogen, and phosphorous atoms are indicated by red, blue, and orange respectively. (B) Hypothetical interactions of AsbB with substrates in the active site. Compound **3** is positioned so that the carboxyl end of the citrate moiety is poised to attack the α-phosphate of ATP. The *N*8 of spermidine is near the same phosphate, poised to attack the ester bond of adenylated **3** for formation of compound **5**. Subsequent molecular modeling allows the *N*1-(3,4-dihydroxybenzoyl)-spermidine "tail" of **3** and spermidine to stretch out within the pocket between the "finger" and "palm" domain in the approximate fashion pictured. Potential protein-substrate interactions include the *N*1and *N*8 of spermidine with Y313 and E459, respectively, and *N*1 and *N*4within the spermidinyl moiety of **3** with E503 and E567, respectively. Residues including H158, H161, R282, K308, and N439 are highly conserved among NIS synthetases (Supplemental Fig. 3-S2) and implicated in coordinating adenylation of the citryl moiety as the first step of catalysis.

positions in the binding pocket similar to that of AcsD or AlcC considering the presence of several highly conserved residues,including nearly all residues implicated in catalytic activity of NIS synthetases (48,49) (Supplemental Fig. 3-S2). Like most other enzymes, the majority of the conserved residues within AsbB reside in the loops—in fact, the binding pocket is made of a number of loops likely arranged to provide flexibility as well as specificity in ligand binding. In this scenario, the substrate conformation is somewhat different from that of AcsD. The number of basic residues in AsbB (i.e. Arg308, Arg282, Lys296) clustered in the loops of residues 296-308 and 280-284, provide a stable binding site for ATP/ADP at the bottom of the pocket as in the cases for AcsD and AlcC (48,49) (Fig. 3-5 A and 3-5 B and Supplemental Fig. 3-S3).

The preferred activity of AsbB, a type C NIS synthetase, requires binding of the relatively complex substrates compound **1** or its dihydroxybenzoylated counterpart **3**. With the location of the triphosphate established, citrate or the citryl moiety of compound **3** most likely positions near the top of the α-phosphate as shown in the co-complex structure of AcsD with ATP and *N*-citryl-ethylenediamine from *P. chrysanthemi* (2X3J) (*41*). In this scenario, the substrate, which is much bulkier in the case of AsbB, requires a larger space for the spermidinyl (in the case of **1**) and/or 3,4-DHB-spermidinyl (in the case of **3**) moiety to be stretched out within the active/binding site. One possible model is depicted in Fig. 3-5 A and 3-5 B. ATP is positioned as suggested by partial electron density of ADP and comparison to the ATP-AlcC co-crystal structure. By adopting orientation and approximate location of the citryl moiety of the AcsD product *N*-citryl-ethylenediamine in the co-complex structure (2X3J) (*34*), the dihydroxybenzoyl-spermidine "tail" of **3** can be stretched out to the direction of the AsbB palm domain,

following the groove formed between the beta loop of Pβ4, Pα8, and Pβ5, and the long alpha-helix Pα3. Along the way, a number of protein residues can interact with the substrate: for example, acidic residues Glu503 and Glu567 are close to *N*1and *N*4, respectively, of the spermidinyl portion of **3**, while Arg497 is near the dihydroxybenzoyl moiety distal to the adenylation active site.

The nucleophilic substrate spermidine is incorporated as a final step, approaching the other side of the citryl moiety of **1** or **3** (near the α-phosphate of ATP where adenylation is likely to occur), and may extend out in the space between the Fingers domain and Palm domain, contacting Tyr313 along the way. Acidic residues Glu459 and/or Glu434 are in position to recruit and stabilize spermidine during the reaction (Fig. 3-5 B). Indeed, the structure reveals sufficient space to accommodate both substrates, a spermidine and an *N*8-citryl-spermidine (**1**) or *N*1-(3,4-DHB)-*N*8-citryl-spermidine (**3**), along with a co-substrate (ATP), without a major change in the main chain conformation of the binding pocket or the additional pocket formed between the two monomers in the AsbB dimer.

Enzymatic characterization of the NIS synthetases AsbA and AsbB.

The crystal structure of AsbB prompted us to further explore aspects of its enzymatic activity and that of its partner NIS synthetase AsbA. Previous work has shown these enzymes catalyze formation of the two amide bonds to the central citrate moiety of petrobactin (Fig. 3-1) (*11, 12, 17*). AsbA regioselectively catalyzes amide bond formation between citric acid and spermidine (*12, 18*). In the case of AsbB, a preference for **1** (the product of AsbA) and spermidine respectively fill this role (*17*). This was demonstrated previously by comparing relative reaction rates using different

substrate sets and also revealed that AsbB readily accepts the 3,4-dihydroxybenzoylated form of **1** (compound **3**), which had been previously proposed as a substrate (Fig. 3-1 C) (*11, 17*).

While relative rates of AsbA and AsbB have been demonstrated under different reaction conditions, kinetic parameters for these enzymes have not been determined. To accomplish this, ATP turnover from synthetase activity was monitored using an enzyme-coupled assay involving conversion of the reporter molecule MESG to its purine base (*42, 43*). This assay was used to empirically establish saturating levels of spermidine, ATP, and Mg^{2+} for AsbA in order to determine reaction rates dependent exclusively on citric acid.

Enzymatic parameters were approximated for AsbA by observing initial reaction rates under varying concentrations of citric acid. Initial experiments suggested that high levels of the substrate inhibited AsbA. Citric acid sequesters divalent cations (including Mg^{2+}) at high concentrations, however, and titration of additional $MgCl_2$ to 0.8 stoichiometric equivalents of citrate restored AsbA activity. The resultant enzymatic activity curve (Supplemental Fig. 3-S4) was sufficient to extrapolate an apparent k_{cat} of $8.90 \times 10^{-1} \pm 0.074$ sec^{-1}, a K_m of $5.65 \times 10^{-3} \pm 0.0016$ M, and an apparent $k_{cat}/K_m = 1.58 \times 10^2$ $M^{-1}s^{-1}$ for purified AsbA-His_6.

Because AsbA and AsbB exhibit such high sequence similarity, particularly between residues in the active sites (Supplemental Fig. 3-S2), and near-identical enzymatic activity (Fig. 3-1 C), optimal spermidine, ATP, and Mg^{2+} concentration was predicted to be similar between the two enzymes. However, substrate-dependent supplementation of additional Mg^{2+} was not required, suggesting the citryl moieties of **1**

and **3** do not sequester divalent cations as effectively as citric acid alone. We sought to determine kinetic parameters for AsbB dependent on the citryl substrate **3** (Supplemental Fig. 3-S4), but UV interference associated with this substrate prevented observation of the reaction at starting concentrations higher than 12 mM. Thus, enzymatic parameters were extrapolated from initial rates occurring between 0-12 mM of **3,** which suggested a V_{max}/K_m=2.40 x 10^2 $M^{-1}s^{-1}$.

Probing acceptance of unnatural nucleophiles for condensation by AsbA and AsbB.

Previous mass spectrometric studies have demonstrated the capacity of AsbA to incorporate a variety of polyamines analogous to spermidine (*18*). Such innate substrate flexibility motivated us to investigate the ability of AsbB to incorporate unnatural ligands as well. Using the MESG assay described above, both AsbA and AsbB enzymes were incubated individually with ATP, $MgCl_2$, and citric acid or **3** (respectively) to compare activity with various nucleophiles related to the preferred substrate spermidine (Fig. 3-6 A). Generally, for both AsbA and AsbB, spermidine remained the preferred nucleophile out of the compounds tested. The one apparent exception was the relatively high activity of AsbA with norspermidine, which has one less carbon atom, and thus bears symmetrical arms. Reaction rate comparison revealed a generally higher promiscuity of AsbB with unnatural substrates. Despite this, the general trend in substrate preference remained consistent between the two NIS synthetases.

Structural basis for polyamine selectivity in AsbB.

In addition to showing a similar profile for distinguishing polyamine nucleophiles as substrates, both AsbA and AsbB regioselectively incorporate spermidine at the *N*8 terminus in the biosynthesis of a symmetrical petrobactin molecule (*12, 17, 18*). To

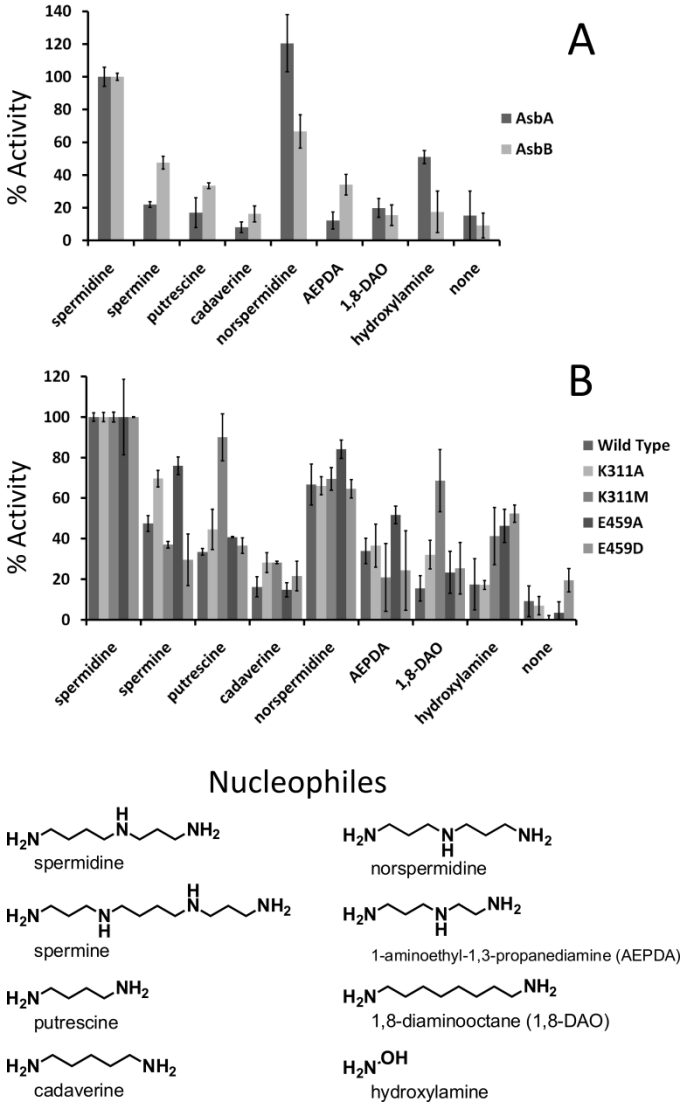

Figure 3-6. AsbA and AsbB display varying selectivity for nucleophilic substrates. A MESG-coupled pyrophosphate detection assay compared relative rate of incorporation of linear nucleophiles by AsbA and AsbB. Data is normalized to the preferred substrate spermidine. (A) AsbB is more promiscuous by comparison; however, the general trend in substrate tolerance is conserved between the two NIS synthetases. (B) Residues in the AsbB substrate-binding cleft hypothesized to interact with spermidine, Lys311 and Glu459, were subjected to site directed mutagenesis. AsbB mutants were compared for relative nucleophile acceptance.

elucidate the basis for this selectivity, a model of the AsbB-substrate complex (Fig. 3-5 B) was used to guide site-directed mutagenesis of residues hypothesized to confer an orientation-specific spermidine binding pocket in both AsbA and AsbB. Among these residues, Lys311 and Glu459 of AsbB align respectively with Lys315 and Gln468 of AsbA. This predictive modeling of the monomeric AsbA polypeptide also suggests that the side chains of Lys315 and Gln468 are solvent exposed in the presumed substrate binding pocket (I-TASSER) (*44, 45*) (data not shown).

An AsbB mutant with alanine substituted for Lys311 was expressed heterologously and purified for comparison of its nucleophile selectivity to that of wild type AsbB (Fig. 3-6 B). While preference for spermidine was not wholly abrogated, activity was elevated in conditions where unnatural nucleophiles were presented. In particular, polyamines of greater length (spermine), or lacking a secondary amine, (l,8-diaminooctane and cadaverine), provided a slightly higher ATP turnover relative to spermidine with the AsbB Lys311Ala mutant than with wild type. Substitution at this position with methionine retains some of the space occupied by the original Lys311, but presents a different charge to the proposed binding pocket. A Lys311Met mutant displayed exclusion of the relatively large spermine molecule as observed with wild type AsbB, but increased acceptance of polyamines lacking a secondary amine still occurred.

Indeed, in the model presented, it appears that the side-chain of Lys311 “pushes” down on spermidine, with multiple positive charges in this space forcing contact between the aliphatic portion of lysine and an alkyl arm of the polyamine. Meanwhile, this conformation facilitates electrostatic interaction between the secondary amine of the substrate and the backbone carbonyl of Glu459. It is possible that partial loss of this

interaction would generate more favorable conditions for binding of substrates lacking a secondary amine.

In addition to the backbone oxygen of Glu459, importance of this residue's side chain in nucleophile selectivity was probed. Substituting this position with alanine demonstrated increased relative acceptance of spermine, norspermidine, and 1-aminoethyl-1,3-propanediamine. Conversely, a less drastically altered Glu459Asp mutant displayed selectivity closer to that of wild type. Considering the substrate conformation model presented (Fig. 3-5 B), the side chain of Glu459 is roughly the same length of the 4-carbon terminus of spermidine and is poised to be positioned parallel to the substrate, extending the *N*8 primary amine to the active site for condensation with adenylated **1** or **3** (Fig. 3-5 B).

Multiple petrobactin biosynthesis intermediates as substrates for AsbCDE.

Spermidine is a nucleophilic substrate of the AsbC-AsbD-AsbE aryl transferase machinery, forming the 3,4-dihydroxybenzoylated product *N*1-(3,4-dihydroxybenzoyl)-spermidine (compound **4**, Fig. 3-1 C) and its regioisomer *N*8-(3,4-dihydroxybenzoyl)-spermidine (compound **4'**) (*11, 13*) (Fig. 3-7, bottom trace). However, a moiety resembling **4'** is not observed within the petrobactin structure (*21, 22*) and more recent relative rate studies demonstrate **4** serves as a relatively poor substrate for AsbA or AsbB (*12, 17, 18*). Indeed, LC-MS analysis of petrobactin generated by *in vitro* pathway reconstitution supports this finding, revealing two peaks with *m/z* ($[M+H]^+$=282.36) corresponding to accumulation of unincorporated **4** and **4'**. Given an abundance of 3,4-DHBA, this reaction will also yield a product with an *m/z* and a fragmentation pattern

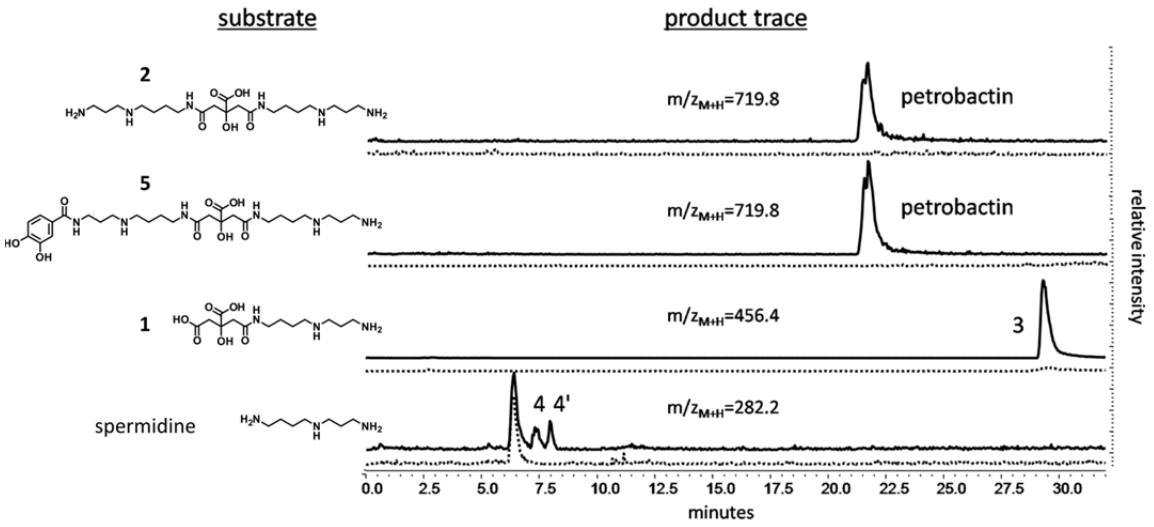

Figure 3-7. 3,4-dihydroxybenzoylation by the aryl transferase components encoded by *asbCDE*. Multiple proposed intermediates of petrobactin biosynthesis contain primary amines and serve as substrates for AsbE. *In vitro* reactions of individually purified His_6-AsbC, His_6-AsbD, and His_6-AsbE with ATP and 3,4-DHBA were extracted using methanol and analyzed by LC-MS. HPLC chromatograms show selected ion monitoring of predicted *m/z* of products. Dashed traces indicate no-enzyme controls.

corresponding to *N*1,*N*8-di-(3,4-dihydroxybenzoyl)-spermidine (compound **6**, Supplemental Fig. 3-S5).

Based on the finding that AsbA and AsbB are both capable of forming products with spermidine (*12, 17, 18*), we were motivated to investigate how these products could be utilized in subsequent biosynthetic steps. Therefore, we considered a more recent hypothesis that, like spermidine, the spermidinylated intermediates **1** and **2** serve as substrates for AsbE in later stages of biosynthesis (*24*). In both molecules, protection of the 4-carbon amino terminus of spermidine (*N*8) through amide bond formation with the central citric acid moiety assures that only the primary *N*1 amine is available for AsbE-catalyzed condensation with 3,4-DHBA (Fig. 3-1 C).

To test this hypothesis directly, **1**, **2** and **5** were incubated with 3,4-DHBA, ATP, $MgCl_2$, and recombinant His_6-AsbC, His_6-AsbD, and His_6-AsbE. Products with *m/z* matching those predicted for 3,4-dihydroxybenzoylation of the substrates were observed by LC-MS (Fig. 3-7): Compound **1**, formed by AsbA, was converted to **3**. As shown previously, **3** has been isolated from iron-depleted cultures of a *B. anthracis* Δ*asbB* mutant (*11*). The products of AsbB, **2** and **5**, functioned as substrates for AsbE as well, participating in amide bond formation with 3,4-DHBA to form petrobactin (Fig. 3-7). In the case of **2**, petrobactin formation likely occurs in two cycles; the first creating **5** which does not appear to accumulate, but instead may be rapidly converted by a second cycle to form petrobactin as the final product. As expected, none of these compounds were observed when AsbC, AsbD, and AsbE were omitted from the reaction mixture.

3.3 Discussion

All products of the *asb* operon implicated in assembly of petrobactin from spermidine, citric acid, and 3,4-DHBA have been heterologously expressed, purified and reconstituted to generate a fully functional petrobactin biosynthetic pathway (Fig. 3-2 A). The absence of AsbA from this reaction resulted in low, but detectable levels of petrobactin formation, suggesting that the similar sequence and enzymatic activity of the partner NIS synthetase AsbB can rescue its function to a modest extent (Fig. 3-2 B). The enantioselective abilities of NIS synthetases have been highlighted previously (*17, 18, 33*); however, AsbB may tolerate both configurations of the chiral citryl moiety of **1** depending on whether this compound exists as a product of AsbA-like activity or as a substrate for condensation to a second spermidine.

The enzymatic activity of AsbA and AsbB during petrobactin assembly was confirmed by LC-MS analysis facilitated by fluorescamine derivatization of siderophore zwitterionic intermediates. Indeed, intermediates of other NIS pathways, including those for rhizoferrin (*46*), staphyloferrin B (*47*), and achromobactin (*23*), have similar charge issues that could be resolved by an analogous derivatization protocol.

By solving the crystal structure of AsbB, we disclose the second structural model of a type C NIS synthetase, and the first to be characterized through concurrent biochemical analysis. Highlighted are residues conserved among other type C enzymes as well as the closely related AsbA. These structural similarities solidify a proposed adenylation mechanism in which attack of the terminal carboxylate within the citryl moiety of one substrate by the α-phosphate of ATP is made energetically favorable by the basic conditions established by surrounding histidines and an arginine (*33*) (Fig. 3-5 A

and 3-5 B and Supplemental Fig. 3-S2). The abundance of conserved polar and charged residues indicates that proper coordination of the substrates is crucial for this first step of the reaction.

Comparison of AsbB to the structures of AlcC (a type C NIS synthetase) and AcsD (a type A NIS synthetase) (Fig. 3-4) highlights differences in substrate binding pocket size and exposure to solvent, which may determine interactions with relatively bulky pathway intermediates as opposed to primary metabolites. In particular, this includes the predominantly acidic face that may tightly accommodate the spermidinyl moiety of **1** or **3** (Fig. 3-5 A and 3-5 B). Considering the structural similarity of the two substrates of AsbB (**1** or **3** and spermidine), it is also possible that they exchange locations and retain the capacity to form an amide bond. This would require deviation from the citrate conformation of previous NIS synthetase-substrate co-crystal structures, but is conceivable considering charge distribution in the AsbB pocket is subtly distinct from that of AcsD, in particular, where a citrate molecule can bind.

High nucleotide sequence identity between *asbA* and *asbB* (46.7%, compared to the 38.4%-41.0% observed between *asbA* and type A NIS synthetases of other species) (*48*) likely results from duplication of an *asbA*-like predecessor gene during evolution of the petrobactin biosynthetic pathway. In support of this, relative catalytic activity values for AsbA and AsbB are now shown to be similar, lying within the same order of magnitude—an observation that is explained by the highly similar primary sequence, substrate structure, and functional activity shared by the two enzymes.

Comparing the relative rates of polyamine incorporation by AsbA and AsbB displayed a similar substrate preference between the two enzymes. Generally, the results

demonstrate that both chain length and general charge are influential factors in nucleophile recruitment to the active site (Fig. 3-6 A). Comparative analysis of the crystal structures for AsbB, AcsD, and AlcC suggests the region likely interacting with nucleophilic substrates extends on the surface of the large solvent-exposed binding cleft from the adenylation active site "upward" towards the solvent, loosely parallel to how **1** or **3** is thought to be binding (Fig. 3-5 A and 3-5 B). Thus, the multiple charged residues along this surface can be envisioned to interact with the amines of spermidine and analogous linear compounds.

Of the residues suggested in binding and selection of nucleophiles in AsbB, Glu434 and Glu459 align closely with Glu442 and Glu466 (respectively) of the type A NIS synthetase AcsD (Supplemental Fig. 3-S2). Docking experiments in the AcsD active site implicate the utility of Glu442 in stabilizing the nucleophile L-serine while Glu466 resides between the nucleophilic alcohol of this substrate and the β/γ-phosphate of ATP (*33*). Indeed, conservation of charged residues at these positions is observed between AsbA, AsbB, AcsD and AlcC, suggesting their importance in coordination of a nucleophilic substrate. Surface exposed AsbB residues Lys311 and Glu459 reside in this patch (Fig. 3-5 B) and also align with similar residues of AsbA (Supplemental Fig. 3-S2). Taking this into account, relative increase in substrate promiscuity with AsbBLys311 Ala/Met and Glu459Ala mutants (Fig. 3-6 B) indicated that these residues, in coordination with Tyr313 interacting with the distal amine of spermidine, might generate a conformation conducive to spermidine recruitment (Fig. 3-5 B).

Activity studies with single amino acid substitutions can partially explain the shared regioselective preference of AsbA and AsbB for spermidine as a nucleophile;

however, factors that cannot be extrapolated from primary sequence undoubtedly play a role, including conserved overall fold and charge distribution within the "fingers" domain. Direct confirmation of whether a loss of substrate specificity is coincident with a loss of regioselectivity will require further investigation, and remains an important factor in the pursuit of chemoenzymatic creation of novel compounds using reconstituted biosynthetic systems.

Work highlighting the incorporation of spermidine by AsbA and AsbB has enabled development of a logical pathway proposal in which 3,4-DHBA is incorporated during late stages of petrobactin biosynthesis exclusively at the *N*1 terminus of spermidine moieties (Fig. 3-1 C) (*4, 12, 17, 24*). *In vitro* results now support this pathway, demonstrating reactivity of AsbE with exposed amino groups of proposed intermediates (Fig. 3-7). **4** and **4',** the previously described products of AsbE aryl transferase activity, and the newly observed but related **6,** accumulate during *in vitro* reconstitution of petrobactin biosynthesis (Supplemental Fig. 3-S5), suggesting they are side-products that are not efficiently incorporated into the siderophore. While **6** may be an artifact of the promiscuity AsbE displays *in vitro*, bis-(dihydroxybenzoyl)-spermidines have been isolated from natural sources including spider venom (*49*) and from bacterial cultures (*50*), and a synthetic compound matching the structure of **6** has shown potential as an antimalarial agent (*51*). Indeed, applications have only been superficially explored for the specific activity combined with substrate flexibility of transferases such as AsbE and siderophore synthetases like AsbB; their potential for expanding chemical diversity is addressed further in Chapter 4 of this dissertation and warrants additional efforts.

The *asb* operon encodes six separate peptides, the products of which clearly can operate *in trans* to form petrobactin. However, interactions between different petrobactin biosynthesis proteins within the cell may specify an exact order of steps in a pathway that appears to include accumulation of unincorporated side-products (e.g. **4'**) and multiple convergent routes *in vitro* (Fig. 3-1 C) (*4, 17, 25, 26*). Indeed, recent pull-down experiments show specific interaction of the His_6-labeled carrier protein AsbD with untagged AsbC and AsbE after co-expression of *asbCDE* in *E. coli* (unpublished data). Understanding how protein-protein interactions between products of *asbABCDEF* confer substrate specificity and reaction efficiency are key future objectives of our group.

The severe virulence of *B. anthracis* combined with its ability to form spores highly resistant to environmental stresses has made it a persisting global health concern and viable security threat (*52, 53*). Current methods for preventing or treating anthrax infection remain limited (*54, 55*). Because abrogation of petrobactin production or uptake has been shown to severely attenuate *B. anthracis* virulence (*6, 10, 15*), enzymes in the biosynthetic pathway remain attractive targets for identification of new antimicrobials. Gaining deeper insights into the details of NIS-associated enzyme function might provide access to mechanism-based inhibitors as have been demonstrated for NRPS-derived siderophore adenylation domains (*13, 56, 57*). Moreover, development of the chemoenzymatic approach described in this work toward creating new siderophore analogs could be applied to generate a class of "Trojan horse" antibiotics, bearing improved target effects and IC_{50} values compared to conventional chemotherapeutics (*58, 59*). These practical considerations further highlight the

importance of expanding our understanding of iron acquisition mechanisms employed by a vast array of pathogenic microbes.

3.4 Experimental Procedures

Chemical and Reagent Origin. Unless otherwise noted, consumable materials were obtained from Sigma-Aldrich (St. Louis, MO) and were of >97% purity. Hydrochloride salts of all polyamines used were either purchased or prepared by titration of stock solutions with HCl to neutral pH.

B. anthracis Strains and Culture Conditions. Targeted mutants of *B. anthracis* Sterne $34F_2$were prepared by the allelic exchange method described by Lee et al. in 2007 (*11*). Δ*asbB* spores were germinated overnight in brain-heart infusion (BHI) broth at room temperature with shaking. After 16-18 hours, vegetative bacilli were diluted 1:100 in BHI broth and grown 1-2 hours to allow cells to enter log phase. Actively growing bacilli were pelleted by centrifugation at 1600 x g for 20 minutes at 25°C and then washed 5x with iron depleted medium (IDM) (*6*) to ensure removal of nutrients and potential iron sources carried over from BHI. Washed bacteria were then used to inoculate 0.5L cultures of IDM in 2L polyethylene flasks at an OD_{600}=0.05. These were grown overnight (16-18 hours) at 37°C with shaking. Vegetative bacilli were removed from the culture supernatant using a 0.22 μm vacuum filtration apparatus (Corning). Catechol presence in the medium was determined using the Arnow assay (*60*) prior to metabolite extraction.

Gene Cloning, Expression and Protein Purification for Enzymology. Supplemental information for expression strain, plasmid, and cloning information is provided in

Supplemental Table 3-S1. Constructs for the expression of AsbB residue-replacement mutant enzymes were produced using protocols provided with the QuikChange (Stratagene) site-directed mutagenesis kit. The addition of 2.5 µl DMSO to 50 µl PCR reactions was required in some instances. Cloning and mutagenesis was confirmed by sequencing (UM DNA Sequencing Core).

To isolate protein for enzymatic analysis, "Z-competent" (Zymo Labs) BLR (Novagen) *E. coli*(DE3) cells were transformed individually with respective *asb* gene-containing plasmids. 5 ml overnight Luria-Bertoni (LB) broth cultures were used to inoculate 2 L baffled flasks containing 500 ml of terrific broth (TB) with 4% (v/v) glycerol and shaken at 37°C. Upon reaching an OD_{600nm} of ~0.8, expression cultures were acclimated to 18°C for 1.5 hours before induction with isopropyl β-D-1-thiogalactopyranoside (IPTG) to a final concentration of 0.25 mM in the medium. In the instance of *asbA*, TB cultures were also supplemented upon IPTG induction with citric acid and spermidine to a final concentration of 1 mM. Over-expression was allowed to continue at 18°C for approximately 16 hours before cells were pelleted and stored at -80°C prior to lysis.

All five over-expressed proteins for enzymatic analysis were purified using standard His_6 Ni^{2+}-affinity chromatography, and are described in detail in Supplemental Methods.

Gene Cloning, Expression and Protein Purification for Crystallization. The *asbB* gene was cloned into the pMCSG7 vector with an N-terminal His_6-tag (*61*) as well as the pMCSG28 vector with a C-terminal His_6-tag (*62*) and over-expressed in *E. coli* BL21 (DE3) - Gold (Stratagene) harboring an extra plasmid encoding three rare tRNAs (AGG

and AGA for Arg, ATA for Ile). To obtain protein from both constructs, recombinant *E. coli* cells were grown using selenomethionine (SeMet)-containing enriched M9 medium (pink medium) under conditions known to inhibit methionine biosynthesis (*63, 64*). Cell cultures were grown at 37°C to an OD_{600} of ~0.95 then cooled down to 18°C before adding Se-Met and 0.5 mM IPTG to induce, and maintained at 18°C overnight. Protein was purified by two-step Ni^{2+}-affinity chromatography following the standard protocol described previously (*65*) and in Supplemental Methods.

The His_6-tag was removed using recombinant TEV protease in a 1:30 ratio by incubating at 4°C for 6 hours. The TEV protease cleavage left six artificial residues (ENLYFQ) at the C-terminus for the pMCSG28 construct protein; however the His_6-tag failed to be cleaved from the N-terminus of the pMCSG7 construct protein. AsbB protein was then further purified by a 5 ml manually packed Ni-superflow affinity column (GE Healthcare). The protein eluted as a flow-through from the column in lysis buffer with 20 mM imidazole. Samples were dialyzed in crystallization buffer containing 20 mM HEPES pH 8.0, 150 mM NaCl, 2 mM DTT and concentrated to 60 mg/ml using an Amicon Ultra centrifugal filter device (Millipore). The protein was then further purified by size exclusion chromatography using a superdex 200 16/60 HiLoad (GE Healthcare) column in the same crystallization buffer.

Protein Crystallization. Crystallization was set up for all AsbB proteins. They were screened for crystallization conditions using a Mosquito robot (TTP Labtech) on sitting drops in 96-well plates (Greiner)at16°C. Each 0.8 µl drop consisted of 0.4 µl of protein from the pMCSG7 or pMCSG28 vectors and 0.4 µl of each crystallization condition. A number of commercially available screens including Index (Hampton Research) and

ANL-1 and ANL-2 (Qiagen) were used for crystallization. AsbB with an N-terminal His_6-tag failed to yield a diffraction quality crystal. The best crystals of AsbB from the C-terminal construct appeared after three days from Index #61 containing 0.2 M L-proline, 0.1 M HEPES pH 7.5, and 10% polyethylene glycol 3350. Prior to data collection, crystals were flash-frozen in liquid nitrogen in the presence of a number of different cryo-protectants. Chunky jewel shape crystals displaying 0.25 x 0.15 x 0.1 mm sides with the ethylene glycol cryo-protectant diffracted to about 2.3 Å and were used for data collection.

Data Collection, Structure Determination, Refinement and Deposition. The single wavelength anomalous dispersion (SAD) data near the Se absorption edge at the peak wavelength 0.9793 Å up to 2.4 Å were collected from a single Se-Met labeled protein crystal at 100° K at the 19ID beam line of the Structural Biology Center at the Advanced Photon Source, Argonne National Laboratory. The crystal was exposed for 5 sec. per 1.0^o rotation of ω circle with the crystal to detector distance of 340 mm. The data were recorded on a CCD detector Q315r from ADSC scanning a full 220º on ω using the SBC-Collect program for data collection and visualization of diffraction images. The space group was $P2_12_12_1$ with cell dimension of a = 64.26 Å, b = 155.92 Å, c = 156.24 Å. All data were processed and scaled with HKL3000 (*66*) (Table 3-1).

The structure was determined by SAD phasing utilizing the anomalous signal from Se atoms with AUTOSHARP (SHARP 2.2.0 and Sushi 3.4.0) (*67*) using the peak data to 2.40 Å.ARP/wARP (*68*) was used to build an initial model that included 495 (out of total 616 residues including the C-terminal artifact residues) and 470 residues for each of two protein chains. Significant manual model building and the subsequent refinement was

Data collection	
Space group	$P2_12_12_1$
Unit cell (Å)	*a* = 64.26
	b = 155.92
	c = 156.24
Wavelength(Å)	0.9793
Highest Resolution bin (Å)	2.44-2.40
Number of observed reflections	62971(3081)
R_{sym}(%)[a]	9.0(63.1)[b]
Completeness (%)	99.8(100)
I/s*I*	10.8(3.2)[b]
Phasing	
Method	SAD
Phasing resolution range (Å)	49.6-2.40
Figure of merit/Phasing power	0.26/1.29
Number of SeMet	26
Refinement	
Resolution range (Å)	49.6 -2.40
R_{cryst} (%)	17.4
R_{free} (%)	22.7
Number of protein residues	1232
Solvent molecules	324
Bond lengths (Å)	0.012
Bond angles (deg)	1.49
Dihedral angles (deg)	17.2
B-factors (Å^2)	59.8
Protein main chain	55.5
Protein side chain	62.2
Others (Water, ADP, Ethylene glycol)	59.6
Wilson B-factor (Å^2)	50.9
Ramachandran Plot (%)[c]	
Preferred	96.4
Generously allowed	3.1
Disallowed	0.5
PDB ID	**3TO3**

Table 3-1. Summary of the AsbB crystallographic data.
[a]$R_{merge} = (\Sigma_{hkl}\Sigma_i \left| Ii - \langle I \rangle \right|)/(\Sigma_{hkl}\Sigma_i \left| \langle I \rangle \right|)$, where *Ii* is the intensity for the *i*th measurement of an equivalent reflection with indices *h*, *k*, and *l*. [b]Numbers in parentheses are values for the highest-resolution bin. [c]Defined in Coot.

performed iteratively by phenix.refine (*69*) and manual adjustment using Coot (*70*) until it converged to the R factor of 0.174, and the free R of 0.227 with the rms bond distances of 0.012 Å and the rms bond angles of 1.49°. The final model included residues 1 - 600 of the chain A and 0 – 600 of the chain B of AsbB, one ADP, one Mg^{2+}, two chloride ions, 3 ethylene glycol molecules, and 324 ordered water molecules. Residues on the surface such as 138-143 of chain A and 139-144 of chain B are not ordered; neither are the C-terminal residues, 601-610 for both chain A and chain B, including those residues introduced during cloning (*62*). The stereochemistry of the structure was checked with PROCHECK (*71*) and the Ramachandran plot. Atomic coordinates and experimental structure factors of AsbB have been deposited in PDB under the code 3TO3.

Purification of N*1-3,4-dihydroxybenzoyl*-N*8-citryl-spermidine* (**3**). All procedures were performed in plasticware thoroughly rinsed with double-deionized water (ddH_2O) or glassware rinsed generously with 6 M HCl followed by ddH_2O. Supernatants from previously described *B. anthracis* Sterne $34F_2$ Δ*asbB* cultures were stirred overnight with 37.5 g of Amberlite XAD-16 resin per liter of supernatant. Prior to mixing with culture supernatants, the resin was equilibrated for an hour in ddH_2O and filtered through a milk-filter that had also been rinsed with ddH_2O. The batch-binding slurry was poured though a glass chromatography column. Retained resin was washed with 1 L of ddH_2O that was collected, followed by 500 ml of methanol (MeOH), which was also collected.

Liquids were evaporated to dryness and re-dissolved in 4 ml of ddH_2O prior to purification on a Beckman-Coulter System Gold HPLC which was conducted as follows: Solvents contained a 0.1% (v/v) mixture of formic acid brought to pH 4 by addition of triethylamine. Separation was conducted on a Waters X-Bridge C_{18} (10x250 mm, 5μm)

column at a flow rate of 2.5 ml/min with an initial concentration of 5% MeOH in ddH_2O for 15 minutes followed by a linear gradient increase to 50% MeOH over the course of 25 min. 100% MeOH was applied for an additional 12 minutes as a cleaning step. Peaks with UV absorption maxima matching that of 3,4-DHBAmoieties (259 nm and 290 nm) were collected and their identity was confirmed by mass spectrometry. To achieve the high degree of purity required for kinetics analysis, collected **3** was evaporated and applied to a second round of HPLC using a Phenomenex Synergi Hydro-RP (10x250 mm, 4 μm) semi-preparative column eluted with solvents containing 0.05% (v/v) formic acid at a flow rate of 2.5 ml/min. 100% ddH_2O was applied for 15 minutes after which MeOH concentration was increased to 50% in a linear gradient over 30 minutes, followed by a 100% MeOH cleanup phase. **3** was collected, confirmed by mass spectrometry, and lyophilized. Prior to use, metabolites were dissolved in ddH_2O to create 100 mM stock solutions that were stored at -20° C.

Synthesis of substrates. **5** and **1** were prepared as previously described (*12, 17*). While **1** was synthesized similarly to previously reported methods, purification of the final product was performed by HPLC on a Beckman-Coulter System Gold in line with a Phenomenex Synergi Hydro-RP (10x250 mm, 4 μm) semi-preparative column with a 100% aqueous mobile phase containing 0.05% (v/v) formic acid at a flow rate of 2.5 ml/min.

In vitro *reconstitution of metabolite biosynthesis.* Small-scale reactions were conducted in 1.7 ml microcentrifuge tubes. Reaction buffer contained 50 mM HEPES pH 8, 15 mM $MgCl_2$, 0.5 mM Tris(2-carboxyethyl) phosphine (TCEP), 10 mM ATP, 2 mM carboxylate substrate (citric acid or **3**), 4 mM nucleophilic substrate (spermidine or

analogs thereof), and 4 mM 3,4-DHBA where applicable. All enzymes were used at a concentration of 1 μM with the exception of AsbD, which was used at 5 μM. All reactions were conducted at 37°C unless otherwise noted. Reactions were quenched in two ways: 1) Adding 0.5 reaction volume of 5% (w/v) trichloroacetic acid (TCA) solution. Reactions were inverted to mix and centrifuged at 16,000 x g on a tabletop centrifuge for 20 minutes. Resultant supernatant was placed into a new tube containing an equal volume of 0.6 M Na-borate buffer pH 8.0. 2) Adding nine reaction volumes of HPLC-grade MeOH spiked with 25μM of *N*-(3-aminobenzoyl)-L-β-alanine as an internal standard. Reactions were inverted to mix and centrifuged at16,000 x g on a tabletop centrifuge for 20 minutes. The resultant supernatant was placed into a new tube and evaporated to dryness by vacuum centrifugation. Samples were re-dissolved in ddH_2O prior to analysis. Enzymatically-derived petrobactin obtained using this method was purified by the same HPLC method applied to **3** (described in a previous section) and retained for further analysis.

Fluorescamine derivatization of polar compounds. 10 μl of TCA-quenched sample was mixed with 10 μl of 200 mM fluorescamine in LC-MS grade acetonitrile (MeCN). Reactions were vortexed, briefly centrifuged, and placed in the dark for 2 hours. Following incubation, reactions were centrifuged in 0.65 ml microcentrifuge tubes at 16,000 x g for 10 minutes. 15 μl of supernatant was then diluted 4-fold in 50:50 MeCN:H_2O for analysis by LC-MS.

LC-MS analysis. 2 μl of MeOH-quenched *in vitro* reaction samples were injected onto a Shimadzu 2010EV HPLC in line with an electrospray quadrupole mass spectrometer running the following chromatographic method: All solvents were LC-MS grade and

contained 0.1% (v/v) formic acid. Separation was conducted on a Phenomenex Luna C_{18} (250x4.6 mm, 5 µm) column at a flow rate of 0.125 ml/min with an initial concentration of 5% MeCN in ddH_2O for 8 minutes followed by a linear gradient of 5% to 95% MeCN over the course of 32 min. 95% MeCN was then applied for an additional 12 minutes. Spectra were scanned in both positive and negative mode over the range of 200 to 1000 *m/z*. Predetermined *m/z* values were also monitored in positive selective ion monitoring (SIM) mode. Similar methods were used for TCA-quenched reactions and biological samples; however, 5 µl were injected and the first 10 minutes of the HPLC protocol was diverted to waste to avoid introduction of salt to the mass spectrometer.

Metabolite analysis by Tandem Mass Spectrometry (MS/MS). Enzymatically prepared products and culture-derived *N*1-(3,4-DHB)-*N*8-citryl-spermidine (**3**) were collected from HPLC purification and stored at -20° C prior to analysis. Using an Agilent Technologies 6500 quadrupole time of flight (Q-TOF) mass spectrometer, 1-3 µl of sample was applied by direct infusion with a 10% MeCN, 0.1% (v/v) formic acid solvent mixture at a flow rate of 0.4 ml/min. Electrospray ionization was used, scanning in positive mode between 100 and 1000 *m/z*. Target ions matching the predicted *m/z* values for analytes were fragmented by collision-induced dissociation at 20 V. An alternative LC-MS/MS method is described in Supplemental Fig. 3-S5.

MESG continuous pyrophosphate detection assay. Reactions were a modification of a previously described protocol (*42, 72*). For kinetics reactions, standard conditions were 50 mM Tris pH 8.0, 15 mM $MgCl_2$, 0.5 mM TCEP, 6 mM ATP, 40 mM spermidine, 0.001 U/µl purine nucleoside phosphorylase, 0.0004 U/µl inorganic pyrophosphatase, 0.4 mM 2-amino-6-mercapto-7-methylpurine ribonucleoside (MESG) (Berry & Assoc.,

Dexter, MI), and 0.2 μM purified enzyme. Varying concentrations of carboxylate-containing substrate (citric acid or **3**) were used to obtain enzymatic parameters. A standard curve was created under these reaction conditions, with the omission of enzyme and including varying concentrations of $Na_4P_2O_7$. Change in A_{360nm} in response to pyrophosphate (PP_i) content remained linear up to 0.05 mM and this relation could be described by the equation $0.394x\Delta A_{360nm}$=mM PP_i. The relative polyamine acceptance assay utilized similar reaction conditions, however 20 mM of analogs of spermidine and 3 mM carboxylate-containing substrate were used.

Assays were conducted in 96-well or 384-well plate format prepared in 80 μl or 40 μl volumes, respectively. A_{360nm} readings were gathered every 15 seconds over the course of 10 minutes using a Molecular Devices SpectraMax M2e plate reader. Kinetics reactions were conducted in triplicate. The initial linear rate under each condition was calculated using the slope function in Microsoft Excel. Subsequent analyses were performed by plotting initial rate versus substrate concentration in Kaleidagraph (Synergy Software) and using nonlinear regression to fit to the Michaelis-Menten equation. Experiments to determine substrate preference were conducted in duplicate; initial rates were zeroed to that of no-enzyme controls and normalized based on the assumption that spermidine acts as a nucleophile to confer 100% activity.

3.5 Supplemental

Protein Purification for Enzymology. All steps were conducted at 4°C. Briefly, harvested cell pellets were resuspended in 5 ml of lysis buffer (20 mM imidazole, 20 mM HEPES, 150 mM NaCl, 1 mM Tris(2-carboxyethyl) phosphine [TCEP], 10% v/v

glycerol, pH 8) per 100 ml of original over-expression culture and lysed by sonication. Insoluble material was removed by ultracentrifugation at 30000 x g for 45 min, and the supernatant was batch-bound for 2 hours to 1 ml of Ni^{2+}-NTA slurry (Novagen) that was previously equilibrated in lysis buffer. This batch-binding mixture was poured through a 5 ml fritted glass column where the retained resin was washed with 1 column volume of lysis buffer, 2 column volumes of wash buffer (40 mM imidazole, 20 mM HEPES, 150 mM NaCl, 1 mM TCEP, 10% glycerol, pH 8), and finally 3 ml of elution buffer (250 mM imidazole, 20 mM HEPES, 50 mM NaCl, 1 mM TCEP, 10% v/v glycerol, pH 8). Protein in the eluate was both exchanged into storage buffer (20 mM HEPES, 5 mM NaCl, 1 mM TCEP, 20% v/v glycerol, pH 8) and concentrated using Amicon Ultra centrifugal molecular weight cutoff filters (Millipore). Resulting samples were flash frozen with liquid N_2 and stored at -80°C prior to analysis.

Protein Purification for Crystallization. Harvested overexpression cells were lysed by sonication in the presence of 1 mg/ml lysozyme and a protease inhibitor cocktail tablet (Complete, Roche) in 35 ml of lysis buffer containing 50 mM HEPES pH 8.0, 500 mM NaCl, 10 mM imidazole, 10 mM β-mercaptoethanol, and 5% v/v glycerol. The lysate was clarified by centrifugation at 30000 x g for 75 min, followed by filtration through a 0.45 μm filter. Protein was purified by two-step Ni^{2+}-affinity chromatography following the standard protocol described previously (*65*). Immobilized metal affinity chromatography (IMAC) was conducted using a 5ml HisTrap Chelating HP column charged with Ni^{2+} ions and buffer-exchange chromatography was performed on a HiPrep 26/10 desalting column (GE Healthcare) on an ***ÄKTAxpress***™ (GE Healthcare).

Gene Name	Number	Expression Vector(s)	Cloning Strategy	Source
asbA	GBAA_1981	pMCSG26	LIC	this work
asbB	GBAA_1982	pET28b/pMCSG28	NdeI-XhoI/LIC	this work
asbC	GBAA_1983	pET28b	NdeI-XhoI	ref. 4
asbD	GBAA_1984	pET28b	NdeI-XhoI	ref. 4
asbE	GBAA_1985	pET28b	NdeI-XhoI	ref. 4

Gene Name	Antibiotic	Expression Strain
asbA	Amp, Spect, Tet	BLR (Invitrogen) cont. the pRARE plasmid (Novagen)
asbB	Kan, Spect, Tet/Amp, Spect	BLR (Invitrogen)/ BL21 (DE3)-Gold (Invitrogen) cont. the pRARE plasmid (Novagen)
asbC	Kan, Spect, Tet	BLR (Invitrogen)
asbD	Kan, Tet/Kan	BLR (Invitrogen)/ BAP1 (Walsh Group, Harvard Univ)
asbE	Kan, Tet	BLR (Invitrogen)

Table 3-S1. Gene, vector, strain, and expression conditions. LIC = Ligation independent cloning. Primer sequences and PCR conditions required for amplification of fragments is available upon request.

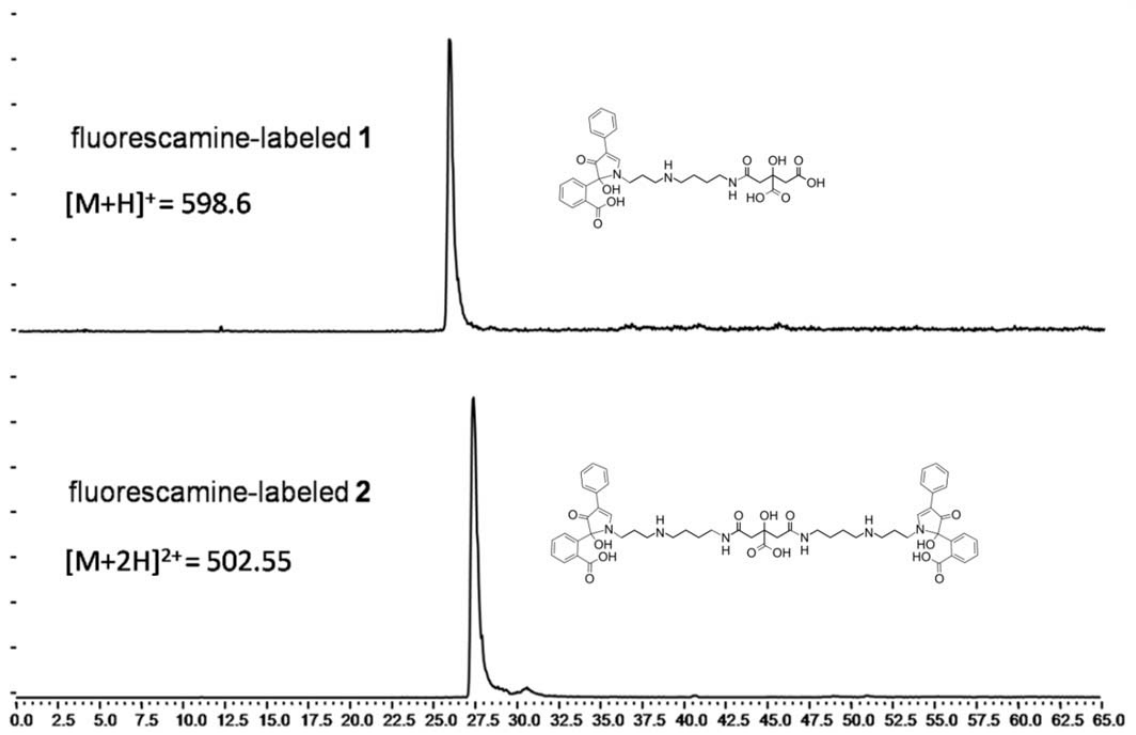

Figure 3-S1. Fluorescamine derivatization of prepared standards. Zwitterionic intermediates of petrobactin biosynthesis were derivatized with fluorescamine and analyzed by LC-MS using selected ion monitoring of predicted *m/z* of products.

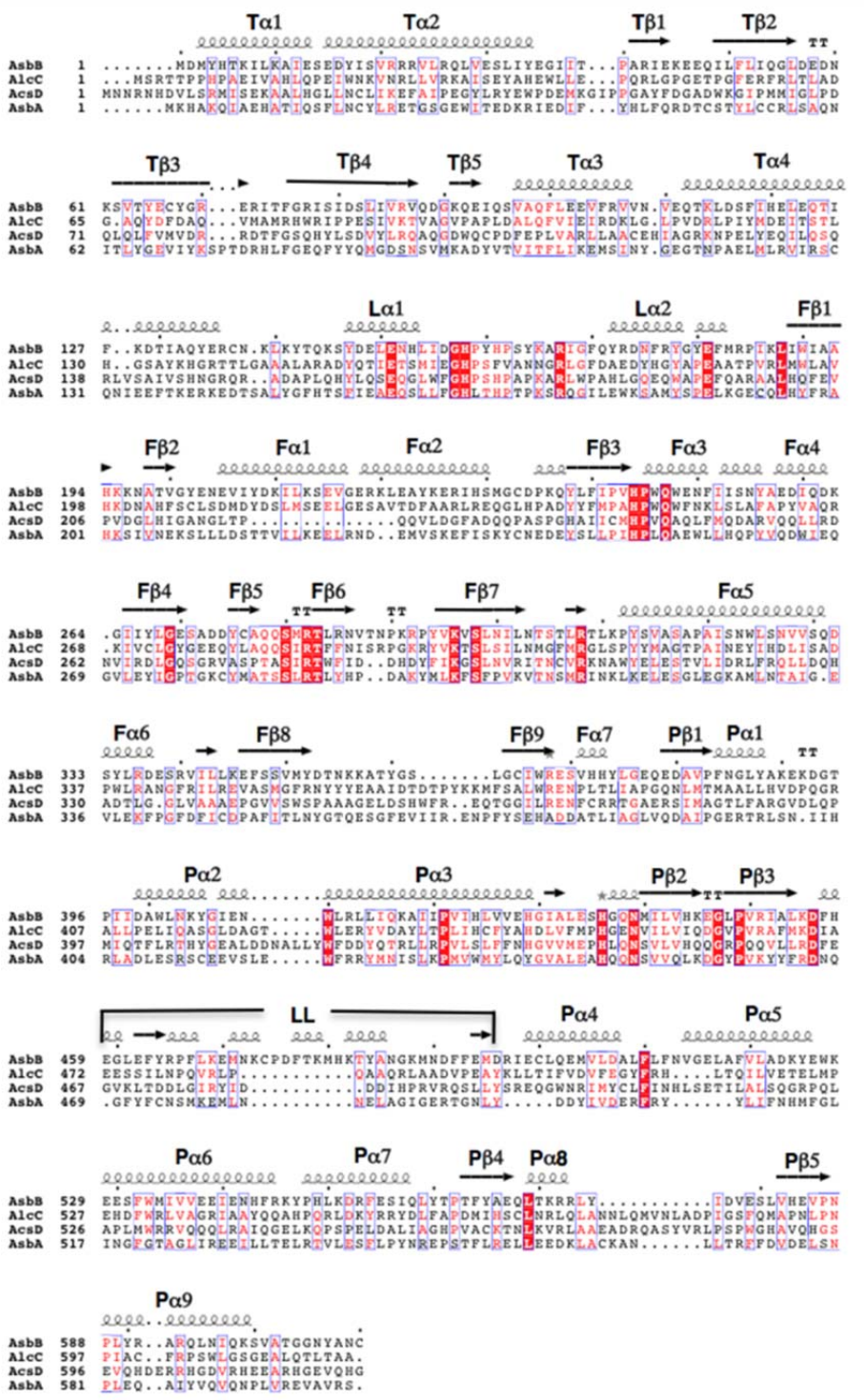

Figure 3-S2. Sequence comparison of AsbB, AlcC, AcsD and AsbA. The secondary structure of AsbB is annotated at the top. Highly conserved residues include H158, H161, R282, K308, E434, and N439 of AsbB. Hypothesized structural interactions with substrates are depicted in Fig. 3-3 D.

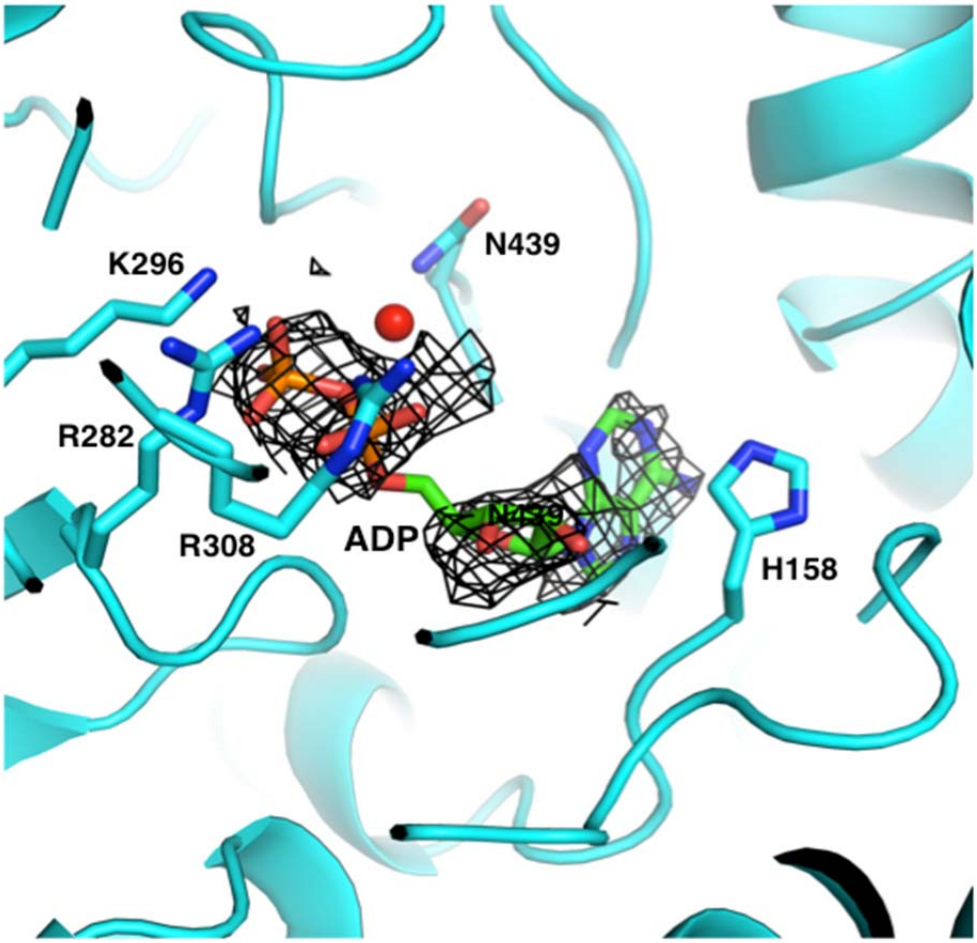

Figure 3-S3. Modeling of ADP binding in the AsbB active site. ADP conformation is modeled and refined with partial occupancies based upon loose electron density data as demonstrated by the difference (Fo-Fc) electron density contoured at 3.0 σ (black mesh). Potential protein-substrate interactions are detailed in Figure 3D.

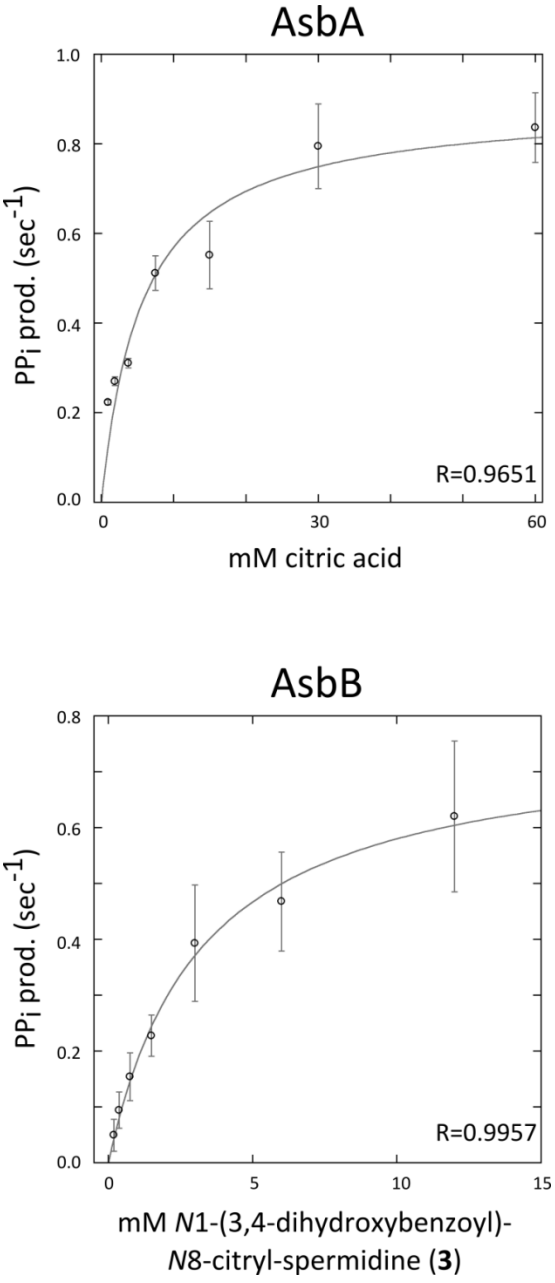

Figure 3-S4. Activity plots for quantification of enzymatic efficiency. His_6-AsbA and His_6-AsbB kinetic parameters were determined through plotting initial reaction rates over varying starting concentrations of adenylation substrate. The additional substrates of ATP and spermidine are at near-saturating levels of 6 mM and 40 mM, respectively. Reaction progress was monitored by observing release of pyrophosphate (PP_i) coupled to hydrolysis of the reporter molecule MESG to establish initial rates that were normalized to enzyme concentration. Only data-points not displaying substrate-associated background interference were used to extrapolate the curves. Nonlinear regression of these data using the Michaelis-Menten equation enabled prediction of V_{max} and K_m for approximation of V/K.

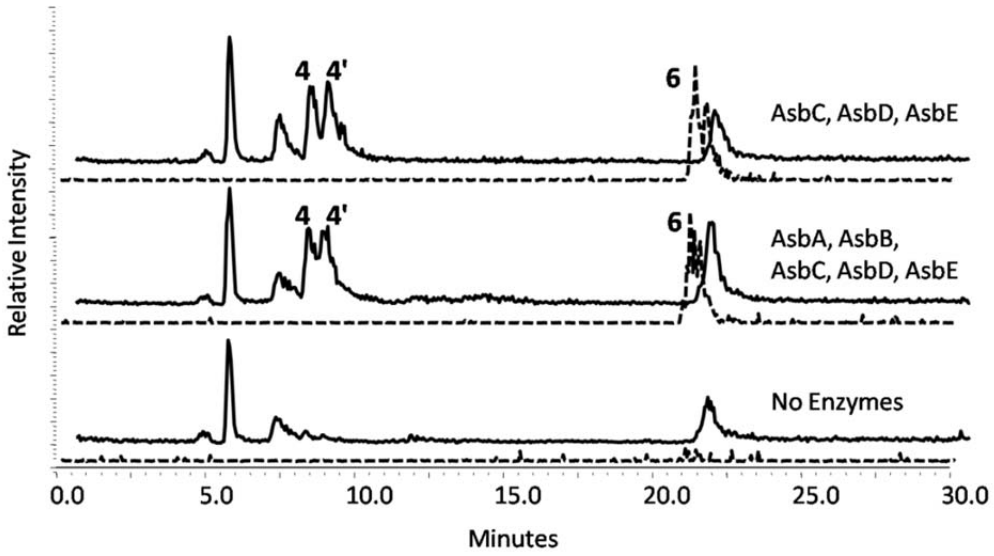
4
4'
6
AsbC, AsbD, AsbE
AsbA, AsbB,
AsbC, AsbD, AsbE
No Enzymes
Relative Intensity
0.0
5.0
10.0
15.0
20.0
25.0
30.0
Minutes

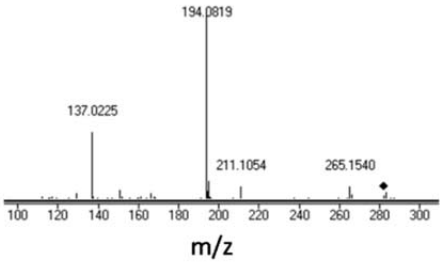
194.0819
137.0225
211.1054
265.1540
m/z

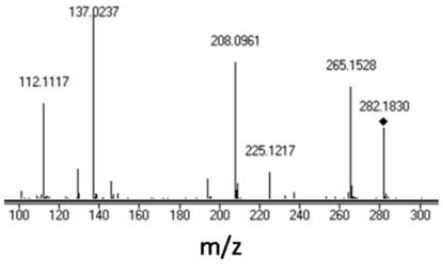
137.0237
208.0961
265.1528
112.1117
282.1830
225.1217
m/z

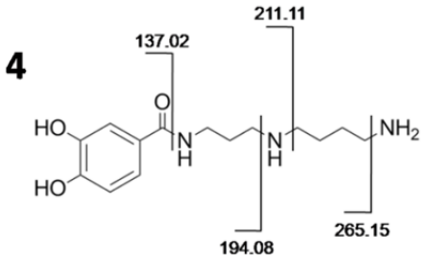
4
137.02
211.11
HO
HO
O
N
H
N
H
NH2
194.08
265.15

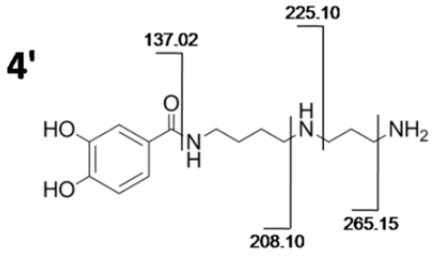
4'
137.02
225.10
HO
HO
O
N
H
H
N
NH2
208.10
265.15

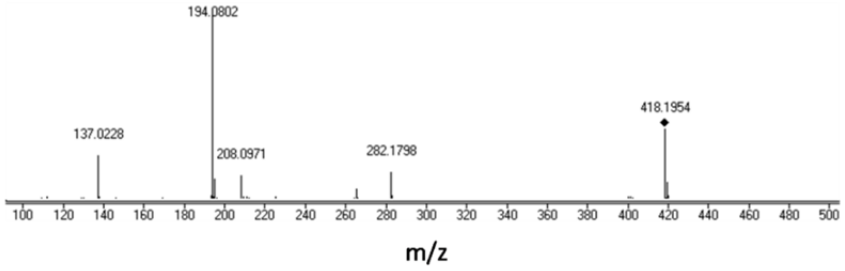
194.0802
137.0228
208.0971
282.1798
418.1954
m/z

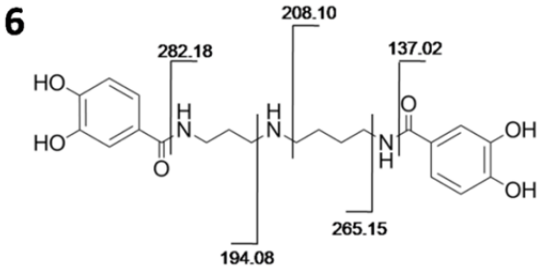
6
208.10
282.18
137.02
HO
HO
H
N
O
H
N
O
N
H
OH
OH
265.15
194.08

Figure 3-S5. Reaction of AsbE with spermidine and 3,4-DHBA. Initial reactions were analyzed by LC-MS as described in the text. Selective ion monitoring (SIM) was conducted in positive mode for predicted *m/z* of **4** and **4'** ($[M+H]^+$=282.2, solid traces). An extracted ion chromatogram (EIC) was rendered to detect compound **6** with a predicted *m/z* of $[M+H]^+$=418.15 (dashed traces). Corresponding peaks are observed in chromatograms of the petrobactin reconstitution enzymatic reaction and in instances where only the 3,4-DHBA - AMP ligase AsbC, the aryl-carrier protein AsbD, and the aryl transferase AsbE are the only proteins present. These results and previous research (*11, 13*) suggest AsbC, AsbD, and AsbE are necessary and sufficient for formation of **4** and **4'** as well as **6**. The accumulation of these molecules during *in vitro* reconstitution of petrobactin biosynthesis (second trace) demonstrates a lack of incorporation into the final product petrobactin. Unlabeled peaks are consistently observed during LC-MS analysis of all reactions, including the no-enzyme control, and represent artifacts from the reaction. Predicted $[M+H]^+$*m/z* of **4**, **4'**, and **6** were used to target corresponding species for MS/MS analysis. Fragmentation spectra confirm the 3,4-dihydroxybenzoylation pattern for all three compounds.

MS/MS settings are described in the main text. Injected reaction samples were separated on a Phenomenex Synergi Hydro-RP (150x4.6 mm, 4 μm) column in-line with the instrument at a flow rate of 0.3 ml/min with mobile phase supplemented with 0.1% formic acid. 100% ddH_2O was applied for 5 minutes followed by a linear gradient of 0% to 95% MeCN over the course of 20 minutes. 95% MeCN was then applied for an additional 10 minutes.

3.6 Notes

Portions of this chapter were originally published in the following:

> Nusca, T. D.[†], Y. Kim[†], N. Maltseva, J.Y. Lee, W. H. Eschenfeldt, L. Stols, M. M. Schofield, J. B. Scaglione, S. D. Dixon, D. Oves-Costales, G. L. Challis, P. C. Hanna, B. F. Pfleger, A. Joachimiak, and D. H. Sherman. 2012. "Functional and structural analysis of the siderophore synthetase AsbB through reconstitution of the petrobactin biosynthetic pathway from Bacillus anthracis". *J Biol Chem*. (Pub. Online March 9th, 2012)
>
> [†]Equal contribution to the work.

Members of the Midwest Center for Structural Genomics and the Structural Biology Center at Argonne National Laboratory and members of the Life Sciences Institute at the University of Michigan lent equipment and assistance in conducting experiments integral to this chapter. This work was supported by NIH grant GM074942 (to Prof. Andrzej Joachimiak), by the U.S. Department of Energy, Office of Biological and Environmental Research, under contract DE-AC02-06CH11357 (to Prof. Andrzej Joachimiak), by the Biotechnology and Biological Sciences Research Council, through grant BB/F013760/1 (to Prof. Gregory Challis), and by the Great Lakes Regional Center for Excellence (GLRCE) in Biodefense and Emerging Infectious Disease U54AI57153, and the H. W. Vahlteich Professorship (to Prof. David Sherman).

3.7 References

1. P. F. Lindley, *Rep Prog Phys* **59**, 867 (1999).
2. S. C. Andrews, A. K. Robinson, F. Rodriguez-Quinones, *FEMS Microbiol Rev* **27**, 215 (2003).
3. M. K. Wilson, R. J. Abergel, K. N. Raymond, J. E. Arceneaux, B. R. Byers, *Biochem Biophys Res Commun* **348**, 320 (Sep 15, 2006).
4. K. Hotta, C. Y. Kim, D. T. Fox, A. T. Koppisch, *Microbiology* **156**, 1918 (Jul, 2010).
5. J. r. J. May, T. M. Wendrich, M. A. Marahiel, *J Biol Chem* **276**, 7209 (March 9, 2001, 2001).
6. S. Cendrowski, W. MacArthur, P. Hanna, *Mol Microbiol* **51**, 407 (2004).
7. A. T. Koppisch *et al.*, *Biometals* **18**, 577 (Dec, 2005).
8. M. K. Wilson, R. J. Abergel, J. E. Arceneaux, K. N. Raymond, B. R. Byers, *Biometals* **23**, 129 (Feb).
9. J. Y. Lee, K. D. Passalacqua, P. C. Hanna, D. H. Sherman, *PLoS One* **6**, e20777 (2011).
10. B. F. Pfleger *et al.*, *Proc Natl Acad Sci U S A*, (Oct 27, 2008).
11. J. Y. Lee *et al.*, *J Bacteriol* **189**, 1698 (Mar, 2007).
12. D. Oves-Costales *et al.*, *J Am Chem Soc* **129**, 8416 (Jul 11, 2007).

13. B. F. Pfleger *et al.*, *Biochemistry* **46**, 4147 (Apr 3, 2007).
14. D. T. Fox, K. Hotta, C. Y. Kim, A. T. Koppisch, *Biochemistry* **47**, 12251 (Nov 25, 2008).
15. A. Koppisch *et al.*, *Biometals*, (2008).
16. A. T. Koppisch *et al.*, *J Org Chem* **73**, 5759 (Aug 1, 2008).
17. D. Oves-Costales *et al.*, *Chem Commun (Camb)*, 4034 (Sep 14, 2008).
18. D. Oves-Costales, L. Song, G. L. Challis, *Chem Commun (Camb)*, 1389 (Mar 21, 2009).
19. M. K. Wilson, R. J. Abergel, J. E. Arceneaux, K. N. Raymond, B. R. Byers, *Biometals* **23**, 129 (Feb, 2009).
20. A. M. Zawadzka, R. J. Abergel, R. Nichiporuk, U. N. Andersen, K. N. Raymond, *Biochemistry* **48**, 3645 (Apr 28, 2009).
21. K. Barbeau, G. Zhang, D. H. Live, A. Butler, *J Am Chem Soc* **124**, 378 (Jan 23, 2002).
22. H. Liu, K. Hakansson, J. Y. Lee, D. H. Sherman, *J Am Soc Mass Spectrom* **18**, 842 (May, 2007).
23. G. L. Challis, *Chembiochem* **6**, 601 (Apr, 2005).
24. S. M. Barry, G. L. Challis, *Curr Opin Chem Biol* **13**, 205 (Apr, 2009).
25. D. Oves-Costales, N. Kadi, G. L. Challis, *Chemical Commun (Camb)*, 6530 (2009).
26. N. Kadi, G. L. Challis, *Methods Enzymol* **458**, 431 (2009).
27. R. J. Abergel *et al.*, *Proc Natl Acad Sci U S A* **103**, 18499 (December 5, 2006, 2006).
28. M. A. Fischbach, H. Lin, D. R. Liu, C. T. Walsh, *Nat Chem Biol* **2**, 132 (Mar, 2006).
29. R. J. Abergel, E. G. Moore, R. K. Strong, K. N. Raymond, *J Am Chem Soc* **128**, 10998 (Aug 30, 2006).
30. R. J. Abergel, A. M. Zawadzka, K. N. Raymond, *J Am Chem Soc* **130**, 2124 (Feb 20, 2008).
31. P. E. Carlson Jr *et al.*, *Mol Microbiol* **75**, 900 (2009).

32. S. A. McMahon *et al.*, *Acta Crystallogr Sect F Struct Biol Cryst Commun* **64**, 1052 (Nov 1, 2008).
33. S. Schmelz *et al.*, *Nat Chem Biol* **5**, 174 (Mar, 2009).
34. M. Oke *et al.*, *J Struct Funct Genomics* **11**, 167 (2010).
35. T. Franza, B. Mahé, D. Expert, *Mol Microbiol* **55**, 261 (2005).
36. A. D. Berti, M. G. Thomas, *J. Bacteriol.* **191**, 4594 (July 15, 2009, 2009).
37. E. Krissinel, K. Henrick, *Acta Crystallogr D Biol Crystallogr* **60**, 2256 (Dec, 2004).
38. R. A. Laskowski, J. D. Watson, J. M. Thornton, *Nucleic Acids Res* **33**, W89 (Jul 1, 2005).
39. R. A. Laskowski, J. D. Watson, J. M. Thornton, *J Mol Biol* **351**, 614 (Aug 19, 2005).
40. Jmol, *Jmol: an open-source Java viewer for chemical structures in 3D.*, http://www.jmol.org/.
41. S. Schmelz *et al.*, *J Mol Biol*, (Aug 1, 2011).
42. R. H. Upson, R. P. Haugland, M. N. Malekzadeh, R. P. Haugland, *Anal Biochem* **243**, 41 (1996).
43. D. J. Wilson, C. C. Aldrich, *Anal Biochem* **404**, 56 (2010).
44. Y. Zhang, *BMC Bioinformatics* **9**, 40 (2008).
45. A. Roy, A. Kucukural, Y. Zhang, *Nat Protoc* **5**, 725.
46. B. Holinsworth, J. Martin, *Biometals* **22**, 625 (2009).
47. J. Cheung, F. C. Beasley, S. Liu, G. A. Lajoie, D. E. Heinrichs, *Mol Microbiol* **74**, 594 (2009).
48. J. D. Thompson, D. G. Higgins, T. J. Gibson, *Nucleic Acids Res* **22**, 4673 (Nov 11, 1994).
49. L. S. Pereira *et al.*, *Biochem Biophys Res Commun* **352**, 953 (2007).
50. G. H. Tait, *Biochem. J.* **146**, 191 (Jan , 1975, 1975).
51. B. Pradines *et al.*, *Antimicrob. Agents Chemother.* **40**, 2094 (September 1, 1996, 1996).
52. A. Casadevall, D. A. Relman, *Nat Rev Micro* **8**, 149 (2010).
53. D. G. Bouzianas, *Trends in Microbiology* **17**, 522 (2009).

54. E. Navas, *Clinical Microbiology and Infection* **8**, 534 (2002).
55. L. Cegelski, G. R. Marshall, G. R. Eldridge, S. J. Hultgren, *Nat Rev Micro* **6**, 17 (2008).
56. E. J. Drake, B. P. Duckworth, J. Neres, C. C. Aldrich, A. M. Gulick, *Biochemistry* **49**, 9292 (2010).
57. A. Gupte *et al.*, *J Med Chem* **51**, 7495 (2008).
58. M. Miethke, M. A. Marahiel, *Microbiol. Mol. Biol. Rev.* **71**, 413 (September 1, 2007, 2007).
59. U. Möllmann, L. Heinisch, A. Bauernfeind, T. Köhler, D. Ankel-Fuchs, *Biometals* **22**, 615 (2009).
60. L. E. Arnow, *J Biol Chem* **118**, 531 (April 1, 1937, 1937).
61. L. Stols *et al.*, *Protein Expr Purif* **25**, 8 (Jun, 2002).
62. W. Eschenfeldt *et al.*, *Journal of Structural and Functional Genomics* **11**, 31 (2010).
63. G. D. Van Duyne, R. F. Standaert, P. A. Karplus, S. L. Schreiber, J. Clardy, *J Mol Biol* **229**, 105 (1993).
64. M. A. Walsh, G. Evans, R. Sanishvili, I. Dementieva, A. Joachimiak, *Acta Crystallographica Section D* **55**, 1726 (1999).
65. Y. Kim *et al.*, *J Struct Funct Genomics* **5**, 111 (2004).
66. W. Minor, M. Cymborowski, Z. Otwinowski, M. Chruszcz, *Acta Crystallogr D Biol Crystallogr.* **62**, 859 (2006).
67. G. Bricogne, C. Vonrhein, C. Flensburg, M. Schiltz, W. Paciorek, *Acta Crystallogr D Biol Crystallogr* **59**, 2023 (Nov, 2003).
68. R. J. Morris, A. Perrakis, V. S. Lamzin, *Methods Enzymol* **374**, 229 (2003).
69. P. D. Adams *et al.*, *Acta Crystallogr D Biol Crystallogr* **66**, 213 (Feb, 2010).
70. P. Emsley, K. Cowtan, *Acta Crystallographica Section D* **60**, 2126 (2004).
71. R. A. Laskowski, M. W. MacArthur, D. S. Moss, J. M. Thornton, *J. Appl. Crystallogr.* **26**, (1993).
72. D. J. Wilson, C. C. Aldrich, *Analytical Biochemistry* **404**, 56.

Chapter 4

Discussion of Research

4.1 Summary

The efforts described in the previous chapters represent a large portion of what is currently understood regarding petrobactin biosynthesis. As highlighted in Chapter 1, the essentiality of this siderophore for mammalian infection by *B. anthracis* and related species has been demonstrated in the past as have certain preliminary aspects of its assembly. However, the origin of 3,4-DHBA necessary for conferring the stealth capacity of petrobactin as well as the function of the protein encoded by the final gene in the biosynthetic *asb* operon, *asbF*, remained unclear. 3,4-DHBA production has now been demonstrated through conversion of the common bacterial metabolite 3-dehydroshikimate (3-DHS) by AsbF – a 3-dehydroshikimate dehydratase. Elucidation of the co-crystal structure of AsbF with 3,4-DHBA, in conjunction with a series of biochemical studies, supports a mechanism in which an enolate intermediate is formed through the action of this 3-DHS dehydratase metalloenzyme.

Uncovering the exact order in which 3,4-DHBA and the other precursors of petrobactin, citrate and spermidine, are enzymatically incorporated into petrobactin not only holds biological relevance in understanding general secondary metabolic pathways, but will guide synthesis of highly specific compounds with the potential antimicrobial effect of inhibiting enzymes involved in petrobactin-dependent iron acquisition.

Experimentation involving Asb proteins *in vitro* now confirms *asbABCDEF* is sufficient for petrobactin biosynthesis, and assembly of petrobactin can only occur along certain pathways to mitigate byproduct accumulation. These pathways are largely dictated by the substrate preference and catalytic activity imparted by the structures of the NIS synthetase AsbB and related AsbA. The work described in the preceding chapters, in conjunction with that of my collaborators and other biologists in the natural product field, have expanded appreciation for how microbes synthesize NRPS-independent siderophores and implement them in essential iron acquisition during environmental colonization and host infection. This chapter aims to discuss the implications and future directions of this research, including an increased understanding of microbial metabolism; the identification of potential therapeutic targets to halt deadly infections caused by *B. anthracis* and other pathogens; and new avenues for the chemoenzymatic synthesis of novel compounds and complexes.

4.2 Microbial Primary Metabolism and the Secondary Metabolism of Siderophore Biosynthesis

The metabolic cost for the biosynthesis of siderophores is relatively high. Multiple stoichiometric equivalents of ATP, NAD(P)H, and other essential primary metabolites are consumed in the active production and secretion of siderophores into the extracellular milieu (with no guarantee of reacquisition) for the sole purpose of maintaining iron homeostasis (*1-5*). This "at all cost" approach to siderophore utilization appears to highlight the essentiality of iron in biology. In the instance of petrobactin, primary metabolite precursors include citric acid, 3-dehydroshikimate, and spermidine,

which must be maintained in precursor pools necessary to drive their enzymatic conversion to a secondary metabolite during host infection by *B. anthracis*.

Bacillus subtilis aconitase, encoded by *citB*, serves a critical role maintaining cytoplasmic citric acid levels in iron-depleted conditions. This dual-role protein contains a reactive Fe-S cluster that is sensitive to endogenous iron levels. In its active form, it functions in the Krebs cycle to convert citrate to isocitrate for further oxidation; however, in iron depleted conditions, aconitase undergoes a conformational change that renders it capable of binding and stabilizing mRNAs containing an iron-regulatory element (IRE) recognition sequence (*6-8*). The end result is not only increased translation of at least 28 gene products, but an accumulation of citric acid that may maximize flux in the reaction catalyzed by AsbA as the first step of petrobactin biosynthesis.

AsbF produces 3,4-DHBA via a dehydratase reaction involving 3-dehydroshikimate. As an intermediate in the production of indole, tyrosine, and phenylalanine, 3-DHS is ubiquitous in microbiology but at low abundance, perhaps even lower than its precursor, quinoic acid, and downstream product in primary metabolism, shikimic acid (*9, 10*). Several bacterial strains have shown an increase in shikimic acid uptake due to stabilization of importer mRNA by the Fur-regulated RyhB gene product (*11, 12*). It has been noted that isochorismic acid, a downstream product of shikimate, is converted to the 2,3-DHBA component utilized by many catecholate siderophores (*2, 11*). It is possible that in securing an exogenous source of shikimate for primary metabolism, *B. anthracis* may benefit as well by shunting more of the direct precursors 3-dehydroshikimate to production of 3,4-DHBA and petrobactin instead.

In addition to comprising the polyamine "arms" of petrobactin, spermidine stabilizes polynucleotides during cell division and translation, functions as a signaling molecule, and mitigates oxidative damage (*13, 14*). During macrophage infection by the *B. anthracis* endospore, a bacterial arginase out-competes host nitric oxide synthase for arginine. This inhibits production of bactericidal NO, but it also increases levels of ornithine, a precursor to putrescine and spermidine biosynthesis (*15, 16*). The effects of polyamines on both host and pathogen life cycles are pleiotropic and at times appear to be conflicting (*17*). Some general infection models demonstrate spermidine and spermine have a suppressive effect on immune cell recruitment and activation (*18, 19*) while these same compounds stimulates immune cell proliferation (*19, 20*) and spermine in particular has a cytotoxic effect on *Staphylococcus aureus* and some other Gram positives during infection (*21*). In Chapter 3, the promiscuity of AsbA and AsbB with polyamine nucleophiles suggests some of the requisite selectivity in incorporating spermidine originates from the fact that it is one of the few polyamines present in the bacterial cytoplasm. Indeed, among other molecules that acted as efficient nucleophiles, spermine is largely a eukaryotic polyamine (*17*) and norspermidine and AEPDA are naturally occurring in only a handful of species (*22*). It is obvious spermidine or its metabolic precursors are present during infection, and while the implications of this during *B. anthracis* infection are complex, the evolutionary steps taken to use this common polyamine in the biosynthesis of petrobactin can be rationalized.

As the structures of additional siderophores are elucidated, it stands to reason that further knowledge of their biosynthetic pathways may harbor insight into global metabolic changes during disease. Many siderophore pathways utilize citric acid,

including some containing type B NIS synthetases that use ketoglutaric or oxaloacetic acid as a substrate instead (*23*). Iron-regulated primary metabolism also affects availability of aromatic chelating groups in siderophores and contributes to other signaling processes. In addition to the Fur-regulated shikimate pathway already described (*11, 12*), this includes the requirement of salicylate in *Mycobacterium* species above incorporation into siderophores (*24*) and the usage of the metal-sensitive quorum sensing molecule PQS which also contributes secondarily to iron entrapment (*25*).

Adverse conditions encountered by bacteria during infection are compounded through antibiotic treatment; recent studies, particularly in *E. coli*, show antibacterial compounds with diverse targets lead to cell death through common perturbation mediated by Fenton reactions of both intracellular redox conditions and iron homeostasis (*26*). Not only does this disrupt Kreb's cycle components (including the aforementioned aconitase), but such global change in cytoplasmic chemistry affects metabolism tied to the shikimate pathway (via indole production) and signals for colony-wide conversion of aspartate to polyamines (*27*); meanwhile *B. anthracis* also draws from the arginine pool for NO synthesis (curbing spermidine production) to mitigate oxidative damage during similar antibiotic challenge (*28*). Just as the cascades resultant from exposure to antibiotics or a hostile host environment are complex, understanding how bacterial siderophore utilization fits to these perturbations is not completely understood. Nevertheless, by looking at the chemical composition and regulation of natural products like siderophores, further connections may be made to seemingly disparate aspects of a microbe's life cycle and metabolism, revealing new layers of control coinciding with unique environmental conditions.

4.3 Macromolecular Organization of the Petrobactin Biosynthetic Complex

My research has primarily revolved around the characterization of individually purified polypeptide products of the *asb* operon. The unincorporated side-products observed and unnatural excesses of substrates applied during the "one-pot" reconstitution reactions described in Chapter 2 and 3 are not present in wild type *Bacillus* culture (*29*). Thus, while it is clear that the functions of AsbA-E *in trans* are sufficient to reconstitute petrobactin *in vitro*, multiple factors suggest that higher order organization of the Asb proteins is necessary for efficient petrobactin biosynthesis within *B. anthracis.*

AsbC, -D, and –E comprise the NRPS-like components encoded by *asbABCDEF* and mediate the transfer of 3,4-DHBA to petrobactin precursors. As described in Chapter 3, the promiscuous aryl-transferase AsbE will condense 3,4-DHBA (that has been loaded onto AsbD) to spermidine *in vitro* (*30*). Products of this reaction are not incorporated into petrobactin efficiently; thus, their formation depletes pools of 3,4-DHBA, spermidine, and ATP that could be applied to further petrobactin biosynthesis (*29, 31*). AsbC adenylates 3,4-DHBA prior to its loading onto AsbD; however, as a further testament to the inefficiency of incorporating the catecholate moiety to petrobactin *in vitro*, adenylation occurs regardless of AsbD being present (*30*). To partially overcome this, AsbD is added at a stoichiometric excess to AsbC, ensuring that most adenylated 3,4-DHBA is incorporated onto a carrier protein and not simply hydrolyzed (which unnecessarily depletes ATP). Unlike many NRPS modules which are covalently bound in a single polypeptide, AsbC-E are translated as separate proteins (*32*). This said, preliminary pulldown experiments suggest the gene products do undergo specific

interaction when co-expressed and observed in a more native state (Fig. 4-1) than the affinity-tagged, individually-purified proteins used in most of the studies I have described. It is easy to envision that formation of an AsbCDE heterotrimer may reduce the promiscuous activity associated with 3,4-DHBA incorporation described above that would otherwise detract from efficient formation of petrobactin *in vivo*.

What is known of the quaternary structure of NIS synthetases primarily stems from the three crystal structures that are now available: the type A AcsD from achromobactin biosynthesis (*33*), the type C AlcC, from alcaligin biosynthesis (*34*), and AsbB, discussed in this work. In these instances, heterologously over-expressed proteins were purified as a homodimer; however, the apparent dimer interface differed between the Type A (AcsD) which positioned active sites of each monomer outward in opposing directions, and the two Type Cs' (AsbB and AlcC) interface over a relatively larger surface area with the two substrate binding pockets forming a larger cleft along the dimer. Though a sufficiently diffractive crystal of AsbA has proven quite difficult to obtain, both anecdotal and computational inferences can be made about its 3-dimensional structure because of its close similarity to AsbB. Sequence conservation in AsbA of residues involved in the AsbB homodimer interface suggest that during native expression of the entire *asb* operon, an AsbAB heterodimer may form in a similar fashion (Fig. 4-2 A and 4-2 B). Conversely, as a type A synthetase, AsbA may utilize a dimer interface similar to AcsD for interaction with an AsbB homodimer in formation of an AsbAB tetramer (Fig. 4-2 C and 4-2 D).

AsbA performs the first committed step in petrobactin biosynthesis, and the preferred substrates of AsbA are primary metabolites kept at a consistent molar order of

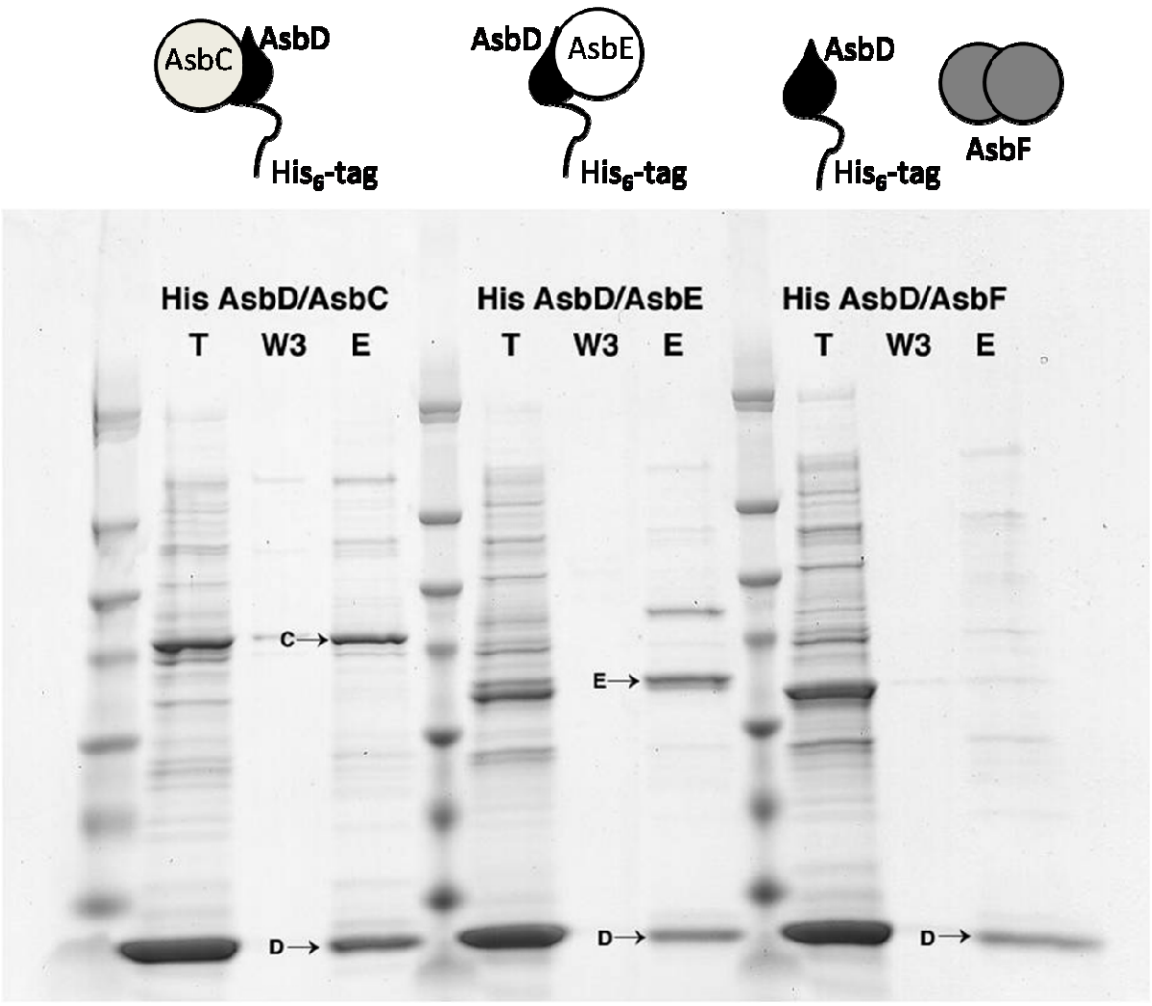

Figure 4-1. Preliminary data suggesting interaction of AsbC, AsbD, and AsbE. His_6-tagged AsbD pulls down co-expressed AsbC or AsbD in *E. coli* using Ni^{2+}-affinity chromatography. The homodimeric cytoplasmic protein AsbF is used as a negative control and does not appear to undergo the same tight interaction when co-expressed with AsbD. *Courtesy of* ***Youngchang Kim*** *and* ***Lucy Stols*** *of the Joachimiak group at Argonne Natl. Laboratory, IL.*

magnitude in the bacterial cytoplasm ($3x10^0$-$2x10^1$ mM) (*17, 35*) necessary for an efficient rate of *N*8-citryl-spermidine formation as suggested by kinetic analysis in chapter 3. AsbB has kinetic parameters similar to AsbA but lacks the abundance of its preferred acidic substrates, *N*1-(3,4-dihydroxybenzoyl)-*N*8-citryl-spermidine or *N*8-citryl-spermidine, that AsbA encounters with citrate. To achieve a similar reaction rate as AsbA, the local concentration of native substrates for AsbB could be increased by a "handoff" from interacting biosynthetic enzymes, overcoming the lag observed *in vitro* as downstream enzymes wait for a diffuse precursor to accumulate to levels where enzymatic activity can occur. Though not experimentally proven, additional association of AsbCDE with upstream siderophore synthetases AsbA and AsbB would ensure presentation of spermidinyl biosynthetic intermediates as preferred nucleophiles for condensation with 3,4-DHBA (Fig. 4-2); meanwhile, this would avoid potential incorporation of unwanted amine solutes like spermidine, putrescine, and lysine. Furthermore, it is likely biosynthetic intermediates would be prematurely secreted if allowed to diffuse through the cytoplasm prior to encountering a trans-acting enzyme; this has been suggested by single *asb* gene deletion mutants of *B. anthracis*, which still secrete petrobactin precursors and side-products to culture media (*29*).

Indeed, a closely-associated "conveyor belt" strategy of natural product biosynthesis is observed in polyketide synthase and NRPS pathways in which multiple catalytic domains are encoded on single polypeptides, which confers reaction order and increases overall flux through the pathway (*36, 37*). Assuming then that polypeptide components of the petrobactin pathway do assemble into a macromolecular biosynthetic complex, the logical organization of this can be explored when considering how petro-

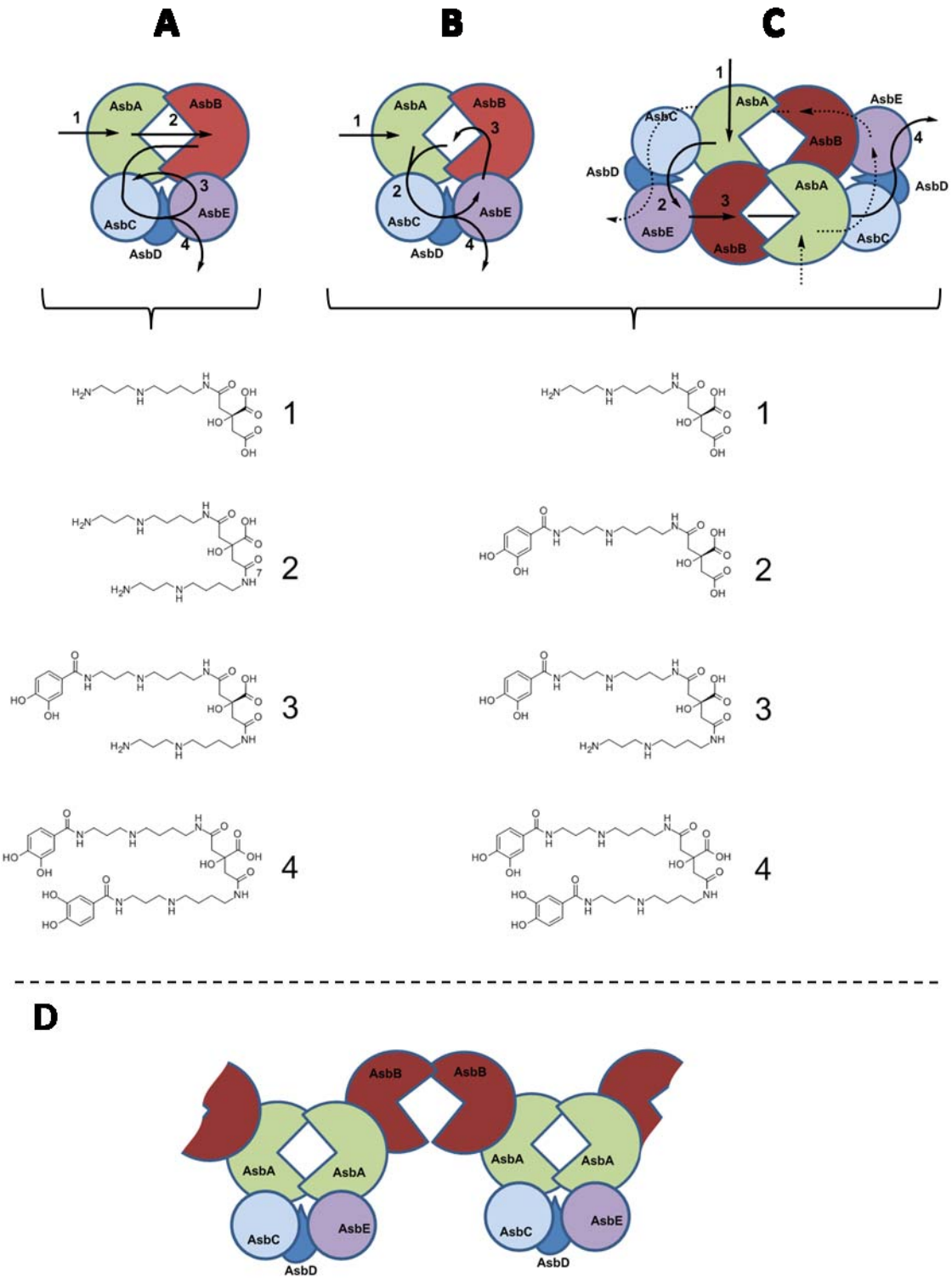

Figure 4-2. Hypothetical quaternary structure of natively expressed *asb* gene products. Stoichiometry of proteins encoded by the *asb* transcript is kept equal in these scenarios. (A) Channeling of biosynthetic intermediates through a putative Asb biosynthetic complex first through an AsbAB heterodimer followed by two consecutive

rounds of an associated NRPS-like AsbCDE complex. (B) An alternate route in which the product of each NIS synthetase is subsequently dihydroxybenzoylated by AsbCDE. (C) Possible pathway through a multimer capitalizing on demonstrated homodimeric interactions of AsbB as well as heterodimeric interactions with AsbA speculated on in this work. Solid and dashed arrows represent two rounds of biosynthesis occurring in parallel through the complex. (D) As a final possibility, homodimers of AsbA and AsbB interact in repeating units for formation of a larger megacomplex.

bactin is constructed. While AsbA and AsbB perform single, early steps, the aryl-transferase complex AsbCDE must perform two dihydroxybenxoylation condensation reactions either consecutively or after incorporation of one spermidine by AsbA and again after a second spermidine by AsbB. How the growing petrobactin molecule is "ping-ponged" in three-dimensional space between siderophore synthetases to aryl-transferase components of the pathway (Fig. 4-2) will likely only be elucidated through expression of the intact *asb* operon under more native conditions (lower copy number of protein, transcribed from a single mRNA, with fewer affinity tags) or by direct imaging of *B. anthracis* during iron-limited growth.

4.4 Chemical and Therapeutic Application

Characterizing the biochemical components of petrobactin biosynthesis was a task that fully occupied the research described in this dissertation; however, it was performed with multiple practical goals in mind. Among siderophores, petrobactin is of particular interest, as it is required for virulence of *B. anthracis* (*32, 38*), and depriving the pathogen of iron acquisition became a logical new target to combat pathogenesis. Along the way, the possibility of petrobactin analogs as therapeutics became apparent, and applying wild type or engineered portions of *asbABCDEF* in a chemoenzymatic approach to create compounds structurally similar to the siderpohore is a logical next step. Indeed, an expansion of chemical diversity, though perhaps without a direct application, has already been achieved in characterizing the promiscuity of condensation enzymes like AsbB and –E. It is possible that upon improving efficient production of petrobactin and analogs thereof, further diverse applications for these compounds may be uncovered.

Siderophore-related antimicrobial strategies

To date, NIS biosynthetic pathways have been described in over 40 species of bacteria; many of these are pathogens. The general activity of NRPS-independent siderophore synthetases is conserved while subtleties of the incorporated substrate vary considerably (*2, 39, 40*). Isolation of an NIS synthetase inhibitor could be applied to a broad spectrum of strains reliant on siderophores, including *B. anthracis*, *S. aureus*, *E. coli*, and *Burkholderia* spp., or, upon discovery, tailored to further mimic a given pathway's intermediate and minimize nonspecific inhibition of commensal strains. While targeted synthesis has produced inhibitors of the AsbC adenylation domain *in vitro*, this activity did not extend to live *Bacillus* (*29*). A separate approach is now being taken where high-throughput adenylation assays involving purified AsbA and the related *S. aureus* synthetase SbnE are screened for inhibitors from natural product extracts at the University of Michigan Center for Chemical Genomics. These experiments are now being conducted by other members of the Sherman group, yielding preliminary hits, some of which are active on multiple synthetases and show bioactivity in a secondary assay.

An alternate route toward capitalizing on *B. anthracis* siderophore dependency during infection focuses on the structure of petrobactin (Fig. 4-3 A). As mimics of the siderophore, petrobactin analogs may bind and block the highly specific components of the now-defined petrobactin ABC importer complexes or function as a molecular "Trojan horse" to deliver antimicrobial chemicals to the bacterial cytoplasm via the same uptake machinery (Fig. 4-3 B). Biophysical characterization of the FpuA receptor, subsequently shown to be the only receptor required for petrobactin uptake in *B. anthracis*, suggest the

central citrate moiety to be crucial for recognition (*41, 42*). For practical purposes, any appending of a petrobactin analog should then occur on portions of the catecholate moieties or polyamine arms. The latter was demonstrated in a proof-of-concept molecular probe that successfully co-precipitated the petrobactin receptor of *B. cereus* (*43*). Ligand-binding of FpuA also becomes more efficient upon complexation of petrobactin with iron (*42*), thus it seems logical that to have much microbiological significance, the chelating capacity—or at least the general 3-dimensional conformation occupied by the ferri-petrobactin complex—should be retained by compounds explored in the future.

Section 4.2 of this chapter discussed the complex downstream effects iron is suggested to have on the eventual redox-associated cytotoxicity of many antibiotics; this highlights the role siderophore-mediated iron uptake might play in affecting potency of new chemotherapeutic methods. Experimentation with siderophore-artemisinin conjugates in both a *Plasmodium* and *Mycobacterium* model demonstrated iron sequestration by test compounds was necessary for optimal bioactivity—presumably via Fenton chemistry with the peroxide moiety of the artimisinin warhead (*44*). Meanwhile, iron is necessary for the full activity of some antibiotics, most notably streptonigrin (*45*), though how efficacy of this compound might be improved as a siderophore conjugate has not been explored. More generally, recent analysis of uropathogenic *Pseudomonas aeruginosa* isolates also demonstrated increased tolerance of antibiotics with disparate cellular targets when strains were cultured in iron-depleted conditions (*46, 47*). It should be noted that despite these intriguing findings, in many cases, depletion of free iron remains an impediment to establishment of a bacterial infection, and preventing the

metal's acquisition still holds promise as a chemotherapeutic method. Whether iron "helps or hurts" appears largely dependent on the redox state a bacterial community resides in and suggests a more thorough comprehension of the multifaceted web of biochemical events mediated by iron is prudent when investigating new antimicrobial targets.

De novo chemoenzymatic production of petrobactin analogs.

Attempts at chemoenzymatically creating petrobactin analogs are still in their nascent phases (Fig. 4-3 C). The tolerance of AsbA for unnatural nucleophiles was described previously (*31*) and expanded on, along with that for AsbB, in Chapter 3. However, *in vitro* enzymatic reconstitution by substituting spermidine with other nucleophiles to create petrobactin analogs that possess two unique polyamine arms has not proven successful. This suggests that unnatural products of AsbA are not efficiently bound downstream at the AsbB active site in an analogous fashion as spermidinyl-citrate, which involves many specific electrostatic interactions (Chapter 3). It has also been speculated that the regioselective capacity AsbA and AsbB have toward spermidine prevents rampant incorporation of multiple repeating polyamine and citryl subunits (*31*). In deviating from the preferred spermidine as the only nucleophile presented to AsbA and -B, perhaps such polymerization occurs—the products of which would not be easily isolated by mass spectrometry due to the multiple charges incorporated. It is in fact the native regioselectivity AsbA and -B place on spermidine that makes it so interesting from a synthetic standpoint. To contrast the singular activity of just AsbA, at least four steps (with much lower yield) are required to produce a racemate of its product with

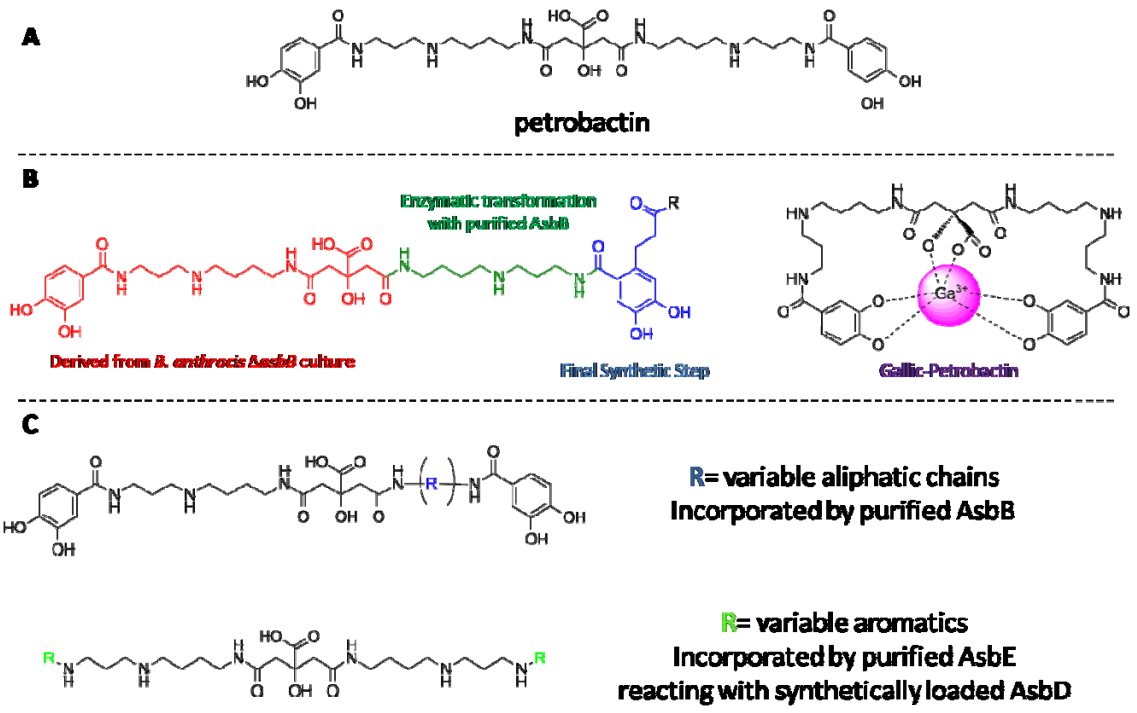

Figure 4-3. Repurposing petrobactin biosynthesis for creation of novel compounds. (A) The structure of petrobactin for reference. (B) Two "Trojan horse" designs demonstrating a combinatorial approach to creating a siderophore analog scaffold and complexation with bactericidal Ga^{3+}. (C) Promiscuity of condensation enzymes including AsbB and AsbE will allow creation of siderophore analogs with variable polyamine arm or aromatic moieties incorporated, respectively.

spermidine in the proper orientation synthetically. It is possible that engineering of AsbA and AsbB could focus this selectivity to other asymmetrical compounds or widen the nucleophile binding pocket to accept larger, branching substrates.

Among NISs characterized, petrobactin is unique in the fact that it contains two aromatic chelating moieties. This not only imbues the compound with a higher affinity for iron, but renders it and many of its precursors much more isolable and observable than similar NISs including the staphyloferrins, achromobactin, and aerobactin (*40, 48*). While AsbE is promiscuous in transfer of 3,4-DHBA from the aryl carrier protein AsbD to nucleophiles, initial activation of 3,4-DHBA by AsbC is much more selective and represents the largest hurdle in chemoenzymatic creation of petrobactin analogs with non-native terminal functionalities (Fig 4-3) (*30*). To overcome this, a fellow graduate student in the Sherman group, Doug Hansen, and I attempted a previously explored methodology (*49*) to bypass AsbC altogether by chemically loading the phosphopantetheine arm of AsbD with thiophenol derivatives of organic acids analogous to 3,4-DHBA (Fig. 4-4 A). In a pilot experiment, synthesized compounds thiophenylated 3,4-DHBA (3,4-DHBA-SPh) and thiophenylated 4-chlorobenzoic acid (4-CBA-SPh) did form an amide bond with spermidine when incubated together; however, this appeared to be independent of the activity of AsbD or AsbE in all but one instance: di-4-chlorobenzoylation of spermidine could not be accomplished without AsbD and –E present (Fig. 4-4 B). Whether or not these proteins will be required in reaction of thiophenylated derivatives with the petrobactin precursors now presumed to be native

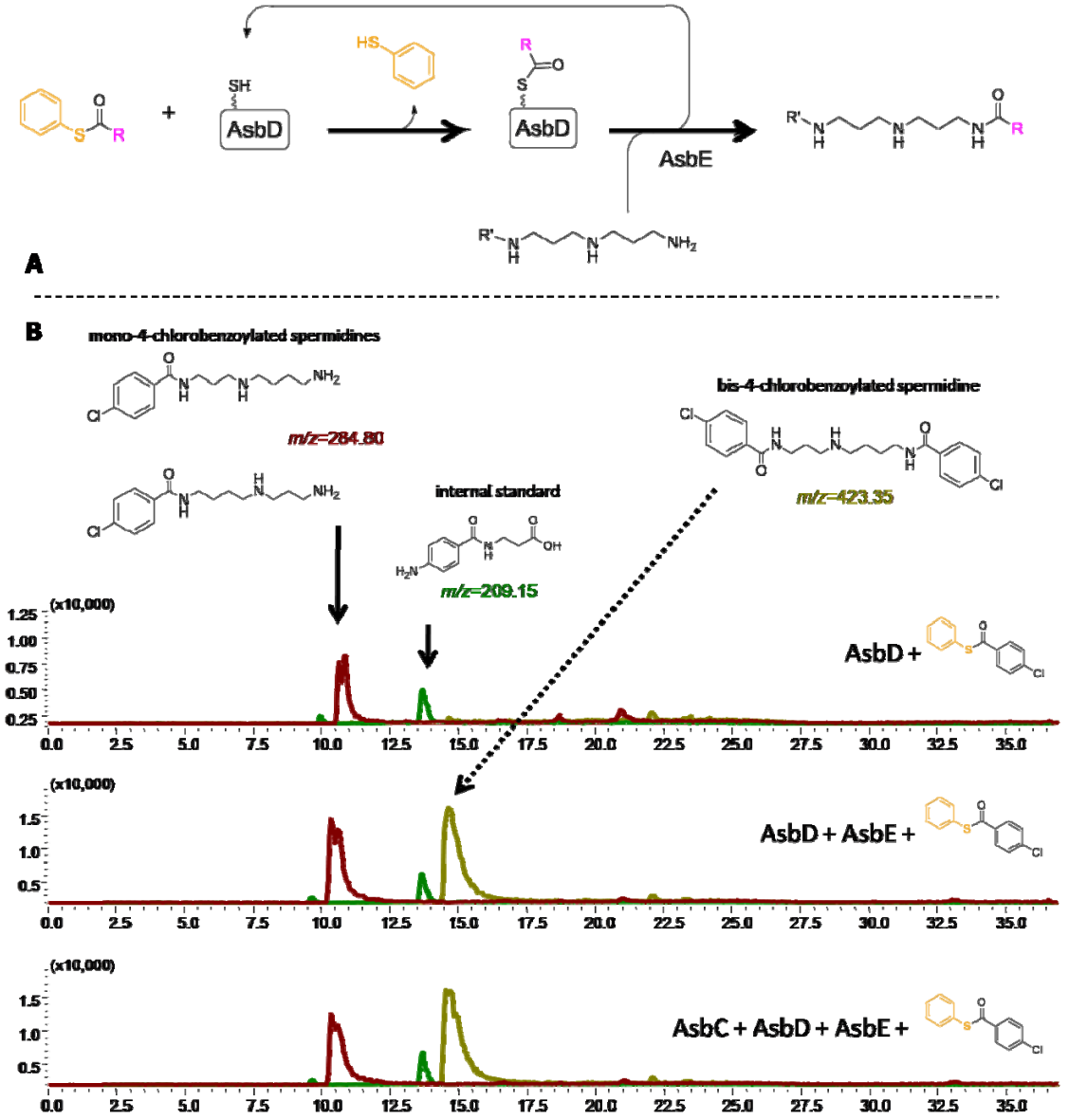

Figure 4-4. Incorporation of unnatural aromatic moieties utilizing thiophenol derivatives. (A) The general reaction with the carrier protein AsbD and the aryl transferase AsbE. (B) LC-MS traces of selected *m/z* depicting enzymatically-dependent formation of bis-(4-chlorobenzoyl)-spermidine and spontaneous mono-(4-chlorobenzoyl)-spermidine products.

substrates of AsbE remains to be determined. Creating petrobactin analogs with replaced aromatic moieties using this strategy requires that the AsbAB reaction be scaled up to obtain the polar bis-spermidinyl-citrate "core" of petrobactin. Ideally, a suite of petrobactin analogs obtained from the methods described would then be probed for bioactivity either as a siderophore or in blocking native siderophore recognition.

Applying isolated natural products.

Purified petrobactin has been used in the characterization of siderophore uptake pathways of *Bacillus (41, 50, 51)*, and also as an exogenous compound in "xenosiderophore" studies with other species (*52*). Complexation of purified siderophores with metals other than iron has been explored, including in bioremediation of heavy metal contaminated ecosystems (*53*) and in delivery of cytotoxic metals to bacteria (*54, 55*). Falling in the latter group, Ga^{3+} has a similar valence and size as Fe^{3+}, but cannot be biologically reduced. Data from the Hanna lab demonstrates gallium exerts a petrobactin-mediated toxic effect on vegetative bacilli (*41, 50*). Furthermore, free gallium salts have shown efficacy in certain bacterial infection models, albeit with expected side effects (*56*). Pre-complexation of petrobactin with gallic ions (Fig. 4-3 B) may target the toxic metal exclusively to cells utilizing the siderophore, perhaps making gallium a druggable option in future anthrax cases.

The gallic-petrobactin complex represents a relatively simplistic approach to the "Trojan-horse" method of drug delivery, which has been applied to siderophore uptake pathways to some success in the past (*44, 55, 57*) and described earlier in this section. In collaboration with Dr. Alex Hoffmaster at the CDC, another method is being explored by

the Sherman group that aims to target *B. anthracis* for destruction. Purified natural product precursors from a Δ*asbB* biosynthetic mutant provide substrate for enzymatic conversion by AsbB to starting material for a final synthetic process that will incorporate a polymorpholino or antibiotic warhead to a petrobactin molecule. The combinatorial approach being taken to produce these petrobactin analogs highlights the two main focuses of my dissertation effort: purification of siderophores or siderophore precursors and analyzing the activity of heterologously-expressed biosynthetic proteins.

Through research that has occurred over the past decade, including the body of work presented in this dissertation, petrobactin has become one of the best characterized siderophores derived from an NRPS-independent pathway. The distribution of the *asb* pathway described in Chapter 2 and the even more expansive utilization of exogenous petrobactin explored by other researchers suggest the implications of this molecule in both pathogenesis and ecology have not been fully uncovered. Terrestrial microbes capable of utilizing but not synthesizing petrobactin extend beyond closely related *Bacillus* species (*32*) to pathogenic strains of *S. aureus* (*52*). Considering the widespread conservation of ABC importer systems homologous to the *fpu* and *fat* genes encoded by *B. anthracis*, the potential for petrobactin recognition is probably more widespread (*3*). Analysis of conserved *asb* operons suggests petrobactin production can be divided into two taxanomic and ecological branches (Chapter 2). Within the marine niche, petrobactin chelates iron for *Marinobacter* spp. among others (*58*). In this non-infectious context, the utility of the stealth 3,4-DHBA moiety as well as the purpose of sulfonated petrobactin derivatives produced by certain strains is unknown, but separate cellular localization or novel signaling function of petrobactin derivatives and alternative chelate

complexes has been speculated on (*59-61*). Furthermore, isolation from oil spills, including the Deepwater Horizon site, of petrobactin-like compounds suggests some importance in bioremediation that warrants further exploration (*62, 63*). The broad impact of fully characterizing petrobactin biosynthesis and understanding the role of this natural product in both disease-associated and environmental iron acquisition has yet to be realized; the foundation established by this body of work and that of my colleagues now sets the stage for future purposeful application of siderophore synthetase pathways in both chemistry and biology.

4.5 References

1. S. C. Andrews, A. K. Robinson, F. Rodriguez-Quinones, *FEMS Microbiol Rev* **27**, 215 (2003).
2. S. M. Barry, G. L. Challis, *Curr Opin Chem Biol* **13**, 205 (Apr, 2009).
3. B. Chu *et al.*, *Biometals* **23**, 601.
4. R. C. Hider, X. Kong, *Natural Product Reports* **27**, 637 (2010).
5. M. Miethke, J. Hou, M. A. Marahiel, *Biochemistry* **50**, 10951 (2012/03/18).
6. H.-J. Kim *et al.*, *Journal of Bacteriology* **185**, 1672 (March 1, 2003, 2003).
7. A. Gaballa *et al.*, *Proceedings of the National Academy of Sciences* **105**, 11927 (August 19, 2008, 2008).
8. G. T. Smaldone *et al.*, *Journal of Bacteriology*, (March 2, 2012).
9. G. Gosset, *Current Opinion in Biotechnology* **20**, 651 (2009).
10. C. T. Walsh, S. W. Haynes, B. D. Ames, *Natural Product Reports* **29**, 37.
11. H. Salvail *et al.*, *Proceedings of the National Academy of Sciences* **107**, 15223 (August 24, 2010).
12. E. MassÃ©, H. Salvail, G. Desnoyers, M. l. Arguin, *Current Opinion in Microbiology* **10**, 140 (2007).
13. J. Schneider, V. Wendisch, *Applied Microbiology and Biotechnology* **91**, 17.
14. H. M. Wallace, A. V. Fraser, A. Hughes, *Biochem J* **376**, 1 (Nov 15, 2003).

15. J. Weaver *et al.*, *Infection and Immunity* **75**, 3894 (August 2007, 2007).
16. S. Porasuphatana *et al.*, *Current Microbiology* **61**, 567.
17. B. Wortham, M. Oliveira, C. Patel, R. D. Perry, J. D. Fetherston. (Springer New York, 2007), vol. 603, pp. 106-115.
18. G. Bjelaković *et al.*, *Amino Acids* **39**, 29.
19. V. Bansal, J. B. Ochoa, *Current Opinion in Clinical Nutrition & Metabolic Care* **6**, 223 (2003).
20. M. Zhang, H. Wang, K. J. Tracey, *Crit Care Med* **28**, N60 (Apr, 2000).
21. L. L. Anzaldi, E. P. Skaar, *Molecular Microbiology* **82**, 1.
22. J. Lee *et al.*, *J Biol Chem* **284**, 9899 (Apr 10, 2009).
23. S. D. Himpsl *et al.*, *Mol Microbiol* **78**, 138 (Oct).
24. T. Adilakshmi, P. D. Ayling, C. Ratledge, *J Bacteriol* **182**, 264 (Jan, 2000).
25. S. P. Diggle *et al.*, *Chem Biol* **14**, 87 (Jan, 2007).
26. M. A. Kohanski, D. J. Dwyer, B. Hayete, C. A. Lawrence, J. J. Collins, *Cell* **130**, 797 (2007).
27. H. H. Lee, J. J. Collins, *Nat Chem Biol* **8**, 6 (2012).
28. I. Gusarov, K. Shatalin, M. Starodubtseva, E. Nudler, *Science* **325**, 1380 (September 11, 2009, 2009).
29. J. Y. Lee *et al.*, *J Bacteriol* **189**, 1698 (Mar, 2007).
30. B. F. Pfleger *et al.*, *Biochemistry* **46**, 4147 (Apr 3, 2007).
31. D. Oves-Costales *et al.*, *Chem Commun (Camb)*, 4034 (Sep 14, 2008).
32. K. Hotta, C. Y. Kim, D. T. Fox, A. T. Koppisch, *Microbiology* **156**, 1918 (Jul, 2010).
33. S. Schmelz *et al.*, *Nat Chem Biol* **5**, 174 (Mar, 2009).
34. M. Oke *et al.*, *J Struct Funct Genomics* **11**, 167 (2010).
35. C. J. Bolten, P. Kiefer, F. Letisse, J.-C. Portais, C. Wittmann, *Analytical Chemistry* **79**, 3843 (2012/03/18, 2007).
36. J. L. Meier, M. D. Burkart, *Chemical Society Reviews* **38**, 2012 (2009).
37. A. C. Jones *et al.*, *Natural Product Reports* **27**, 1048 (2010).
38. M. K. Wilson, R. J. Abergel, K. N. Raymond, J. E. Arceneaux, B. R. Byers, *Biochem Biophys Res Commun* **348**, 320 (Sep 15, 2006).

39. N. Kadi, G. L. Challis, *Methods Enzymol* **458**, 431 (2009).
40. D. Oves-Costales, N. Kadi, G. L. Challis, *Chemical Commun (Camb)*, 6530 (2009).
41. P. E. Carlson Jr *et al.*, *Mol Microbiol* **75**, 900 (2009).
42. A. M. Zawadzka *et al.*, *Proc Natl Acad Sci U S A* **106**, 21854 (Dec 22, 2009).
43. N. Bugdahn *et al.*, *Angew Chem Int Ed Engl* **49**, 10210 (Dec 27).
44. M. J. Miller *et al.*, *J Am Chem Soc* **133**, 2076 (Feb 23, 2011).
45. H. N. Yeowell, J. R. White, *Antimicrob Agents Chemother* **22**, 961 (Dec, 1982).
46. M. Narten, N. Rosin, M. Schobert, P. Tielen, *Curr Microbiol* **64**, 7 (Jan, 2012).
47. D. Nguyen *et al.*, *Science* **334**, 982 (November 18, 2011, 2011).
48. J. Cheung, F. C. Beasley, S. Liu, G. A. Lajoie, D. E. Heinrichs, *Mol Microbiol* **74**, 594 (2009).
49. S. A. Sieber, J. Tao, C. T. Walsh, M. A. Marahiel, *Angewandte Chemie International Edition* **43**, 493 (2004).
50. S. D. Dixon, B. K. Janes, P. E. Carlson, Jr., P. C. Hanna, *Mol Microbiol*, (2012).
51. A. Koppisch *et al.*, *Biometals*, (2008).
52. F. C. Beasley, C. L. Marolda, J. Cheung, S. Buac, D. E. Heinrichs, *Infection and Immunity* **79**, 2345 (June 1, 2011, 2011).
53. M. Rajkumar, N. Ae, M. N. V. Prasad, H. Freitas, *Trends in Biotechnology* **28**, 142.
54. M. Miller *et al.*, *Biometals* **22**, 61 (2009).
55. M. Miethke, M. A. Marahiel, *Microbiol. Mol. Biol. Rev.* **71**, 413 (September 1, 2007, 2007).
56. C. R. Chitambar, *Int J Environ Res Public Health* **7**, 2337 (May).
57. U. Möllmann, L. Heinisch, A. Bauernfeind, T. Köhler, D. Ankel-Fuchs, *Biometals* **22**, 615 (2009).
58. K. Barbeau, G. Zhang, D. H. Live, A. Butler, *J Am Chem Soc* **124**, 378 (Jan 23, 2002).
59. W. R. Harris, S. A. Amin, F. C. KÃ¼pper, D. H. Green, C. J. Carrano, *Journal of the American Chemical Society* **129**, 12263 (2012/03/18, 2007).

60. V. V. Homann, K. J. Edwards, E. A. Webb, A. Butler, *Biometals* **22**, 565 (Aug, 2009).
61. G. Zhang *et al.*, *Inorganic chemistry* **48**, 11466 (2009).
62. J. M. Gauglitz, H. Zhou, A. Butler, *J Inorg Biochem* **107**, 90 (Feb).
63. R. A. Gardner, R. Kinkade, C. Wang, O. t. Phanstiel, *J Org Chem* **69**, 3530 (May 14, 2004).

Appendix

Further Comparison of Putative *asb* Gene Clusters

In conjunction with Fig. 2-S2 in Chapter 2, following is a description of further bioinformatic analyses of genes homologous to those encoded by the *asbABCDEF* in *B. anthracis*. The BLAST tool on the National Center for Biotechnology Information (NCBI) website was used for initial queries. Sequences of individual protein products of the *asb* operon were applied to homology searches. *Bacillus* and closely related genera were excluded to survey a wider range of diverse organisms' transcribed genomes. Hits ranged between 42% and 75% in primary sequence similarity.

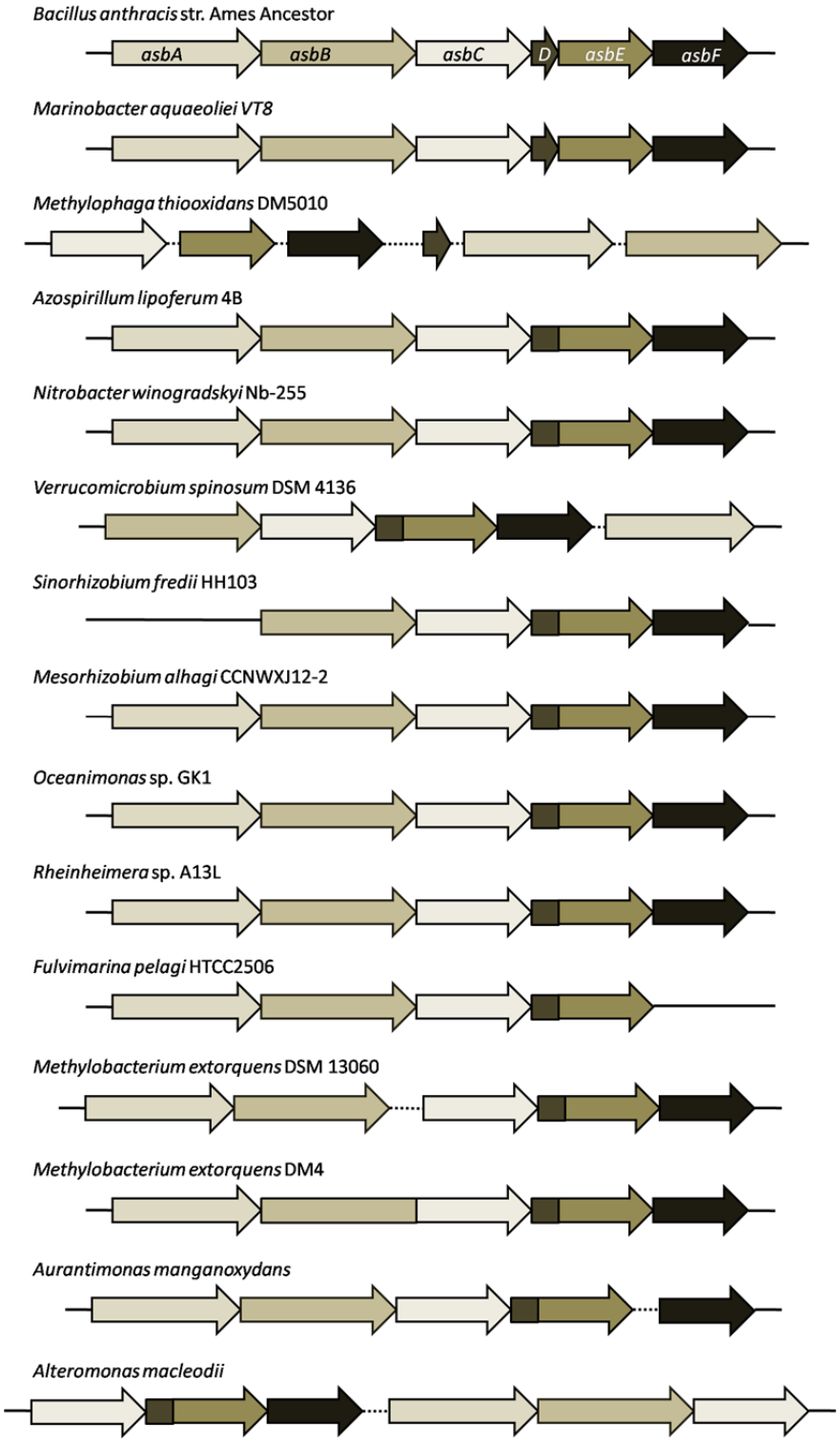

Figure A-1. Synteny in *asb* genes from select species. Each arrow is indicative of a separate open reading frame. The color theme of each *asb* product is kept consistent throughout to indicate homologues (multicolored arrows indicate a fusion). Dashed lines indicate separation of different cluster components onto different loci on the genome.

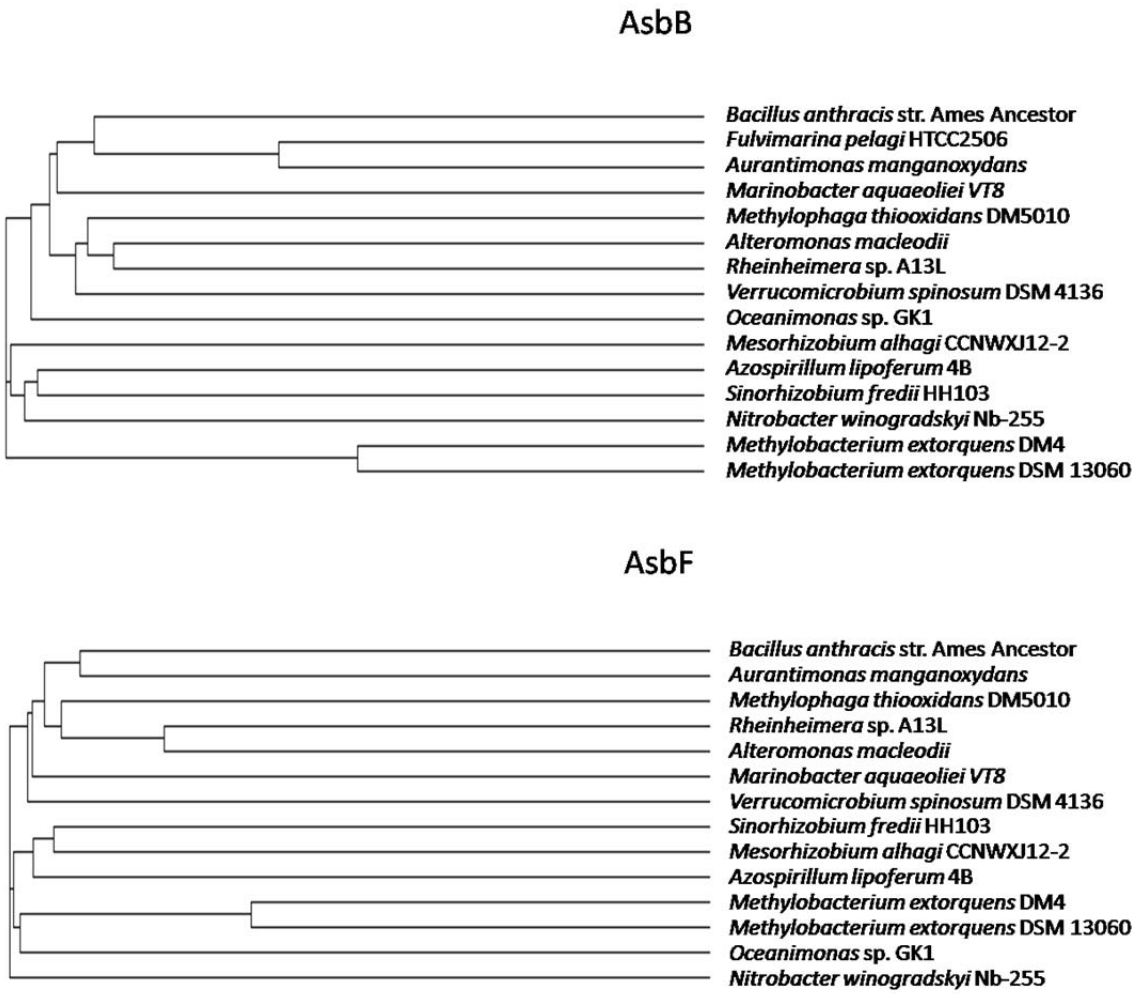

Figure A-2. Divergence of selected *asb* products. Cladograms display the probable evolutionary relationship of AsbB and AsbF based upon primary sequence similarity. Though not identical, general clade separation is similar between AsbB and AsbF among their respective homologues. Generated from alignments performed on ClustalW2 on the European Bioinformatics Institute (EMBL-EBI) website.

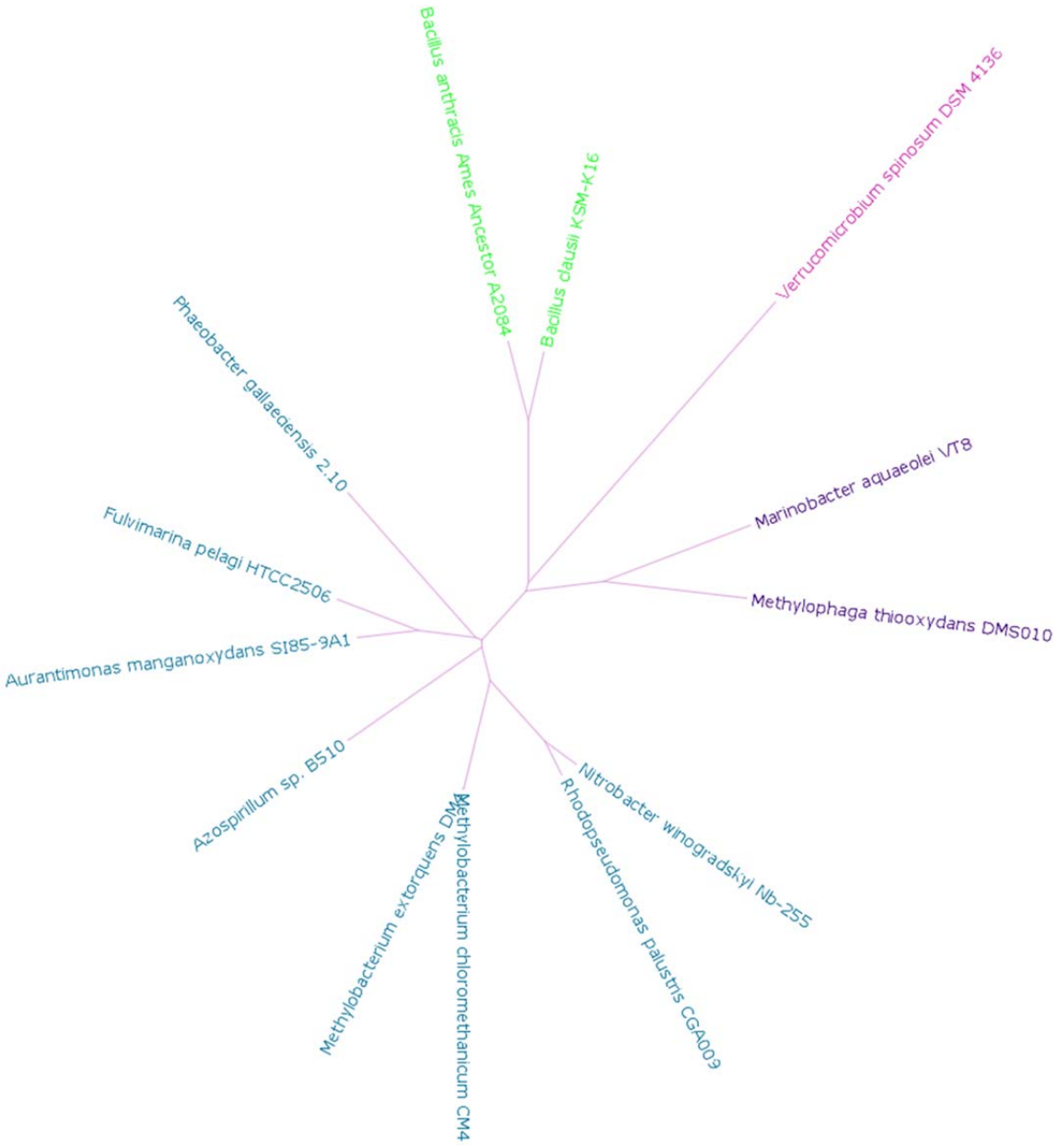

Figure A-3. Phylogeny of select species harboring an *asb*-like gene cluster. Relative distance of some *asb*-containing genomes is shown. Though incomplete, organisms in diverse ecological niches and disparate taxonomy that likely have the capacity to biosynthesize petrobactin are depicted. Such distribution of the *asb* cluster probably results from one or more horizontal gene transfers. Based on the cladograms of Fig. A-2, homologues of AsbB and AsbF with primary sequences most similar to those from *B. anthracis* appear to originate from the branch containing *F. pelagi* and *A. manganoxydans*. Possibly, a shallow-water relative of these species is responsible for the gene transfer events that allowed terrestrial *Bacillus* spp. and deep water *Marinobacter* spp., among others, to produce petrobactin. Generated using the distance function on the U.S. Department of Energy Integrated Microbial Genomes (IMG) website.